UNIVERSITÀ
DEGLI STUDI
DI PADOVA

University of Padua

Department of Cardiac, Thoracic and Vascular Sciences

PhD PROGRAMME IN MEDICAL, CLINICAL AND EXPERIMENTAL SCIENCES
CURRICULUM: NEUROSCIENCE
29th SERIES

DEVELOPMENT AND *IN VITRO* CHARACTERIZATION OF NANOPARTICLES FOR INNER EAR DRUG DELIVERY

Coordinator: Prof. Gaetano Thiene
Supervisor: Prof. Alessandro Martini
Co-Supervisor: Dr. Laura Astolfi

PhD Student: Filippo Valente

Abstract

An innovative drug delivery system for inner ear therapy is based on the use of nanoparticles (NPs): they can be considered good carriers for therapeutic drugs within the inner ear, because they increase drug diffusion and are detected in all parts of the cochlea when applied near the round window. In this study liquid crystalline NPs based on glycerol monooleate were developed and conjugated with two hydrophobic drugs, coenzyme Q10 and dexamethasone, already used for inner ear therapies but limited in their efficacy by low solubility and bioavailability. These conjugated NPs were tested *in vitro* on two different cell lines, as models of the inner ear cell populations: thePC12 cells, neural-like cells used as a model of neuronal differentiation, and OC-k3, derived from the organ of Corti of transgenic mice as a model of inner ear sensory cells. The NPs conjugated with coenzyme Q10 or dexamethasone were tested against cisplatin (cis-diamminedichloroplatinum(II)), a cytotoxic agent widely used for treatment of solid tumors. Although effective as antitumor agent, cisplatin induces serious collateral effects, among which ototoxicity on the auditory nerve, the stria vascularis and hair cells. The results showed that NPs conjugated with drugs are well tolerated by both cells lines and are uptaken by cells in the first few hours after treatment, delivering the conjugated compounds inside the cells. Moreover, NPs conjugated with dexamethasone were able to counteract damages caused by cisplatin, preventing apoptosis in OC-k3 cells, and increased the concentration of drug uptaken by the cells compared to the free drug treatment. Based on these results, NPs have an interesting potential as inner ear drug delivery systems.

Index

1 Introduction

1.1 The auditory system: anatomy and physiology

1.1.1 Anatomy of the ear

The auditory system enables the hearing perception (hearing function) and the regulation of the sense of balance (vestibular function). It is anatomically divided into three parts: outer, middle and inner ear. The outer part is composed of the pinna and the auditory canal. At the bottom of the canal the tympanic membrane (eardrum) creates a barrier protecting the middle ear. The middle ear consists of the tympanic cavity, containing the ossicular chain composed by the malleus, the incus and the stapes. The Eustachian tube opens in the middle ear and allows the ventilation of the tympanic cavity via the nasopharynx (1). The outer ear and middle ear redirect and amplify the sound vibration coming from the outside towards the inner ear, connected to the tympanic cavity by the round window membrane (RWM) and the oval window (2). The inner ear is inserted in the petrous part of the temporal bone and contains the organ of sensorineural hearing (the cochlea), the organs of balance (utricle and saccule) and the semicircular canals (1) (Fig. 1.1).

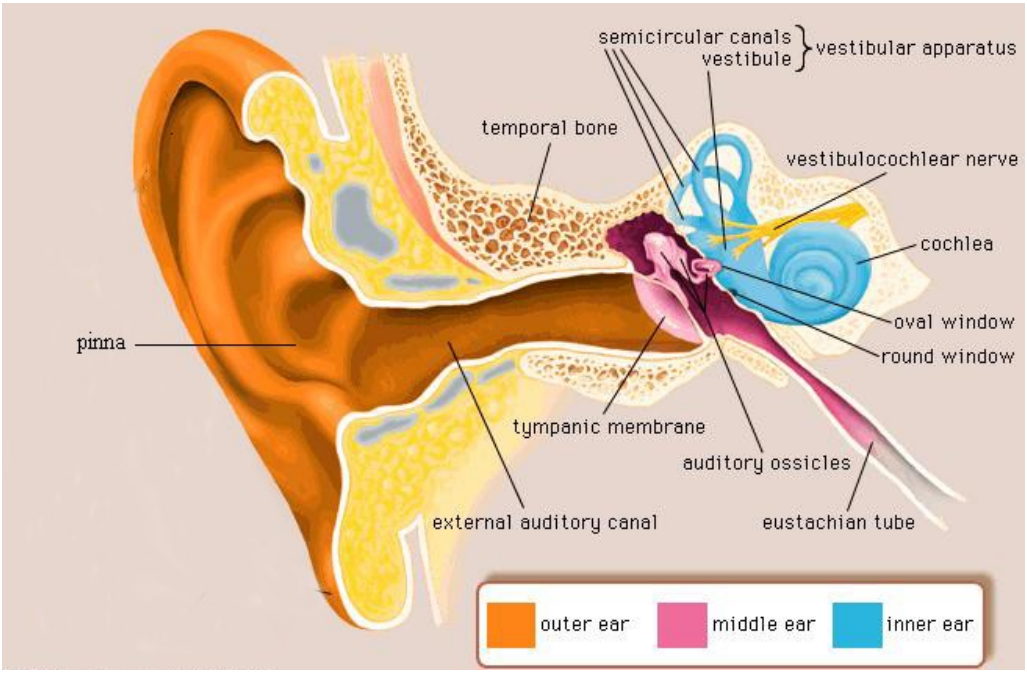

Fig. 1.1. Anatomical scheme of the human ear (redrawn from: ©1997 Encyclopedia Britannica, Inc.).

1.1.2 The cochlea

The cochlea is a coiled tube, about 30 mm long in humans, making 2 and ¾ turns around a mass of fibrous tissue called modiolus. The internal structure of the cochlea is composed of three fluid filled compartments located inside the petrous temporal bone. The middle channel, called scala media or cochlear duct, is filled with endolymph, while the lower and upper compartments, respectively called scala tympani and scala vestibuli, are both filled with perilymph. Scala tympani and scala vestibuli are connected at the apex of the cochlea through a passage known as helicotrema (3) (Fig. 1.2). The scala media contains the organ of Corti, responsible for the transduction of the auditory signal to the brain; the organ is shielded above by the Reissner's membrane and at the bottom lays on the basilar membrane. The scala media is anchored to the outer bony structure by the spiral ligament, made of connective tissue. The ligament is highly vascularised by a tissue named stria vascularis.

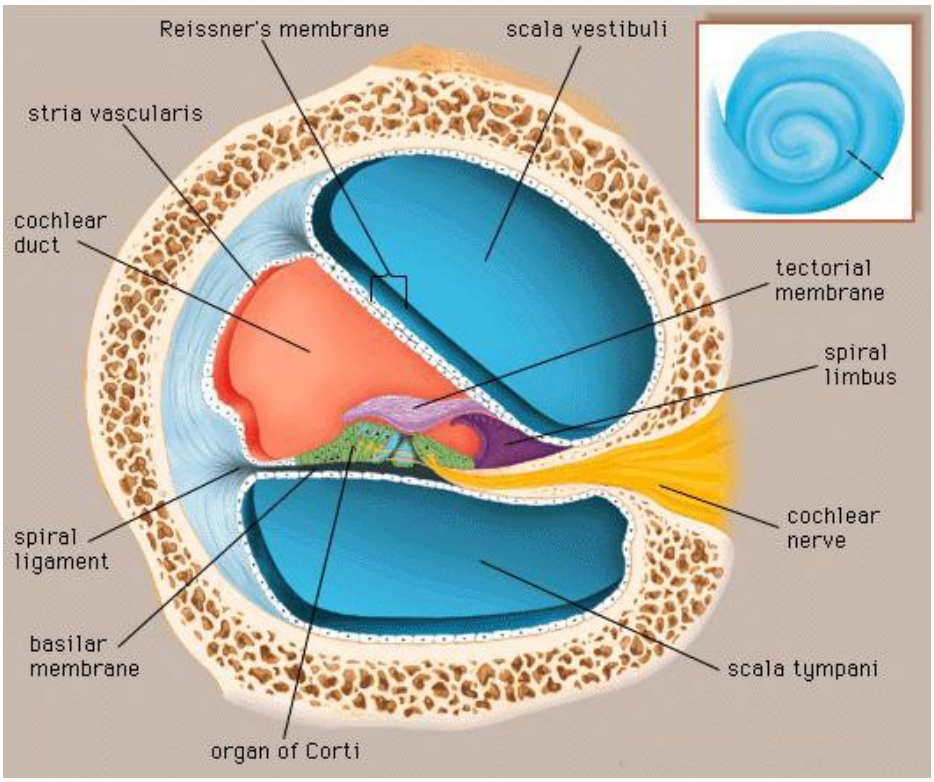

Fig. 1.2. Section of the cochlea (redrawn from: ©1997 Encyclopedia Britannica, Inc.).

1.1.3 The organ of Corti

The organ of Corti is composed of two different kinds of cells: the sensory ones, called hair cells because of the presence of stereocilia at the cellular apex, and the supporting cells (Fig. 1.3). Other cells rich in cytoskeleton, called pillar cells, cover the cochlear duct. Hair cells are arranged in longitudinal rows, divided in one row of inner hair cells and three rows of outer hair cells. The inner hair cells differ from the outer ones in number (in humans the proportion is about 1:10) and in shape and structure of the stereocilia. Above the organ of Corti there is the tectorial membrane, in direct contact with the stereocilia. The hair cells are connected to the central nervous system by afferent nerve fibers projecting to the auditory cortex. A long nervous ganglion, called spiral ganglion, is located inside the modiulus: it is made of cell bodies of the neurons related to the cochlea, whose combined processes form the acoustic nerve. Together with the vestibular nerve, the spiral ganglion forms the vestibulocochlear nerve (eighth cranial nerve). About 95% of the nerve fibers of the spiral ganglion individually innervate the inner hair cells which are able to discriminate among incoming sound vibrations; the remaining 5% take multiple contacts with the outer hair cells, whose role is to increase the sound signal sensitivity (2).

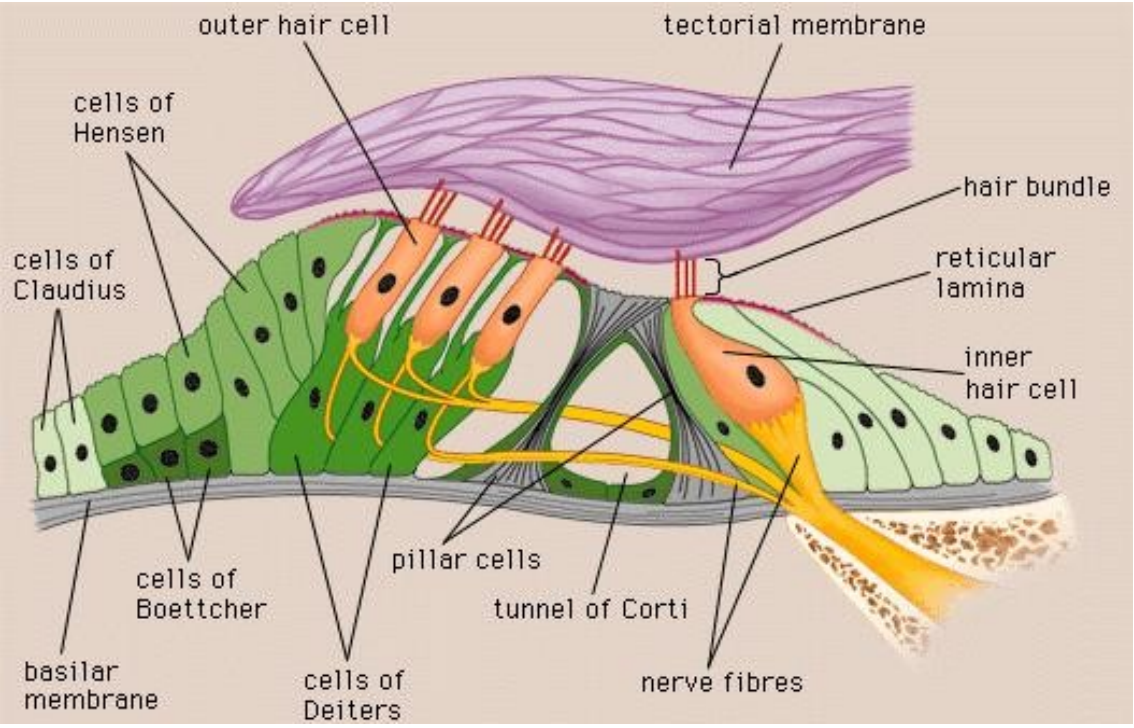

Fig. 1.3. Structure of the organ of Corti (redrawn from: ©1997 Encyclopedia Britannica, Inc.).

1.1.4 Transmission of the acoustic signal

In the auditory process, the acoustic waves are channelled by the pinna into the auditory canal, inducing the vibration of the eardrum. The vibrations cause the movement of the ossicular chain, which transfers the mechanical pressure waves to the inner ear fluids through the oval window. During their passage, the pressure waves cause vibrations of the basilar membrane and thus of the organ of Corti. The resulting vibrations of stereocilia of the hair cells are responsible for acoustic signal transduction: the mechanical waves are transformed into an electric signal by inducing a variation of intracellular potential leading to the release of neurotransmitters. The signal is then transmitted via the cochlear nerve to the auditory cortex to be processed (4). The hair cells and the neurons of the inner ear are in a state of terminal differentiation and have lost the ability to regenerate or proliferate: thus, once the inner ear tissue is damaged by an external agent, the loss of function in the auditory system becomes permanent (2).

1.1.5 Ototoxicity

The medical condition of unilateral or bilateral hearing impairment is defined as hypoacusis (hearing loss): it is called transmission hypoacusis when it is related to alterations of the external or middle ear and sensorineural hypoacusis when it is related to the inner ear. The latter is classified according to whether the deficit concerns the cochlea (cochlear hearing loss) or the related nerve pathway (retrocochlear hearing loss) (5). According to World Health Organization data published on March 2015, about 360 million people worldwide have disabling hearing loss, referring to hearing loss greater than 40 decibels (dB) in the better hearing ear in adults and greater than 30 dB in the better hearing ear in children. According to the same data, one-third of people over 65 years of age are affected by disabling hearing loss caused by congenital or hereditary factors or induced by exogenous ones. Exogenous hearing loss can be caused by numerous stress factors such as noise, trauma, infections and ototoxic effects of drugs. Among the drugs there are substances which cause the loss or dysfunction of the auditory cells (hair cells and neurons), and the induced damage can be reversible or permanent (2). Among pharmacological drugs widely used in clinical practice that cause a loss of the hearing function there is cisplatin.

1.2 Cisplatin

1.2.1 Structure and characteristics

Cisplatin ((*SP*-4-2)-diamminedichloroplatinum(II)) (CDDP) is a chemotherapeutic agent belonging to the class of platinum containing anti-cancer drugs. It was the first platinum antitumor drug introduced in clinical practice (6) and is still one of the most powerful and widely used agent to treat solid tumors affecting head, neck, lungs, oesophagus, stomach and genitourinary tract (7, 8).

The structure of the CDDP includes a central platinum atom with four ligands, two amino groups and two hydrochloric groups (Fig. 1.4): when the last two groups are disposed in *cis* conformation, the molecule exhibits chemotherapeutic activity (9). The cellular uptake of CDDP, although not fully understood, is thought to occur because of passive diffusion via transmembrane channels and facilitated diffusion processes (10). Once inside the cells, the two chlorine atoms are substituted with two molecules of water, forming a monohydrate complex: this turns the CDDP into a very reactive and cytotoxic molecule, able to interact with the cellular proteins, the phospholipid membrane, the cytoskeleton microfilaments, RNA, nuclear and mitochondrial DNA (11). All these effects may induce cell death by apoptosis, which is at the base of the antitumor role of CDDP (12).

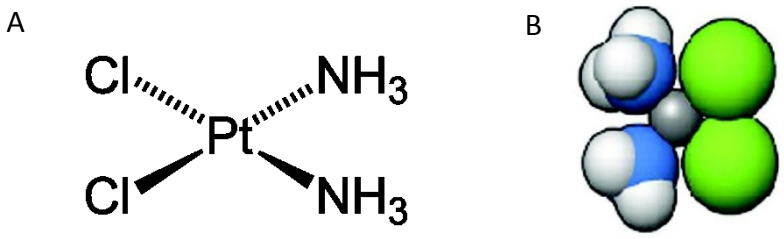

Fig. 1.4. A. Structure of cisplatin ((SP-4-2)-diamminedichloroplatinum(II)). B. *cis*- conformation of cisplatin (redrawn from Goodsell, 2006).

1.2.2 Cisplatin ototoxicity and cytotoxicity

The clinical administration of CDDP induces severe dose-dependent side effects, including neurotoxicity, nephrotoxicity and ototoxicity. A major limitation of the chemotherapy is also the

development of a serious drug resistance of the cancer cells (13). In detail, the CDDP ototoxicity is dose-dependent, affecting the hearing capacity and inducing the occurrence of tinnitus in patients (14). However, there is a high variability of individual response due to metabolism, genetic factors, age, combination with other drugs and pre-existing hearing problems (14, 15). CDDP affects the cell population of the organ of Corti, the spiral ganglion and the stria vascularis, causing morphological alterations and cell death. The treatment with CDDP induces first the death of the hair cells of the basal turn of the cochlea and the neurons connected to them (15-19).

The mechanism of CDDP cytotoxicity, although not fully understood, includes the interaction of the drug with DNA and the formation of DNA adducts (7): these bonds cause inhibition of the nucleic acid production (7) and the arrest of the cell cycle (20-23). Some studies have also shown that CDDP induces mitochondrial dysfunction and production of reactive oxygen species (ROS) in the cochlear cell population (24-29): in the adult inner ear, where the cells are mostly post-mitotic, the CDDP toxicity could be less related to DNA damages, but ROS production could play a major role in the mechanism of ototoxicity (30). The increased ROS production could be caused by a decrease of antioxidant enzymes or by direct ROS activation: CDDP administration has been recently associated to a decrease of activity of superoxide dismutase, catalase, glutathione peroxidase and reductase in the cochlea (16) and to higher levels of superoxide anion (31) and nitric oxide (32). The inhibition of antioxidants and the overproduction of ROS may increase calcium concentration in hair cells and in cochlear neurons, impairing the signal transmission and triggering the apoptotic process (25, 33).

1.3 The apoptotic process

Apoptosis, or programmed cell death, is an ATP-dependent physiological cell process (34), highly conserved (35) and aimed to regulation and maintenance of cell populations and development of the organism (36). Apoptosis is characterized by an ordered sequence of events: in the initial step the cell undergoes a shrinkage due to cytoskeleton degradation, leading to the loss of some membrane properties and to detachment from nearby cells. The next step is the condensation of the chromatin, followed by nuclear envelope discontinuity and chromatin fragmentation by endonucleases. Finally the cell organelles are degraded and the cells undergo a process called blebbing, a division into small apoptotic bodies, engulfed by phagocytosis by nearby macrophages without any inflammatory reaction (37).

The initial phase of the apoptotic process can be regulated by two different signal pathways, called extrinsic (receptor based) and intrinsic (mitochondrial). Both ways can be regulated or reversed, and converge in the late phase of apoptosis by activating the same effector enzymes (37).

The extrinsic apoptotic pathway is activated by the cell membrane death receptors, which transmit intracellular pro-apoptotic signals as a consequence of binding with specific ligands (38). The subsequent steps are mediated by the cytoplasmic part of the activated receptor: a highly conserved sequence called "death domain" recruits and binds the cytoplasmic protein Fas associated to death domain (FADD), forming a complex called "death inducing signalling complex" (DISC). The DISC proceeds by activating the initiator of the apoptotic cascade, pro-caspase 8, that in turn activates the effector caspases (39).

The apoptotic signal can be either amplified or directly activated in the intrinsic apoptotic pathway in mitochondria (40, 41): the link between the extrinsic and intrinsic way is the BH3 interacting-domain death protein (Bid), belonging to the Bcl-2 family: Bid is cleaved by caspase 8 and its truncated form translocates to the mitochondria (42). Together with other mitochondrial proteins, such as BAX, it induces the release of cytochrome *c* and other pro-apoptotic factors in the cytoplasm.

The protein Bid acts by directly activating BAX, that accumulates near the mitochondrial membrane and causes the opening of the mitochondrial voltage-dependent channels, favouring the leakage of cytochrome *c* (43). The expression of Bid and BAX is upregulated by numerous factors, among which p53, an antitumor protein and transcriptional factor overexpressed in response to cellular stress (44).

The activation of the intrinsic pathway of apoptosis involves the protein procaspase 9 (45): once cytochrome *c* is released from mitochondria to cytoplasm, it induces the formation of a pro-apoptotic protein complex, the apoptosome, which directly cleaves the procaspase 9 (46). When caspase 9, the initiator of the apoptotic intrinsic pathway, is activated, it exerts proteolitic activity on the effector caspases (3, 6, 7) (47), leading the cell to the final phase of the apoptosis. Caspase 3 acts in the late apoptotic stage by regulating the activity of deoxyribonucleases (DNases) responsible for DNA degradation, such as poly (ADP-ribose) polymerase (PARP), inducing morphological changes of the nucleus and of the entire cell (48, 49).

Cisplatin (CDDP) induces cytotoxic effects on DNA and causes signal transduction in several molecular pathways, including those of p53 and of the family of mitogen-activated protein kinases (MAPK), which lead the cell to apoptosis (50). An overexpression of p53 has been shown to

activate the apoptotic cascade including Fas/FADD, caspase 8 and caspase 3 (51, 52). The MAPK is a family of numerous protein kinases involved in cell metabolism and proliferation (53, 54); the overexpression of the subfamily of extracellular signal-regulated kinases (ERK) has been associated to the effects of CDDP-induced apoptosis, the release of cytochrome *c* and the activation of caspase 9 and 3 (13) (Fig. 1.5). When the DNA damage induced by CDDP becomes irreversible, a concomitant activation of the intrinsic apoptotic pathway has been observed, with translocation of BAX into the mitochondria and activation of caspase 9 and 3 (13, 55).

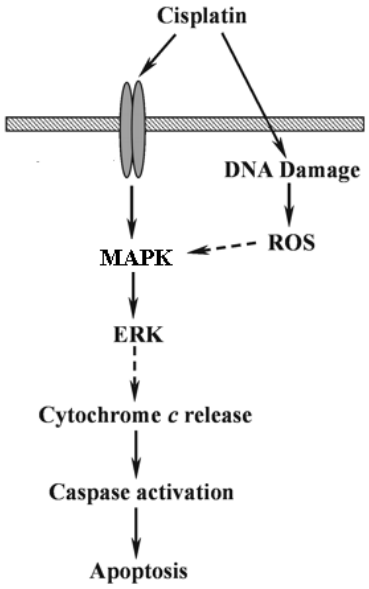

Fig. 1.5. Model of CDDP-induced signaling pathways leading to ERK activation and apoptosis (redrawn from: Wang et al., 2000).

1.4 Treatment of drug-induced ototoxicity

Several compounds have been tested in clinical practice and basic research against drug-induced ototoxicity, in order to reduce or mitigate cellular stress, ROS production and/or DNA damages. Among these compounds there are the coenzyme Q10 and the dexamethasone.

1.4.1 Coenzyme Q10

Coenzyme Q10, also called ubichinone (2, 3-dimethoxy-5-methyl-6-decaprenyl-1,4 benzoquinone, CoQ10), ubiquitous molecule in human and animal body, is a vitamin-like antioxidant (Fig. 1.6) involved in electron transport along the mitochondrial respiratory chain. It reacts with ROS and lipoperoxidases preventing damages to cells and tissues (56-58). As a ROS scavenger, CoQ10 may be used as antiapoptotic agent (59): it works by inhibiting the mitochondrial membrane depolarization, thus the consequent release of cytochrome *c* into cytoplasm and the activation of procaspases 9 and 3 (60). In animal models the antioxidants can be administrated locally or systemically (61): the local administration of antioxidants through the round window *in vivo* increases the glutathione level and reduces the effects of noise induced hearing loss (62). The administration of antioxidants before noise exposure significantly reduces the threshold shift and the death of hair cells (63).

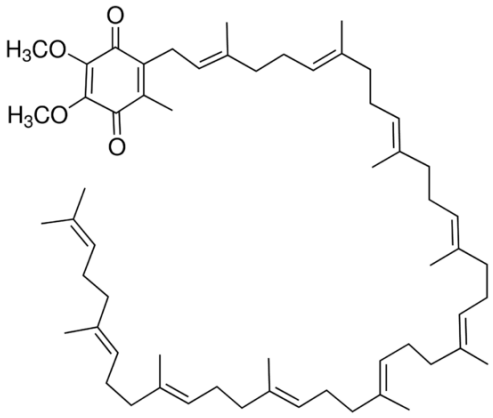

Fig. 1.6. Structure of coenzyme Q10 (2, 3-dimethoxy-5-methyl-6-decaprenyl-1,4 benzoquinone, CoQ10) (retrieved from http://www.sigmaaldrich.com/catalog/product/sigma/c9538?lang=it&region=IT).

1.4.2 Dexamethasone

Dexamethasone is a synthetic drug belonging to the family of the glucocorticoids and used for a wide variety of clinical therapies (Fig. 1.7). In inner ear therapies, steroids are mostly administered via the systemic route, but in this way it is very difficult to reach the therapeutic concentration

within the inner ear because of the inner ear blood barrier (64). Moreover, the systemic use of high steroid doses causes numerous side effects to other organs. Dexamethasone has been administrated with local inner ear applications in cases of autoimmune diseases (65), sudden hearing loss (66) and currently for treatment of Meniere's disease (67). Dexamethasone has been shown to reduce the toxicity caused by administration of aminoglycosides: it has been reported that glucocorticoids may reduce cell stress and inner ear cell death rate *in vivo* on Guinea pigs (68). In the same animal model, other studies verified that dexamethasone was able to reduce CDDP ototoxicity *in vivo* (69), induce overexpression of antioxidant enzymes (26) and reduce the levels of NADPH oxidase 3 (NOX-3) (70). The *in vitro* treatment with dexamethasone affects the expression of MAPK pathway, with increased activation of Jun and p38 protein subfamilies, but not of the ERK subfamily (71).

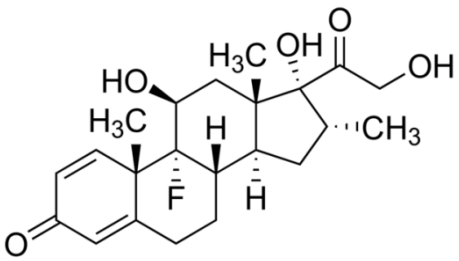

Fig. 1.7. Structure of dexamethasone (retrieved from: https://pubchem.ncbi.nlm.nih.gov/image/fl.html?cid=5743).

1.5 Nanoparticles based systems for inner ear drug delivery

The treatment of inner ear diseases through drug delivery (DD) faces numerous challenges (72) such as the limited blood flow to the inner ear (73), the presence of physical barriers acting as a selective filter for drug transportation from circulatory system to inner ear (74), the small size of the cochlea and its isolated anatomical position. Research in local drug applications and medications has recently attracted interest because it is a better and more effective treatment than the systemic one. Case studies involving antioxidants (56), steroids (75) and gentamicin in treatments for Meniere's disease (76) have been documented, but these approaches have not yet been applied in clinical protocols due to the lack of controlled and targeted delivery systems.

Nanoparticles (NPs) are a possible option to improve existing therapeutic strategies (77). The NPs with size between 10 and 100 nm could be applied in biology and medicine as innovative DD system: this strategy could be more efficient and reduce drug-associated side effects because of the ability of NPs to deliver the therapeutic agent to the target site. Moreover, the controlled release of compounds conjugated to NPs results in a lower dose of drug required to achieve the therapeutic effects (78).

The cochlea is a good model for studying NP-based DD because of its isolated structure and of the perilymph rheology that facilitates the distribution of administered compounds. The intratympanic delivery of NPs could be suitable to treat the induced hearing loss and prevent its progression when hair cells and spiral ganglion neurons are damaged (79).

1.5.1 Ear barriers limiting drug intake

The afflux of molecules and compounds in the inner ear is selectively regulated by a system of physical barriers: the round window membrane (RWM) and the blood inner ear barrier (BB) isolate the cochlea respectively from the middle ear and from the circulatory system (Fig 1.8). The RWM is a three-layer semi-permeable membrane composed of an outer epithelial cell layer, a middle connective layer and an inner connective layer facing the perilymph of the scala tympani (80). In humans, the variable thickness of RWM affects the response of patients to DD treatments. In animal models, the RWM has different thickness according to the species but its composition is similar (81).

The RWM is the main passage for DD from the middle ear cavity to the cochlear perilymph. The passage of molecules across this membrane is influenced by its thickness, morphological integrity, inflammation and weight, but also by concentration, liposolubility and external charge of the therapeutic compound (82). The drugs deposited topically in the middle ear cavity are internalized by pinocytosis and transported to the perilymph through blood vessels or by diffusion. The direct application of drugs in the proximity of RWM is therefore a suitable approach for treatment of inner ear pathologies (83).

The BB is a major barrier in the stria vascularis separating the cochlear tissues from the circulatory system (84, 85). Its main components are the endothelial capillaries whose cells are connected by tight junctions. The role of BB is to maintain the homeostasis of cochlear fluids and protect the

inner ear integrity. The BB acts as a physical and biochemical barrier through an efflux pump, the P-glycoprotein 1 (86), therefore it is considered a rate-limiting barrier in the passage of therapeutic agents from the circulatory system to the inner ear. However, the current knowledge about drug transportation processes through BB is limited (87).

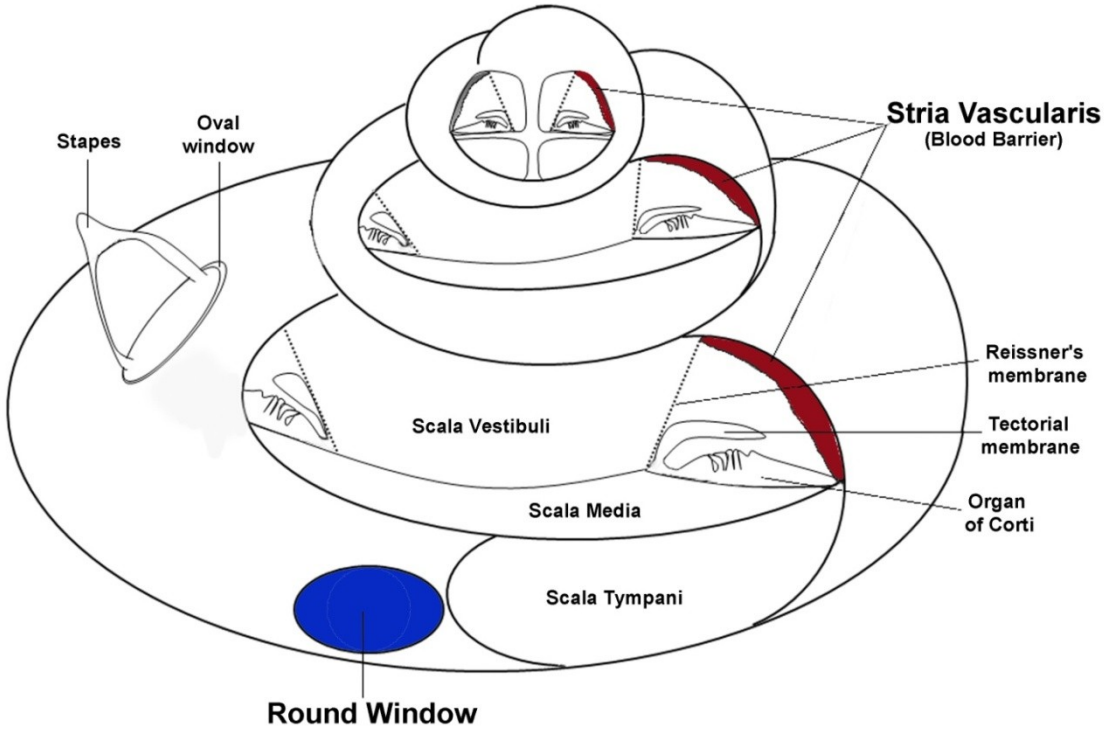

Fig. 1.8. Cochlear barriers. Image of Guinea pig cochlea in longitudinal section near the round window. RW, round window; BB, blood barrier.

1.5.2 Administration routes for drug delivery to the inner ear

To date the clinical protocols for inner ear therapies rely on systemic and local DD routes (Fig. 1.9). The systemic administration represents a classical route for DD, but in the inner ear only few drugs may reach the target site at therapeutic concentrations. High doses of systemic drugs often induce the development of side effects (88, 89). Systemic applications of nanoparticles in the inner ear have been recently investigated: poly(lactic-co-glycolic acid) NPs conjugated with rhodamine B and applied systemically were detected in the liver, but not in the cochlea (90). The limited

bioavailability of NPs after systemic administration could be due to the rapid clearance from the circulation in liver and spleen (91).

Local administration appears more suitable for inner ear DD (19) because it allows a quick distribution of the drug inside the cochlea, improving delivery to the target site; it also requires lower drug doses, avoiding side effects (92). Two main routes are presently used for this purpose, the intratympanic (IT) or the intracochlear administration, but the second one is rarely performed because it is highly invasive and limited to surgery cases (93). On the contrary, the IT injection is minimally invasive and relies on passive diffusion of the active molecules through RWM. This technique does not cause trauma or hearing loss in patients or in the animal model. However, local delivery trials show a high variability in results (94) because of some key factors: 1) the drug clearance within the middle ear through the Eustachian tube; 2) the permeability of RWM; and 3) the residence time of the drug in contact with RWM (95). A method to reduce variability of results and increase the drug concentration in the perilymph could be to better control the residence time of the drug at close range with RWM, using specific delivery systems based on NPs (96).

The NPs used in DD (also called nanocarriers or nanovectors) are artificial compounds with size below 1 μm, which should compensate for adverse drug properties such as low solubility, degradation and short half-life (1). The NPs may also be adapted to target a specific tissue of the inner ear. However, when injected in the middle ear as a liquid suspension, NPs will undergo clearance through the Eustachian tube (97), thus significantly reducing their residence time near RWM. The NPs suitable for DD systems should therefore increase the residence time, together with the ability to cross RWM and biocompatibility.

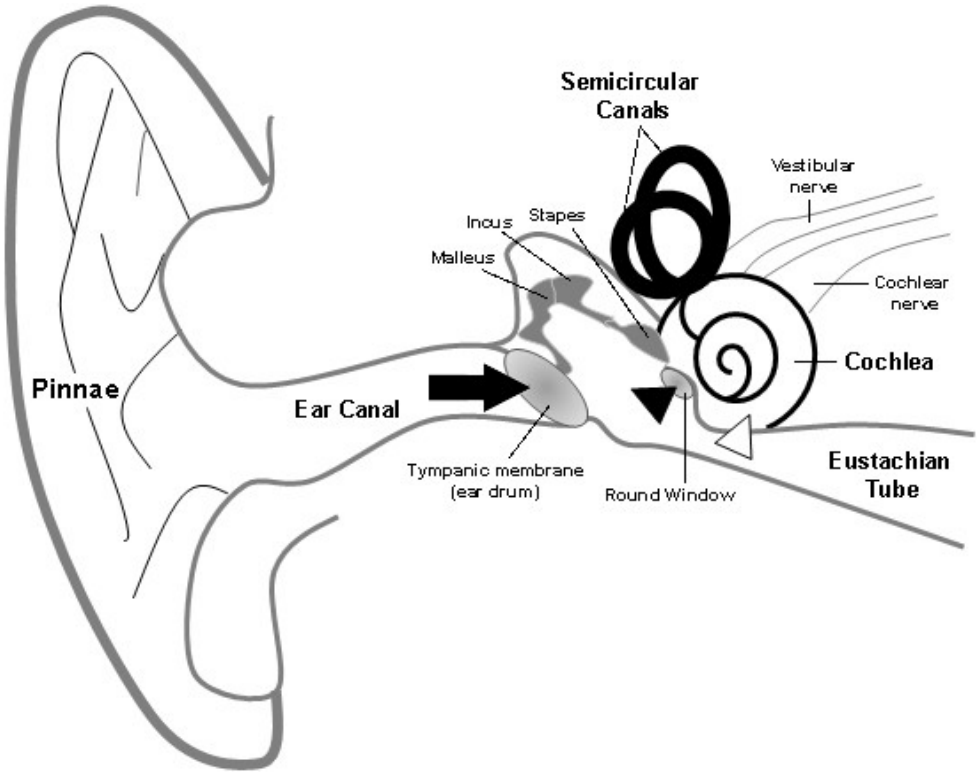

Fig. 1.9. Scheme of nanoparticle administration routes. Arrow, intratympanic route; arrowhead, intracochlear route: black by round window and white by cochleostomy.

1.5.3 Liquid Crystalline NPs

Lyotropic liquid crystalline structures based on polar lipids may be used as carriers and delivery system for different substances, due to their ability to solubilize and encapsulate both hydrophilic and hydrophobic compounds (98). Due to the three-dimensional nanostructures with hydrophilic or hydrophobic domains, liquid crystalline phases have been used for pharmaceutical DD applications: their large exchange surface area provide a complex diffusion pathway for conjugated compounds and their lipid constituents are biocompatible, bioadhesive and digestible (99).

Depending on the surrounding environment and its molecular conditions, the amphiphilic components may self-assemble in different liquid crystalline phases: lamellar, reversed hexagonal or reversed bicontinuous cubic phase (100, 101). The bicontinuous cubic phase is composed by lipid bilayers arranged in periodic tridimensional structures turning into a shape with minimal surface (Fig. 1.10) (102). The interconnections of this structure transform this material into a

viscous gel (also called bulk gel) (103): this arrangement minimizes the molecular stress and free energy waste and produces bicontinuous lipid/water domains (104).

The system may be in equilibrium with an excess of water that, in presence of a suitable surfactant agent, induces fragmentation of the bulk gel into a particulate dispersion of liquid crystalline nanoparticles (LCN) called cubosomes (105).

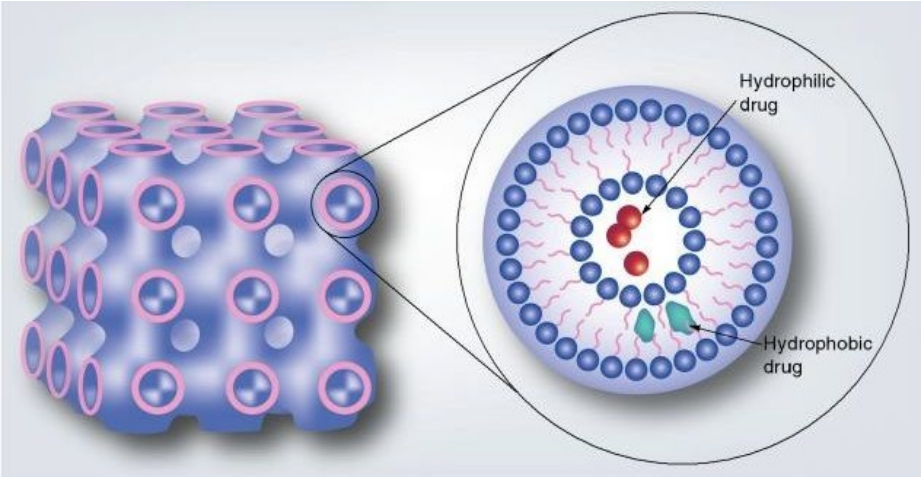

Fig. 1.10. Scheme of cubosomes, showing the internal cubic structure and membrane composition with different drug-loading modalities (redrawn by Bei et al., 2010).

Although several methods have been tested for producing the cubic phase dispersion, no standard process is presently available to develop and control the properties and characteristics of such materials (106). In the past, cubosomes have been produced by combining polar lipids with water and feeding the system with heat energy. The resulting cubic liquid crystalline gel could be dispersed into particles by applying mechanical or ultrasonic energy. The energy input could be replaced by a hydrotrope, defined as a molecule with amphiphilic properties, but unable to display surfactant phase behaviour (i.e. micelle formation) (103). The hydrotrope can simplify the dispersion of liquid crystal particle formation (107): for example, ethanol can be used as a precursor able to spontaneously produce cubosomes when diluted (Fig. 1.11). The addition of the hydrotrope does not induce by itself cubosomes production, but increases the solubility of water-insoluble molecules such as polar lipids (103). The presence of stabilizer agents in solution, such as lecithin, polyethylene glycol or poloxamers, is known to help stabilization of the cubic phase dispersion, located on the surface of the cubosomes while preserving the inner structure of the particles (108,

109). In presence of an excess of water and mechanical stirring, the polar lipids swell and precipitate, forming a coarse dispersion, but preserving the inner cubic structure of the particles. Further reductions in size can be achieved by using ultrasonication or high pressure homogenization (110). The maintenance of the inner cubic structure is an important property for application since the lipid phase structure must maintain its integrity in the diluted media (106).

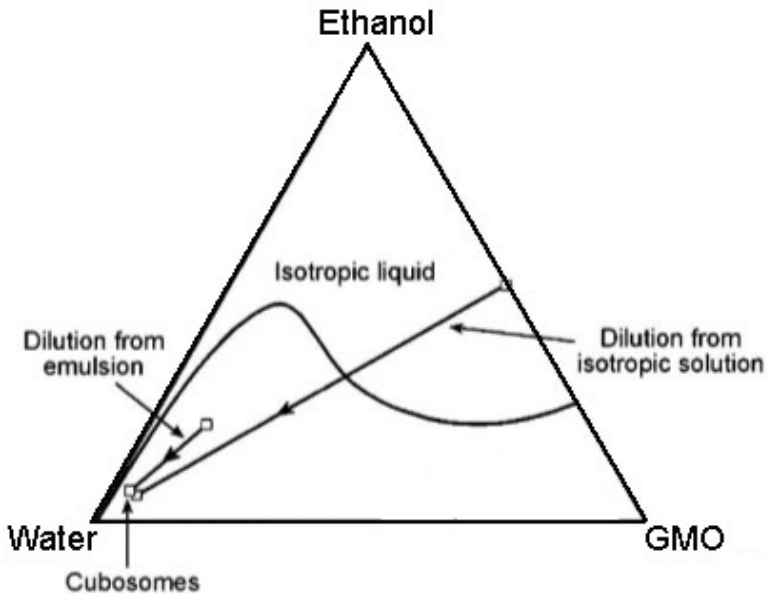

Fig. 1.11. Ternary phase diagram for a glycerol monooleate (GMO)/ethanol/water system, whose lines indicate the water dilution values at which cubosomes are formed from an isotropic solution and an emulsion system (redrawn from: Malmsten, 2006).

1.5.4 Glycerol monooleate

Glycerol monooleate (Glyceryl oleate; (Z)-1-oleoyl-sn-glycerol; 1,2,3-propanetriol, 9-octadecenoic acid; monoolein) (GMO)/water system is one of the best known liquid crystalline systems for DD (111), due to its extensive polymorphism and widespread use in industrial products, e.g. food and cosmetics (Fig. 1.12). The GMO is a biocompatible and biodegradable polar lipid (99), which may swell in water, regardless of its very low water solubility (approximately 10^{-6} mol/l^{-3}). This polar lipid may form a reversed bicontinuous cubic phase that in excess of water is thermodynamically stable (112) and exhibits mechanical stiffness (113). The cubic phase has a tridimensional periodic

conduit structure, composed by a network of surfactant bilayers and water channels, with a surface area of highly specific exchange. The properties of GMO-based cubic phases, among which an easy preparation process, biocompatibility, low cost of raw materials, temperature stability, bicontinuous structure, high internal surface area and solid-like viscosity, make them suitable for high rate production and pharmaceutical applications (103).

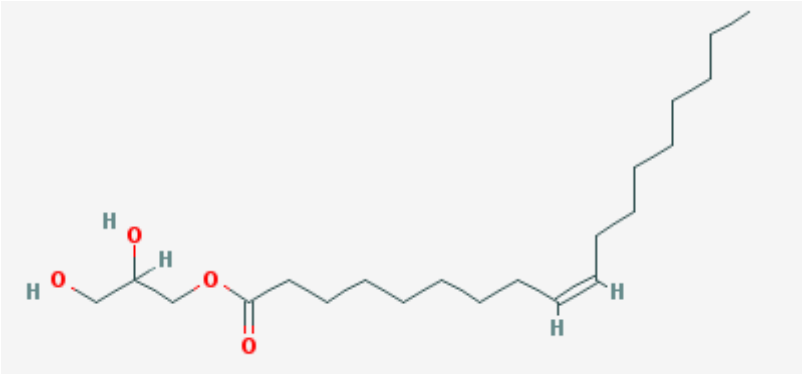

Fig. 1.12. Structure of glycerol monooleate (retrieved from https://pubchem.ncbi.nlm.nih.gov /compound/5283468#section=Top).

1.5.5 Drug delivery with liquid crystalline nanoparticles

Polar peptides, proteins and drugs can be conjugated in a self-assembled lipid structure (liquid crystalline nanoparticle, LCN), becoming less vulnerable to chemical and proteolytic degradation (114, 115). Depending on its polarity and molecular structure in LCN, the conjugated compound will be located either in water or in the lipid domain of the system (116). The LCN structure may also be modified to include different types of drugs and control the kinetics of drug release (117). It has been shown that the addition of lipophilic compounds to GMO-based cubic LCN may induce a shift into a reverse hexagonal phase, while hydrophilic molecules can induce a transition to a lamellar liquid crystalline phase (111, 118). To date, LCN have been studied *in vitro* and *in vivo* on animal models for the delivery of numerous compounds: peptides (98), proteins such as insulin (119), ovalbumin (120), somatostatin (121), cyclosporin A (122), and drugs such as acetyl salicylic acid (aspirin) (123), lidocaine (124), sodium diclofenac (123), theophylline (125), timolol maleate (126) and vitamin E polyethylene glycol succinate (123). The results are encouraging because of sustained release *in vitro* (123-126) and *in vivo* (127) and increase of half-time life of the

conjugated compound (121). The rate of drug release *in vitro* is diffusion dependent (124, 128). The LCN have been tested *in vivo* through several delivery routes, including depot (129) and transdermal injections (130) and mucoadhesive applications(99).

1.5.6 Liquid crystalline nanoparticles in the inner ear

The LCN possessing a lipid core matrix with a surrounding shell of stabilizing agents have been tested in the inner ear. These NPs do not induce toxicological effects *in vivo* in mice after systemic applications (12 mg/kg intravenously for five days) (131) and their cell uptake and cell viability *in vitro* has been verified on fibroblasts by confocal scanner laser microscopy (132). In rat animal model LCN are able to cross the RWM and reach inner ear targets after middle ear application, without affecting hearing capacity (133). Their preferred pathway of diffusion inside cells has been investigated: LCN follow a "nerve pathway", diffusing from the perilymph in the scala tympani to the spiral ganglion and nerve fibres, and later approaching inner and outer hair cells (134). The LCN diffusion variability and ability to cross the RWM depend on their lipid composition, size and external charge. The ability to cross the middle ear barrier has been shown to be size-dependent, because the percentage of particle diffusion is inversely proportional to their size (132). Surface charge may also affect uptake and biodistribution of LCN: after an *in vivo* application nearby RWM of LCN with different external charges, those expressing stronger positive charges were detected in the deeper turns of the cochlea. However, an increasing positive charge has been also related to a higher toxic effect in inner ear tissues (135). The LCN have also been tested as drug carriers, delivering dexamethasone in the inner ear through IT injection and comparing the results with a systemic application. The amount of dexamethasone detected in cochlear fluids after local LCN application is significantly higher compared to the systemic application, also increasing the drug half-life and average residence time in the perilymph by 1.9 folds (136). All these results indicate that LCN are suitable for sustained drug release and targeting of inner ear tissues after local administration.

1.5.7 Other nanoparticle-based drug delivery systems

Several nanoparticle systems based on different materials and with different properties have been studied *in vitro* and *in vivo* with the aim of improving DD to the inner ear. A short description of physical-chemical characteristics of these NPs and their applications is reported below.

Liposomes. They are artificial phospholipid bilayers, similar to those found in the cell membrane, but surrounding an aqueous core. They have a wide size range (between 50 nm and 5 μm) and morphology, depending on phospholipids used and on preparation method (137). Liposomes may encapsulate either hydrophobic molecules in the phospholipid bilayer or hydrophilic molecules in their aqueous core (138). The uptake of these NPs *in vitro* or *in vivo* usually relies on passive diffusion inside the cell, depending on their size (139, 140).

Polymersomes. They are a wide class of amphiphilic copolymers, consisting of a self-assembled membrane of hydrophobic units, surrounding an aqueous core, and of a hydrophilic corona (141). Structurally similar to liposomes, their membrane thickness can be controlled by the molecular weight of the hydrophobic block of copolymers, achieving stronger, thicker and more stable membranes. The hydrophilic corona can be modified to regulate the biodistribution of polymersomes and to induce a specific cellular uptake (142). The hydrophilic drugs can be loaded in the core, while the hydrophobic ones in the membrane (143). Different multifunctional polymersomes have been studied for inner ear DD, including PEG-*b*-PCL (144), PHEA (145) and PLGA (90, 146-148).

Silica NPs. They are modified colloidal silica particles (149) used for *in vitro* transfection of plasmid DNA (150), but also as a DD system. Applied near the RWM, these NPs were later found inside the inner hair cells, the vestibular hair cells, the spiral ganglion neurons and the supporting cells, without causing any hearing impairment (151).

Supermagnetic iron oxide NPs. Magnetic NPs are synthetic Fe_3O_4 (magnetite) particles with a core diameter around 15 nm, that can be widely applied for magnetic targeting of cells(152). Unlike large ferromagnetic materials, the smaller supermagnetic iron oxide NPs (SPION) do not exhibit residual magnetic interactions when the magnetic field is not active, thus are more suitable for biomedical applications (153). The SPION, derivatized to increase biocompatibility and cell interactions, could be guided by an external magnetic field to a specific biological target, but they cannot encapsulate any drug (154). For *in vivo* applications, SPION were coated with organic compounds to prevent particle aggregation and facilitate dispersion (155). In inner ear DD, SPION

have been encapsulated in PLGA (156), silica (154) and dextran (155) and their biocompatibility was tested and verified *in vitro* and *in vivo* (155).

Hyperbranched poly-L-lysine (HBPL). They are highly cationic charged dendrimers widely used for non-viral gene transfer (67, 68). The HBPL were applied *in vivo* in Guinea pig inner ears without any sign of cell toxicity or permanent hearing loss: they were detected in the stria vascularis and hair cells (132).

1.5.8 Key aspects for nanoparticle-based drug delivery in the inner ear

Several parameters should be considered for nanoparticle-based local DD in the inner ear: the RWM permeability, the NPs cochlear targeting, their payload ability and controlled drug release, the biocompatibility and stability in cochlear fluids and tissues. All these aspects have been evaluated *in vitro, ex-vivo* or *in vivo* in animal models, but studies on their therapeutic efficacy are still in progress (1).

The RWM is considered the main access to the inner ear after drug administration in the middle ear (157). The NPs with different composition and size between 10 nm and 640 nm are able to cross RWM. The size and the surface charge are key factors affecting NPs diffusion through RWM. The amount of NPs crossing from middle ear to inner ear is inversely proportional to the size of lipid NPs (139). In the cochlea the positively charged glycerol monooleate NPs achieve a larger distribution than neutral or negatively charged molecules (135). The process responsible for this passage was first described for lipid NPs as a paracellular pathway (134). Recent studies in the rat model suggest that the passage of liposome NPs may occur either by the paracellular pathway, or by endocytotic mechanisms based on clathrin and caveolin (144).

In numerous studies NPs have been loaded or labelled with a fluorescent dye (rhodamine B, carboxycyanine, nile-red) or a contrast agent (gadolinium) for visualization of particles in cochlear cells or fluids by imaging techniques: nevertheless, the presence of NP was detected in inner ear tissues without a quantitative analysis. Liposome NPs have been detected in the cochlea until 6 days post-injection (157) and LCN until 7 days post-injection (134). The NPs surface has been also modified to improve DD target specificity: NPs functionalized by conjugation with nerve growth factor-derived peptides have shown specificity for spiral ganglion neurons and nerve fibres (158).

One of the major concerns in NPs clinical applications is biocompatibility. To date no hearing impairment, loss of hair cells or histological damages have been reported in studies with NPs (132, 133, 159, 160), thus these systems appear reasonably safe. However, SPIONs tend to gather together when the magnetic field is removed, thus they form aggregates within the cell (144). The effects of LNC have been evaluated 20 days post-injection and no toxicity has been detected (157). Topic applications of liposomes in rats do not affect hearing, but a NP concentration-dependent toxicity has been observed *in vitro* in primary cochlear cell cultures (133). In most of these studies, a single intratympanic administration was employed: however, in order to improve liposome efficiency, a continuous NP release has been recently obtained through a high-performance polymide tubing equipped with a micro-pump*;* liposomes loaded with gadolinium-tetra-azacyclo-dodecane-tetra-acetic acid have been visualized both *in vitro* by TEM and *in vivo* by MRI. *In vitro* intact NPs are free to diffuse in the medium, and *in vivo* are detected in the cochlea without adverse effects within six days (157). Again, no long-term effects of exposure to NPs after multiple applications in the inner ear have been detected up to date.

The ability of NPs to carry drugs into the cochlea through the RWM is shown *in vivo* by several studies. Some SPION coated with PGLA and conjugated with dexamethasone enable the release of the drug in inner ear fluids, resulting in a higher concentration of dexamethasone in the perilymph compared to the pure drug diffusion (10% higher after 60 minutes, $p<0.01$) (161). The PLGA loaded with coumarin-6 enhance up to 10.9 times the local bioavailability of the dye in the perilymphin comparison to pure drug solution (147). Liposome loaded with the neurotoxic agent disulfiram induce a significant decrease of the number of spiral ganglion cells after two days from the administration (144). However, drug release by NPs has not yet been examined by long-term studies.

The residence time of the drug within the middle ear cavity may be increased by NPs, but this does not guarantee direct contact between the loaded NP sand the RWM. The NPs also undergo the middle ear clearance through the Eustachian tube (162). A possible solution is to incorporate the NPs into a hydrogel, increasing their residence time in the middle ear and enhancing the drug release in the perilymph (26). The hydrogel applied near the RWM releases the loaded NPs in the perilymph along with its degradation. This approach has been recently reported: a poloxamer 407 hydrogel combined with SPION was successfully applied on *ex vivo* models (in human temporal bones and explanted mouse inner ear cultures) (163); also a nanohydrogel based on chitosan polymer incorporating liposomes was tested *in vitro* and *in vivo* in the mouse model (73). The *in vitro* results show that NPs persisted without significant degradation for at least two weeks and

were released in a controlled and continuous way by the nanohydrogel. The *in vivo* results showed that NPs were successfully released by the nanohydrogel across the RWM and were able to reach the perilymph and the organ of Corti (164).

Although NPs research in local DD for inner ear therapy appears promising, there are still many difficulties to overcome, mostly related to the inner ear anatomy, to the complexity of the cochlea and its highly differentiated cell populations, as well as the possibility to cause hearing loss using microsurgical approaches. The *in vivo* analyses of perilymph samples represent a technical challenge (97), because of the small volume of inner ear fluids in animal models (the total volume of perilymph in a Guinea pig amounts to about 10 µl) (165), and the possible contamination of samples by cerebrospinal fluid (97). The pharmacokinetics of drugs in the inner ear is therefore still unclear and there are no reliable quantitative data about local bioavailability, drug distribution and RWM permeability (1). Recently a computer pharmacokinetic software for inner ear fluids and drug distribution has been developed (166). The software outlines a model based on inner ear anatomy in humans and rodents, including the pharmacokinetic and the solute distribution parameters. This model has been used to simulate the distribution of therapeutic drugs and other compounds in the perilymph (95, 167). However, because of intraspecific variability of inner ear fluid volumes, and of RWM thickness and conditions, it is difficult to compare all current studies using different DD systems and draw quantitative conclusions about drug pharmacokinetics in the inner ear.

1.6 Cell cultures as model for inner ear studies

Numerous studies are involved in analysing the molecular mechanisms and the effects of drugs and new devices on the auditory system, with the aim to develop new therapeutic approaches. The *in vivo* studies nevertheless have to deal with key issues: the scarcity of the inner ear tissue, the variability of the response due to highly differentiated cell populations and the small size of the cochlea (168). To overcome these limits, cell cultures have been set up as *in vitro* models of inner ear cells. Two different cell lines were employed in this study to test toxic and protective effects of various compounds: an Organ of Corti cell line (OC-k3) and a cell line derived from rat pheochromocytoma (PC12).

1.6.1 The OC-k3 cell line

The OC-k3 cells were isolated in 1999 and derive from the inner ear of an immortalized mice. When cultivated in permissive conditions (33 °C and medium culture enriched with interferon-γ) these cells exhibit a fusiform aspect and a highly replicative capacity: they can be replated up to 50 times without losing their characteristics (169). The OC-k3 express an inner ear unique protein, called Organ of Corti Protein 2. This cell line shows specific epithelial characteristics: they are positive for nestin, a marker of epithelial precursors; they express markers typical of the auditory sensory cells (such as myosin VII and acetylcholine α-9 receptor) and of the supporting cells (such as connexin 26), but not the markers of neurons or glia cells. They are therefore considered a good *in vitro* model to study hair cells of the inner ear and have already been used for studies on ototoxicity induced by drugs such as gentamicin and cisplatin (170-173).

1.6.2 The PC12 cell line

The PC12 cells were isolated in 1976 from rat pheochromocytoma, a tumour of the chromaffin cells of the adrenal gland (174). When cultivated in permissive conditions they have a rounded shape and they can be reseed up to 70 times without losing their characteristics. The PC12 cells can differentiate into neural-like cells when treated with 50 ng/ml of nerve growth factor for 7 days: they lose their replicative capacity and start growing typical neural cell processes, known as neurites. The PC12 cells can synthesize neurotransmitters such as norepinephrine and dopamine, possess type N and T calcium channel (175) and may release calcium-dependent exocytotic vesicles (174). For all the above characteristics they are considered a good model for study of neural cells. Only a few studies have been performed on the effects of oxidants (176) and cisplatin (177) on undifferentiated PC12 cells, and others have dealt with the effects of cisplatin on differentiated PC12 (178).

2 Aim of the work

The aim of this thesis is to develop a new nanoparticle-based system conjugated with two hydrophobic drugs, coenzyme Q10 and dexamethasone, and test it *in vitro* on PC12 and OC-k3 cells, used as a model of inner ear cell populations, to evaluate the protective effects against cisplatin cytotoxicity.

Nanoparticles (NPs) represent an innovative approach for inner ear treatments; when applied nearby the round window, NPs are known to be detected in all parts of the cochlea, improving the distribution and the half-life of the conjugated compound. Liquid crystalline NPs based on glycerol monooleate are a promising NPs system that can internalize hydrophobic drugs in their lipid matrix. The aim of this work is to produce NPs highly biocompatible that can be conjugated to improve the delivery of hydrophobic drugs compared to the treatment with the drug alone, achieving better results while reducing the amount of drug used.

Among drugs tested against noise or drug induced ototoxicity there are antioxidants and glucocorticoids. Antioxidants, such as coenzyme Q10, are known to reduce the formation of reactive oxygen species (ROS) in the cochlea when applied as a pre-treatment, but have a very low solubility and bioavailability. Steroid drugs, such as dexamethasone, are currently used for inner ear therapies but, besides their low solubility, their high dosage may induce numerous side effects. Local application of drugs within the inner ear also relies only on passive diffusion, which requires high amounts of drugs. It is therefore necessary to develop a system for a controlled and sustained delivery of drugs within the cochlea.

Cisplatin is a widely used antitumor agent: it is highly cytotoxic and its use leads to numerous side effects, including ototoxicity through the formation of ROS, inflammation and DNA damages to the inner ear tissues. The development of a specific NPs system for local treatment of the inner ear could prevent the occurrence of ototoxicity and hearing loss, without affecting the anticancer effects of cisplatin applied systemically.

The studies performed for this thesis represent a preclinical work on the effects of NPs *in vitro* on PC12 and OC-k3 cell lines and on the protective effects of NPs conjugated with two compounds (coenzyme Q and dexamethasone) against cisplatin cytotoxicity.

3 Materials and methods

3.1 Nanoparticles production and physical-chemical characterization

3.1.1 Reagents

Glycerol monooleate (GMO RYLO MG 19 Pharma) was purchased from from Danisco A/S (Grindsted, Denmark). The composition of the sample according to the manufacturer was minimum 95% monoglycerides, maximum 10% diglycerides and maximum 2% triglycerides. The fatty acid content was minimum 88 % oleoyl (C18:1). The triblock copolymer poly(ethylene oxide)(PEO)-poly(propylene oxide)(PPO)-poly(ethylene oxide)(PEO) (trade name Lutrol F127) was obtained from BASF (Lundwigshafen, Germany) and its approximate formula is PEO101PPO56PEO101 and have an average molecular weight of 12600 g/mol.

Coenzyme Q10 (C9538, powder, purity ≥ 98% for HPLC, formula weight 834.34 g/mol) and dexamethasone (9α-fluoro-16α-methylprednisolone, D1756, powder, purity ≥ 98% for HPLC, molecular weight 392.46) were purchased from Sigma-Aldrich (St Louis, Missouri, U.S.A.).

3.1.2 Preparation of liquid crystalline nanoparticles

Nanoparticles (NPs) were prepared by dilution of an isotropic mixture of 5% wt lipid and 5% wt ethanol in F-127 1% solution. Incorporation of CoQ10 and dexamethasone was performed dissolving the active compounds in the lipid blend. The coarse samples were then homogenized five times for 5 minutes through a microfluidizer (MF) (Microfluidizer M-110s, Microfluidics Corp., Newton, USA) equipped with a Z-type interaction chamber with a minimum passage of 100 μm. The fine liquid crystalline nanoparticle dispersions were heated in a steam sterilization autoclave Laboklav 25 (SHP Steriltechnik AG, Detzel Schloss/Satuelle, Germany) at 121 °C for 20 min. The total time for sterilization and cooling was about 1 hour. Samples were then stored at 4 °C.

3.1.3 Dry content and concentration of active compound

The dry content of the LCNP dispersions was analysed by freeze-drying a pre-weighed sample using a Epsilon 2-4 LSCplus freeze drier (Martin Christ Gefriertrocknungsanlagen GmbH, Osterode am Harz, Germany). The concentrations of active compounds in the LCNPs were assessed by diluting the freeze-dried particles in ethanol followed by analysis by UV spectrometry (Lambda 650, PerkinElmer instruments LLC, Shelton, USA) at 274 nm for CoQ10 and at 278 nm for dexamethasone.

3.1.4 Particle size

The size of the NPs was detected by a Zetasizer Zen3600 measurer (Malvern Instruments Ltd., Worcestershire, U.K.) using disposable cuvettes. The samples were diluted 10 times in purified water prior to analysis in disposable cuvettes, and measured 3 times: each measurement consisted of 12 sub-runs. Refractive indices were set to 1.47 and 1.33, for lipids and water, respectively, and the temperature were kept at 25 °C during measurements. Data presented in this study correspond to the zeta-average particle size.

3.1.5 Zeta potential

The zeta potential of particles with and without drug loaded was determined by measuring the electrophoretic mobility with the Zetasizer Zen3600 (Malvern Instruments). Samples were diluted in purified water or 5 mM acetate buffer (pH 5.5) to a particle concentration of 0.5-2.0 mg/ml, and analysed in disposable measuring cells at 25 °C. Each sample was measured in triplicate.

3.1.6 Cryogenic Transmission Electron Microscopy (CRYO-TEM)

The samples were prepared in a vitrification system with controlled environment, kept at 25 °C and with humidity close to saturation to prevent evaporation from the sample during preparation. A

droplet of each dispersion was placed onto a carbon-coated "holey" polymer film supported by a copper grid, gently blotted with a filter paper to from a thin liquid film (10-500 nm) and plunged into liquid ethane at -180 °C. The sample was then transferred into liquid nitrogen at -196 °C into a Zeiss LIBRA-120 transmission electron microscope (Carl Zeiss, Oberkochen, Germany) operating at 80kV and with a working temperature below –160 °C to prevent formation of ice crystals.

3.2 *In vitro* analyses

3.2.1 Cell cultures

The OC-k3 cells were cultured at 37 °C and 10% CO_2 with complete culture medium DMEM (Dulbecco Modified Eagle's Medium; Gibco BRL, Gaithersburg, Maryland, U.S.A.), 10% FBS (Fetal Bovine Serum; Gibco BRL), L-glutammine 2 mM (Gibco BRL), 50 U/ml Interferon γ (IFN, Genzyme, Cambridge, Massachusetts, U.S.A.), 1% penicillin – streptomycin (Gibco BRL).

The PC12 cells were cultured at 37 °C and 5% of CO_2 with complete culture medium RPMI 1640 (Roswell Park Memorial Institute Medium, Gibco BRL), 10% HS (Horse Serum, Gibco BRL), 5% FBS (Fetal Bovine Serum, Gibco BRL), L-glutammine 2mM (Gibco BRL), 1% penicillin – streptomycin (Gibco BRL).

3.2.2 Treatments and co-treatments

For all the treatments and for the co-treatments including the NPs and the cisplatin (CDDP, 1 mg/ml - Accord Healthcare, Milan, Italy), performed on both PC12 and OC-k3 cell lines several concentrations of the different compounds have been tested (Table 1). For every different condition, all the following test were performed, for the times indicated for each of the methods.

When performing co-treatments analyses, CDDP was added to cells 24 hours after the treatment with NPsD and NPsQ. The culture medium was replaced in order to avoid interferences between CDDP and NPs. The protection rate was detected after 24/48 hours from the CDDP treatment. The control samples were treated only with CDDP, NPsD or NPsQ.

Table 1. Concentrations of nanoparticles (NPs) (µg/ml) and cisplatin (CDDP) (µM) tested on OC-k3 and PC12 cell lines. *= concentrations used in the protection analyses. NPsA: non-conjugated nanoparticles. NPsQ: NPs conjugated with coenzyme Q. NPsD: nanoparticles conjugated with dexamethasone.

Treatment	NP concentrations (µg/ml) tested in OC-k3	NP concentrations (µg/ml) tested in PC12
NPsA	10-25-50-75-100-125-150	10-25-50-75-100-125-150-200
NPsQ	10*-25*-50*-75-100-125-150	10-25*-50*-75*-100*-125-150-200
NPsD	10*-25*-50*-75-100-125-150	10-25-50-75-100-125-150-200
NPs + rodhamine B	25-50	50-100
CDDP	2.5-5*-13*-25-50	2.5-5*-13-25-50

3.2.3 Viability assays

Cell were spread on a 96-wells plate adding 5000 cells in 100 µl of medium per well. After 24 hours, cells were treated with different concentration of NPs or CDDP. Each concentration was tested in threefold and every experiment was repeated three times against suitable controls. Cells were tested by adding 20 µl of a tetrazolium compound [3-(4,5-dimethylthiazol-2-yl)-5-(3-carboxymethoxyphenyl)-2-(4- sulfophenyl)-2H-tetrazolium, inner salt; MTS] (CellTiter 96® AQueous MTS Reagent Powder, Promega, Woods Hollow Road, Madison, Wisconsin, U.S.A.) and an electron coupling reagent (phenazine methosulfate, PMS) (Sigma Aldrich) at rate 20:1. After 3 hours of incubation at 37 °C the plate was read at 492 nm, using a SIRIO plate reader (SEAC s.r.l, Florence, Italy). The absorbance value obtained for each sample, expressed as optical density (OD), was normalized to the mean value of the respective non-treated sample, considered as 100% viability rate.

3.2.4 Cell cycle analyses

For analyses of the cell cycle, about 150000 cells were spread into six-well plates in 2 ml of medium. After treatments, cells were collected into a sterile test tube, centrifuged at 1500 rpm for 5

min and the resulting pellet was washed with PBS 1X while the supernatant was discarded. The pellet was fixed in 70% ethanol, added dropwise while stirring. In these conditions samples could be stored for one month at -20 °C. Before performing flow cytofluorimetry analyses, the samples were centrifuged and washed twice with PBS 1X. The pellet was resuspended in a solution of PBS 1X, RNase 100 µg/ml and PI 50 µg/ml, and left at room temperature for 1 hour. Samples were analysed in a BD FACSCalibur cytofluorimeter (BD Biosciences, San José, California, U.S.A.) to study the cell cycle. The Standard Optical Filter 585/42 nm (FL2) channel was used to discriminate the percentage of cells in each phase of the cell cycle and the values obtained were indicated as an area (FL2-A) in the results.

3.2.5 Morphological analyses

For both OC-k3 and PC12 cell lines, about 150000 cells per well were seeded and spreaded on a glass slide, with pre-addition of collagen layer for PC12 cells. Treated cells were stained with annexin V-fluorescein isothiocyanate (FITC) and propidium iodide (PI) kit (Abcam, Cambridge, U.K.) to evaluate the presence of apoptosis. To evaluate the state of cytoskeleton and nucleus, cells were fixed in Glyo –fixx (Thermo Scientific) for 30 min at room temperature, then permeabilized and stained with phalloidin – tetramethylrhodamine (TRITC) 1 µg/ml (Sigma Aldrich) for 2 hours at room temperature. After being washed in PBS 1X, cells were stained with 4',6-diamidino-2-phenylindole (DAPI) 1 µM (Sigma Aldrich) for 5 min in the dark. The slides were then mounted on a microscope slide with glycerol 20% for observation at the fluorescence microscope. For internalization tests, NPs were administered to cells attached to the slides and then observed at the optical fluorescence microscope after 1-2-4-8-24-48 hours. The optical fluorescence microscope used was a Nikon Eclipse TE2000-U model (Nikon, Milan, Italy) and the images were acquired using the programme Nis-Elements 3.0 Image Analysis System software (Nikon).

3.2.6 Real time quantitative polymerase chain reaction

For Real time quantitative polymerase chain reaction (RTqPCR), total RNA was isolated from cultured OC-k3 and PC12 cells using innuPREP Micro RNA Kit (Life Science, Jena, Germany). Total RNA extracted was processed with DNAase I (RNase-free) M0303S kit (New England

Biolabs, Ipswich, USA). Retrotranscription was performed using Euroscript M-MLV Reverse Transcriptase kit (Euroclone, Milan, Italy): 0.5 µg RNA, 0.5 µg oligo (dT), 0.2 µg random hexamers and H_2O up to 12.5 µl were incubated at 65 °C for 5 min. Afterwards, 4 µl of reaction buffer, 0.5 µl RNase inhibitor (20 units), 2 µl of dNTP (10 mM) and 1 µl Euroscript Reverse Transcriptase (200 units) were added to the solution. The final mix was incubated at 60 min at 42°, then 10 min at 70°. The primers (forward, F, and reverse, R) were designed using the PerlPrimer software 1.1.21 (Sourceforge; http://perlprimer.sourceforge.net/). RTqPCR was performed with Chromo4™ system (BioRad, Milan, Italy) adding 5 µl of SSoFast™ EvaGreen® Supermix, 100 ng cDNA, 1 µl primer forward + primer reverse mix in ratio 1:1 (final concentration 300 nm) and H_2O up to 10 µl, using Opticon Monitor™ 3 software (BioRad). Every reaction ran for 31 amplification cycles for a total time of 80 minutes; the reaction temperature depended on the used primers specification. Every analysed condition was repeated in threefold. RTqPCR data of interest genes are analysed with comparative CT methods using GenEx 6.1 software (bioMCC, http://www.biomcc.com/genex-software.html) taking as reference at least three housekeeping genes. The primer used are listed in Table 2.

Table 2. Primers used for RTqPCR analyses.

Primer	Sequence	Species (F + R)	Annealing temperature (°C)
ACTB forward ACTB reverse	CGTTGACATCCGTAAAGACC TAACAGTCCGCCTAGAAGCA	Mouse	60
Caspase 3 forward Caspase 3 reverse	GTTACTATTCCTGGAGAAATTC GACACAATACACGGGATCTGT	Mouse/rat	60
Caspase 8 forward Caspase 8 reverse	CGGACTTCAGACAAAGTTTACCA ACTCAGAGCCTCTTTATCACAG	Mouse/rat	60
Caspase 9 forward Caspase 9 reverse	GCAGATATGGCATACACCCT GGATGACCACCACAAAGCAG	Mouse/rat	60
BAX forward BAX reverse	CTAGCAAACTGGTGCTCAAGG CTCAGCCCATCTTCTTCCAG	Mouse/rat	60
p53 forward p53 reverse	CTCCTCCCCAGCATCTTATCCG CTGTCCCGTCCCAGAAGGTTC	Mouse	60
Bid forward Bid reverse	ACTTGGTTAGAAACGAGATGGAC GGCGTAAACTCTTCAGATACACTC	Mouse	58.4
β_2 microglobulin forward β_2 microglobulin reverse	CGAGACCGATGTATATGCTTGC GTCCAGATGATTCAGAGCTCCA	Mouse/rat	60
ACTB forward ACTB reverse	CGTTGACATCCGTAAAGACC GATAGAGCCACCAATCCACAC	Rat	60
Caspase 3 forward Caspase 3 reverse	GAACCAGATCAGAAGCTCCT CTTTCCAAGTCCCGTGTG	Rat	57.4
Caspase 8 forward Caspase 8 reverse	CCAAATGAAGAGCAAACCTCG GATACTAGAACCTCATGGATTTGAC	Rat	60
Caspase 9 forward Caspase 9 reverse	TTTCTTAGCAGTCAGGTCGT GCCACCTCAAAGCCATGGT	Rat + Mouse/rat	59
p53 forward p53 reverse	TTTGAGGTTCGTGTTTGTGC TTTTATGGCGGGACGTAGAC	Rat	61
Thrombomodulin forward Thrombomodulin reverse	GCTCTGTACCTCTCCTTTCTC TTCAAGTCCTCCCTACCCTC	Mouse/rat	60

3.2.7 Western blot

A SDS-PAGE gel was used to evaluate the expression of proteins extracted from cells. The total protein concentration was determined using the Pierce™ BCA Protein Assay Kit (Thermo Scientific, Waltham, Massachusetts, U.S.A.). The acrylamide percentage varied from 10 to 20 % depending on the analysed proteins. Gel electrophoresis ran with an intensity between 30 and 80 mA; proteins were then transferred to a 0.2 or 0.45 µm polyvinylidene difluoride (PVDF) blotting membrane (GE Healthcare, Amersham, Buckinghamshire, U.K.) by Semi-dry transfer system (Celbio S.p.a., Milan, Italy). To verify if the transfer is successful blots were stained with Ponceau Red or Pierce® Reversible Protein Stain Kit (Thermo Scientific), while the SDS-PAGE gel was stained with Coomassie blue to detect residual proteins.

Primary antibodies were dissolved in 5 % (w/v) milk in TBST buffer (10 mM Tris-HCl, pH 7.4, 137 mM NaCl, 0.1% (v/v) Tween-20) or in 3 % (w/v) BSA in PBST buffer (PBS 1X, 0.1% (v/v) Tween-20). Each final concentration followed the manufacturer's instructions (Table 3). Blots were exposed to primary antibody for 2 hours at room temperature or overnight at 4 °C. Secondary antibodies were dissolved in 5% milk (w/v) (Table 4). Blots were exposed to secondary antibody for 1 hour at room temperature.

Table 3. Primary antibodies used for Western Blot. All antibodies were obtained from Santa Cruz Biotechnology (Dallas, Texas, U.S.A.).

Antibody	Produced in	Molecular weight	Dilution	Commercial/catalog n°
Caspase 3	Rabbit	32 - 17	1:250	sc-7148
ERK-1	Rabbit	42 - 44	1:500	sc-94
pERK	Mouse	42 - 44	1:500	sc-154
HSP 70	Goat	70	1:500	sc-1060
PARP 1/2	Rabbit	116	1:500	sc-7150
β-actin	Mouse	43	1:500	sc-47778

Table 4. Secondary antibodies used for Western Blot.

Antibody	Species	Dilution	Company and catalog n°
Anti goat IgG	rabbit	1:1000	Santa Cruz Biotechnology sc-2768
Anti rabbit peroxidase IgG	goat	1:1000	Sigma Aldrich A4416
Anti mouse peroxidase IgG	goat	1:1000	Sigma Aldrich A6154

3.2.8 Ultra performance liquid chromatography (UPLC)

The drug loading efficiency in NPs was quantified by separating the NPs from the suspension liquid by centrifugation at 15000g for 30 min through Amicon Ultra-0.5 filter devices (Ultracel-100 K, Merck Millipore Ltd., Cork, Ireland). To analyze the release of dexamethasone from NPsD in OC-k3, cells were spread as a monolayer on a Petri dish and treated with NPsD 50 µg/ml for 4, 24 and 48 hours. After each exposure time, the cell medium was collected while cells were harvested and treated with lysis buffer (NaCl 300 mM, EDTA 5 mM, Triton X-100 0.5%, H_2O), centrifuged at 15000g for 20 min. Finally, the supernatant and the cell pellet (dispersed in H_2O) were collected separately. Cell medium, lysate and pellet samples were prepared for UPLC analysis diluting 100 µl each sample with 100 µl dichloromethane (DCM), then centrifuging at 14000g for 4 min at 4 °C and collecting 100 µl of the separate phase on the bottom of the vial. The drug concentration in the filtrate was quantified using an UPLC system (Waters Corp., Milford, Massachusetts, USA) with an ultraviolet (UV). The system was equipped with a C18 column (1.7 µm, 2.1 mm X 150 mm; Model Acquity BEH300, Waters Corp.) operating at 40 °C. The mobile phase was acetonitrile/water 1:9 plus 0.03% of trifluroacetic acid (phase A) and acetonitrile/water 1:9 plus 0.03% of trifluroacetic acid (è uguale??) (Phase B) at a flow rate of 500 µl/min. A gradient was used where the mobile phase composition was changed from 100% phase A to 39% (phase B) over a period of 3.4 min. The injection volume is 10 µl and the absorbance was measured at 292 nm (dexamethasone). The concentration of the drug in the filtrate was determined using a calibration curve and a correction factor compensating for adsorption to the filter. The amount of drug conjugated to the NPs could then be calculated as ng/ml.

3.2.9 Statistical analyses

Data were analysed by the program GraphPad Prism 7 (GraphPad Software, Inc., La Jolla, California, U.S.A.) to perform t-test and one-way ANOVA tests to identify significant results.

4 Results

Nanoparticles (NPs) were characterized in this study according to their physical chemical properties and their interactions with cells. In detail, the effects of treatment with NPs were studied in two cell lines used as model for inner ear tissues, examining the toxicity, the cell uptake, the cell morphological variations, the activation of molecular pathways and the expression of genes related to cell stress. All analyses were also performed on NPs conjugated with anti-inflammatory and antioxidant compounds, with the aim to develop ways of prevention of cisplatin ototoxicity.

4.1 Physical chemical characterization of NPs

The NPs produced as previously described in the Materials and Methods section were analysed for their physical chemical properties and stability in time; moreover, their morphology was examined by cryogenic transmission electron microscopy (CRYO-TEM). For each NPs batch produced, viability tests were performed *in vitro* on two cell lines, the rat pheochromocytoma PC12 line and the organ of Corti OC-k3 line, in order to evaluate the effects of NPs on inner ear cell models.

Four types of NPs were produced for this study: a control NP without any conjugated drug called NPsA; a NP conjugated with coenzyme Q10 (2,3-dimethoxy-5-methyl-6-decaprenyl-1,4 benzoquinone, CoQ10) called NPsQ; a NP conjugated with dexamethasone called NPsD; a NP conjugated with the fluorescent dye rhodamine B. The NPs size ranged from 150 and 250 nm (Table 5) and were highly homogeneous, with a low polydispersity index (PDI). All NPs have a slightly negative surface charge (Table 5), due to the properties of the lipid used for particle synthesis, the glycerol monoleate (GMO). A slight surface charge is required for nanomaterial cohesion and guarantees its stability over time, preventing autoaggregation of NPs.

The physical chemical parameters of all NPs, that is size in nm, PDI, electrokinetic potential in colloidal dispersions (Z potential, mV), active concentration expressed as percentage of total dry weight over percentage of total weight in formulation, are indicated in Table 5. The differences among the physical chemical parameters are probably due to the conjugation of NPs with the drug, involving steric bulks and variations of the surface charge. The stability of physical chemical NPs stored a 4°C (except NPs plus rhodamine B) was verified at day 0. day 30 and day 60 after

preparation: the data are shown respectively in Table 6 and Table 7. No significant variations were detected in physical chemical parameters up to 60 days after preparation.

Table 5. Physical chemical parameters of the nanoparticles studied. Active concentration is expressed as percentage of total dry weight over percentage pf total weight in formulation. SD, standard deviation.

Nanoparticle	Size (nm ± SD)	PDI	Z potential (mV)
NPsA	190.7 ± 1.1	0.026	-21.4
NPs + rhodamine B	250.1 ± 1.1	0.150	-15.0

Table 6. Variations of size and polydispersity index (PDI) of NPs stored at 4°C, measured at different time intervals.

Nanoparticle	Day 0		Day 30		Day 60	
	Size (nm ± SD),	PDI	Size (nm ± 0.1),	PDI	Size (nm ± 0.1),	PDI
NPsA	212 ± 1.1	0.026	211 ± 0.9	0.050	246 ± 1.4	0.064
NPsQ	177 ± 1.2	0.179	142 ± 1.3	0.173	158 ± 0.9	0.14
NPsD	262 ± 1.9	0.036	227 ± 1.2	0.042	226 ± 1.4	0.026

Table 7.Variations of the surface charge of NPs, stored at 4 °C, measured as electrokinetic potential in colloidal dispersions (Z potential) at the same time intervals as in Table 6.

Nanoparticle	Day 0	Day 30	Day 60
NPsA	-21.4	-14.7	-18.8
NPsQ	-22.9	-26.9	-22.5
NPsD	-20.4	-17.3	-20.5

The physical chemical analyses by cryogenic transmission electron microscopy (CRYO-TEM) allowed to visualize the structure of NPs produced and to evaluate in detail their size and variations.

The NPsA showed a cubic structure ("cubosome") and size about 200 nm, but several lamellar structures were interspersed among the cubic particles (Fig. 4.1A, B).

The NPsQ and NPsD analysed by CRYO-TEM exhibited a different morphology: they had a rather roundish (Fig. 4.2A, B) or hexagonal ("hexosome") (Fig. 4.3A, B). The conjugation of NPs with the drug induced therefore a change in the morphology of NPs.

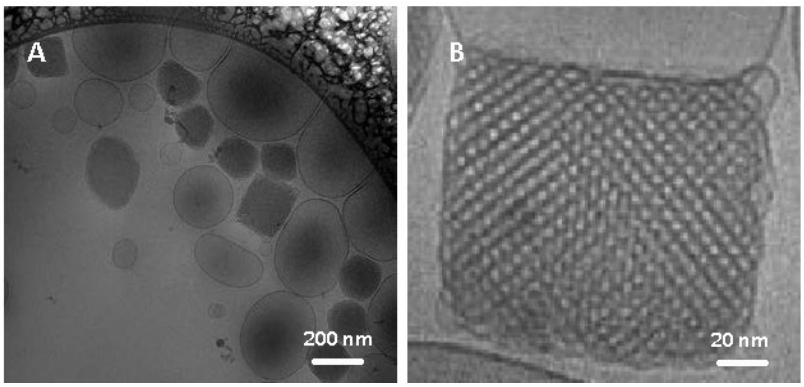

Fig. 4.1. Structure of NPsA by CRYO-TEM. A. Image at low magnification. B. Detail of a NPsA. Scale bars as indicated.

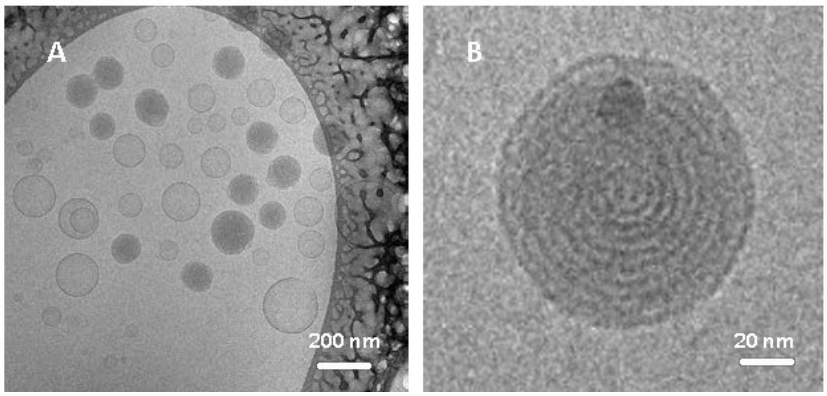

Fig. 4.2. Structure of NPsQ by CRYO-TEM. A. Image at low magnification. B. Detail of a NPsQ. Scale bars as indicated.

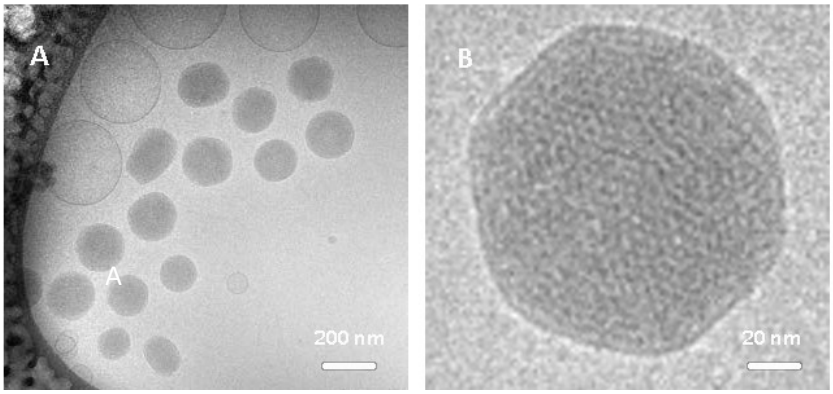

Fig. 4.3.. Structure of NPsD by CRYO-TEM. A. Image at low magnification. B. Detail of a NPsD. Scale bars as indicated.

4.2 Characterization of NPs in vitro

The *in vitro* toxicity of NPs was evaluated on cell lines by a tetrazolium reduction assay (MTS), as described in the Materials and Methods section. This test allows to identify the best dosage of NPs with no toxic effects for morphological and molecular experiments, and allows also to verify the reproducibility of results and the standardization of NPs preparation processes.

4.2.1 Characterization of NPsA

For PC12 cell line, the percentage of viability significantly increased when the cells were treated with NPsA up to 100 µg/ml for 24 hours and up to 150 µg/ml for 48 hours (Fig. 4.4). At 24 hours, the difference in comparison to untreated controls (0 µg/ml NPsA, 100% viability) was significant from 75 µg/ml ($p<0.05$) to 100 µg/ml ($p<0.001$). At 48 hours, the difference in comparison to untreated controls was significant from 25 µg/ml ($p<0.05$) to 125 µg/ml ($p<0.001$). Viability was different between the two exposure times after 24 hours of treatment compared to the 48 hours at NPsA concentration 175 µg/ml ($p<0.05$), while it was higher after 48 hours of treatment compared to the 24 hours values at NPsA concentrations 75 µg/ml and 125 µg/ml ($p<0.05$). From 100 µg/ml on, the cell viability decreased and a slight toxicity was detected. The effect of NPsA on PC12 may therefore be described as dose and time dependent. Based on the above data, the concentration range chosen for all analyses conducted on NPsA was 50 - 100 µg/ml.

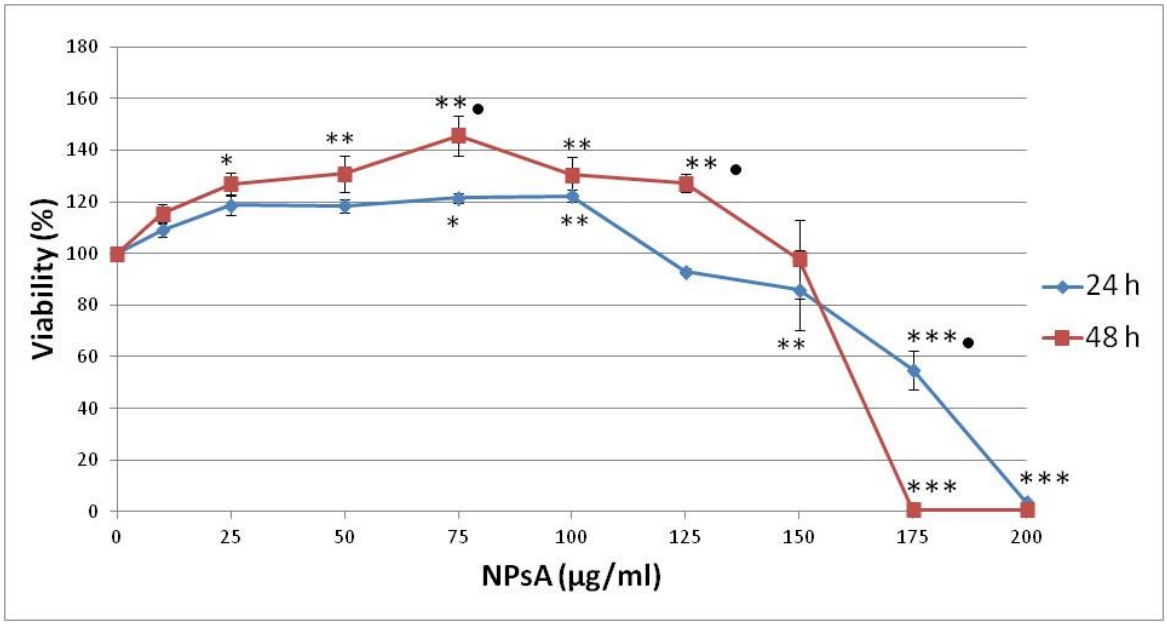

Fig. 4.4. *In vitro* toxicity of NPsA on PC12 cells, expressed as percentage of cell viability vs. NPsA concentration. Bars represent the standard errors. Asterisks indicate significant differences in comparison to untreated controls and dots represent significant differences between exposure times. * = $p<0.05$; ** = $p<0.01$; ***= $p<0.001$; • = $p< 0.05$.

In order to verify whether the variations in cell viability could be associated to alterations of the cell cycle, PC12 cells treated with NPsA up to 100 µg/ml were analysed by flow cytofluorimetry after 24 and 48 hours of treatment. The results did not show any significant variation of cell distribution in the cell cycle phases in comparison to controls (Fig. 5A, B). No increase in hypodiploid cell population (thus with fragmented nuclear DNA because of the onset of apoptosis) was detected at the concentrations tested. No significant differences were also observed between the two exposure times (Fig. 5C, D).

The absence of cell cycle alterations after treatment with NPsA, together with the results of cell viability tests (Fig. 4.4), suggests that concentrations of NPsA up to 100 µg/ml do not cause significant damage to cells, because they maintain a normal ability to reproduce and show a higher viability after 48 hours of treatment in comparison to 24 hours.

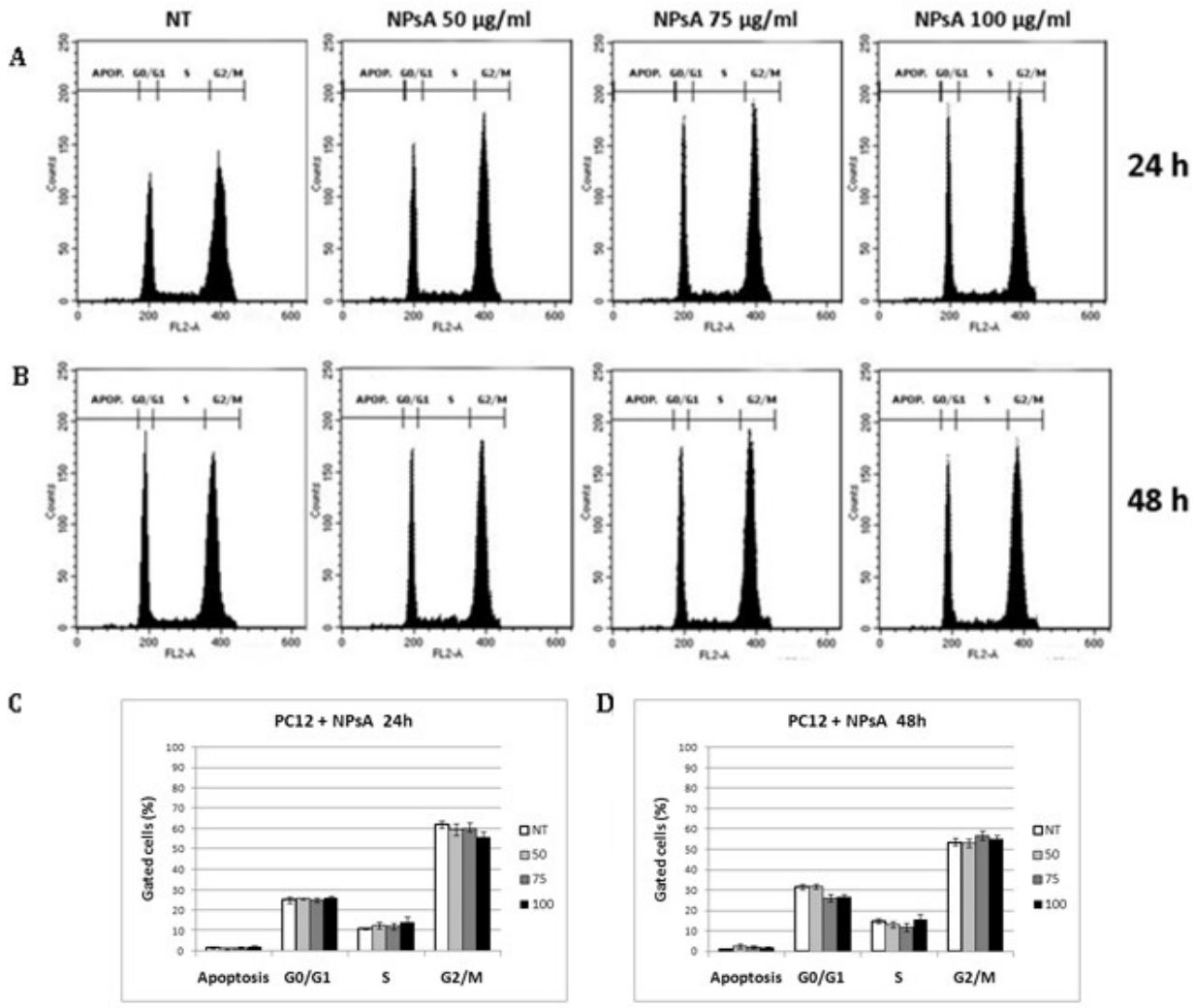

Fig. 4.5. Analyses by flow cytometry of PC12 cells treated with NPsA at 50, 75 and 100 µg/ml for 24 and 48 hours. A, B. Number of cells (expressed as counts) in each phase of the cell cycle. For each experimental condition, about 20000 events were analysed. NT, untreated control. APOP, apoptosis. C, D. Distribution of cells expressed as percentage of gated cells± standard error in each cell cycle phase.

The next analysis conducted on PC12 treated with NPsA was the morphological one. When cells were observed by phase contrast optical microscopy, small vesicles could be detected inside the cells in the perinuclear region (Fig. 4.6A). At increasing concentrations of NPsA, the number of vesicles increased. At very high concentrations (200 µg/ml, thus toxic according to the cell viability tests) large vesicles were visible inside the cells, which appeared swollen and deformed. This dose dependent effect is apparently due to the uptake of NPsA inside the cell (although it is unclear

whether these vesicles actually contain the internalized NPs) and to the consequent increased osmotic stress.

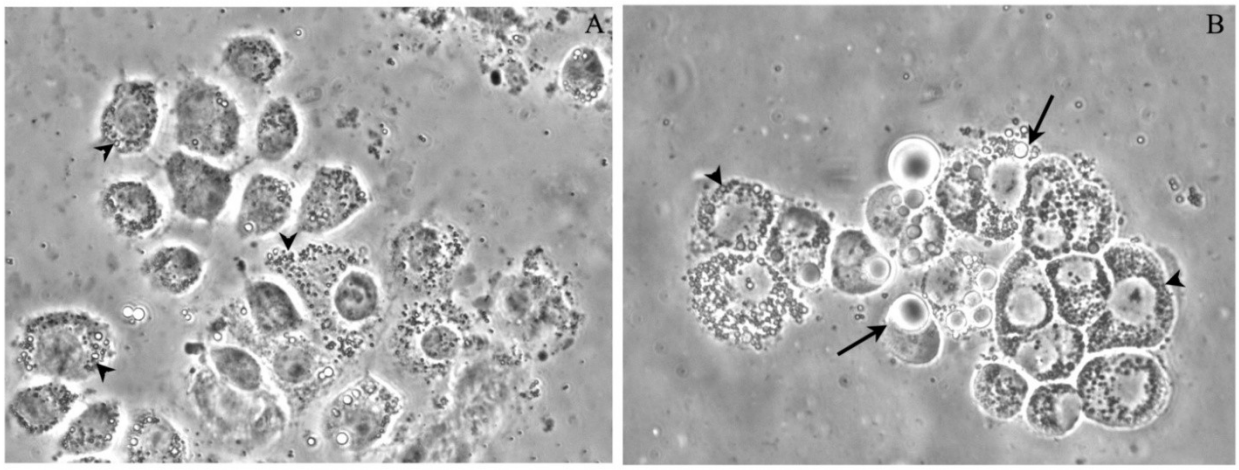

Fig.4.6. Phase contrast images of PC12 cells treated with NPsA. Magnification 40x. A. 75µg/ml: arrow heads indicate small perinuclear vesicles. B. 200µg/ml: arrows indicate large vesicles.

To verify the uptake of NPs within the cell, analyses by fluorescence microscopy were therefore performed by treating PC12 cells with concentrations of 50 µg/ml and 100 µg/ml of NPs conjugated with the fluorescent dye rhodamine B (9- (2- carboxyphenyl)- 6- diethylamino- 3-xanthenylidene]- diethylammonium chloride). The cells were monitored up to 48 hours (Fig. 4.7).

In the first four hours of treatment no signal was detected, but from 8 hours on an intense fluorescent signal was detected inside the cells, showing that NPs were internalized. The signals inside the cells remained dot-shaped and localized in the perinuclear region. A detailed comparison with the phase contrast images showed that the signal was not restricted to the vesicles observed in the previous stage. Although a quantitative analysis was not performed, the signals resulted intense and stable at 24 hours of treatment, indicating that most NPs were internalized within that time interval. At 48 hours the signals clearly decreased.

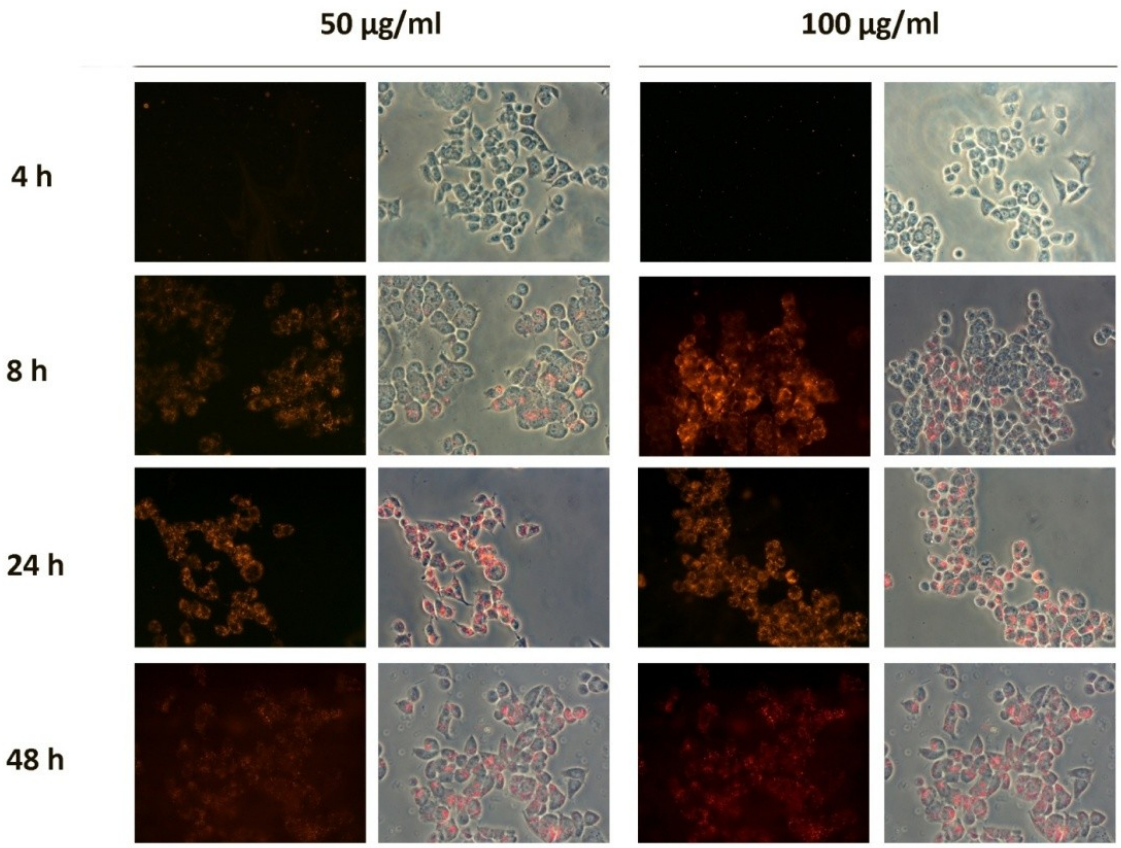

Fig. 4.7. Fluorescent microscope images and colour-combined (phase contrast plus fluorescence) images of PC12 cells treated with 50 and 100 µg/ml NPs conjugated with rhodamine B up to 48 hours. Magnification 40x.

The morphological observations of treated cells was integrated by analyses with fluorescent cell markers: annexin V conjugated to the green dye fluorescein isothiocyanate (annexin V-FITC) and propidium iodide (PI), respectively markers of the initial and late apoptotic phases; 4',6-diamidino-2-phenylindole (DAPI) and phalloidin-tetramethyl rhodamine B isothiocyanate (phalloidin-TRITC), respectively markers of cell nuclei and cytoskeleton.

When PC12 cells were treated with NPsA up to100 µg/ml, and marked with annexin V-FITC and PI, no double green-red fluorescent signal was observed, therefore no apoptosis occurred in these cells (Fig. 4.8). The staining by DAPI did not show any variation in nuclei (Fig. 4.9, blue stain) and no alterations were detected in the cytoskeleton marked by phalloidin-TRITC (Fig. 4.9, red stain). Although the cytoskeleton was not completely visible because of the roundish and flattened shape of PC12 cells, the conservation of their shape after treatment with NPsA represented a good indicator of the cytoskeleton normal condition.

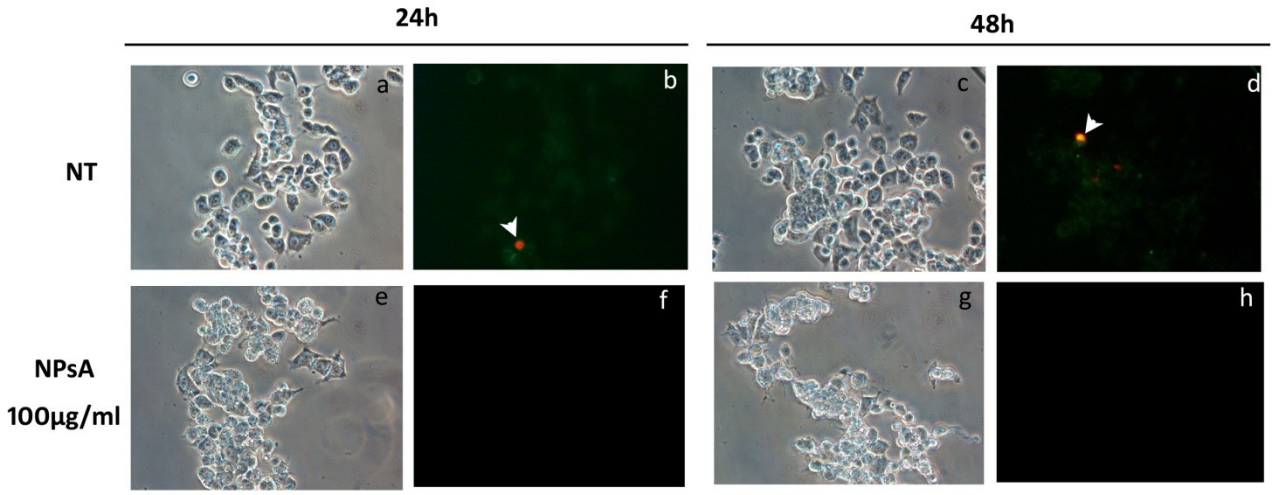

Fig.4.8. Morphological investigations with the fluorescent markers annexin V-FITC (green) and propidium iodide (PI) (red) on PC12 cells treated with NPsA 100 µg/ml at 24 and 48 hours. Images a, c, e, g are phase contrast. NT, untreated control. White arrows indicate cells in apoptosis or necrosis. Magnification 40x.

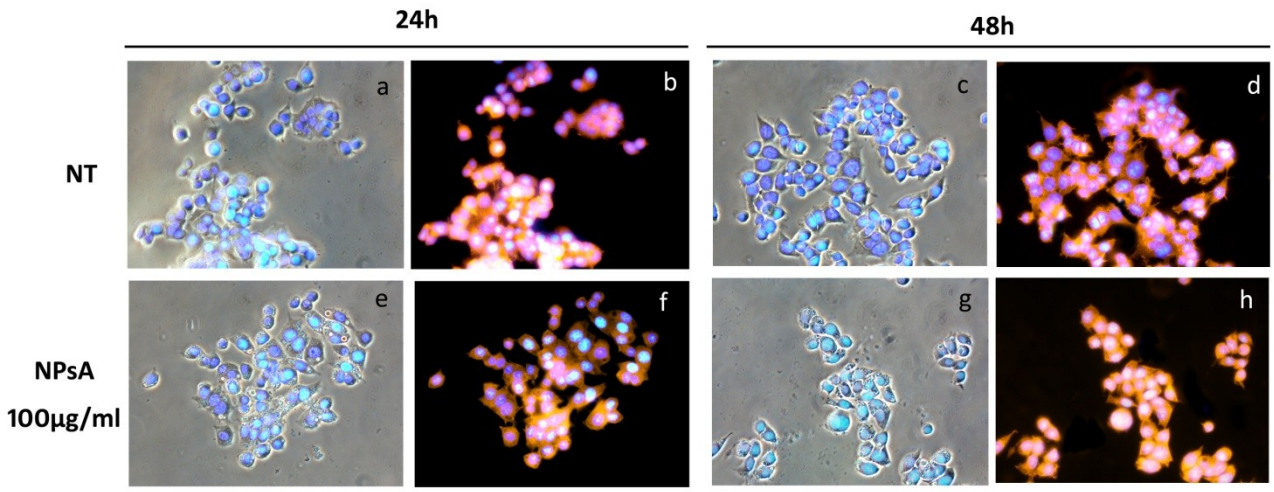

Fig. 4.9. Morphological investigations with 4',6- diamidino- 2-phenylindole (DAPI) (blue) and phalloidin-tetramethyl rhodamine B isothiocyanate (phalloidin-TRITC) (red) on PC12 cells treated with NPsA 100 µg/ml at 24 and 48 hours. Images a, c, e, g are colour-combined DAPI-phase contrast. NT, untreated control. Magnification 40x.

The analysis of gene expression profiles by real time quantitative PCR (RTqPCR) concerned some genes related to the apoptotic process, with the aim to connect all results and identify the signal pathways activated in the cell after NPs treatments. Both pathways of apoptosis, the extrinsic and the intrinsic one, were examined. The results of gene expression profiles showed that the exposure

of PC12 cells to NPsA induced a general stress condition, because a dose dependent increase in expression of genes related to both extrinsic and intrinsic pathways of apoptosiswas was observed (Fig. 4.10). The intrinsic pathway initiated by caspase 9 appeared the most activated, however an increase in expression of caspase 8 was observed; the overexpression of tardive apoptotic markers, such as caspase 3, or other markers playing a key role in cell regulation, such as p53, generally indicate a stress condition in the cell.

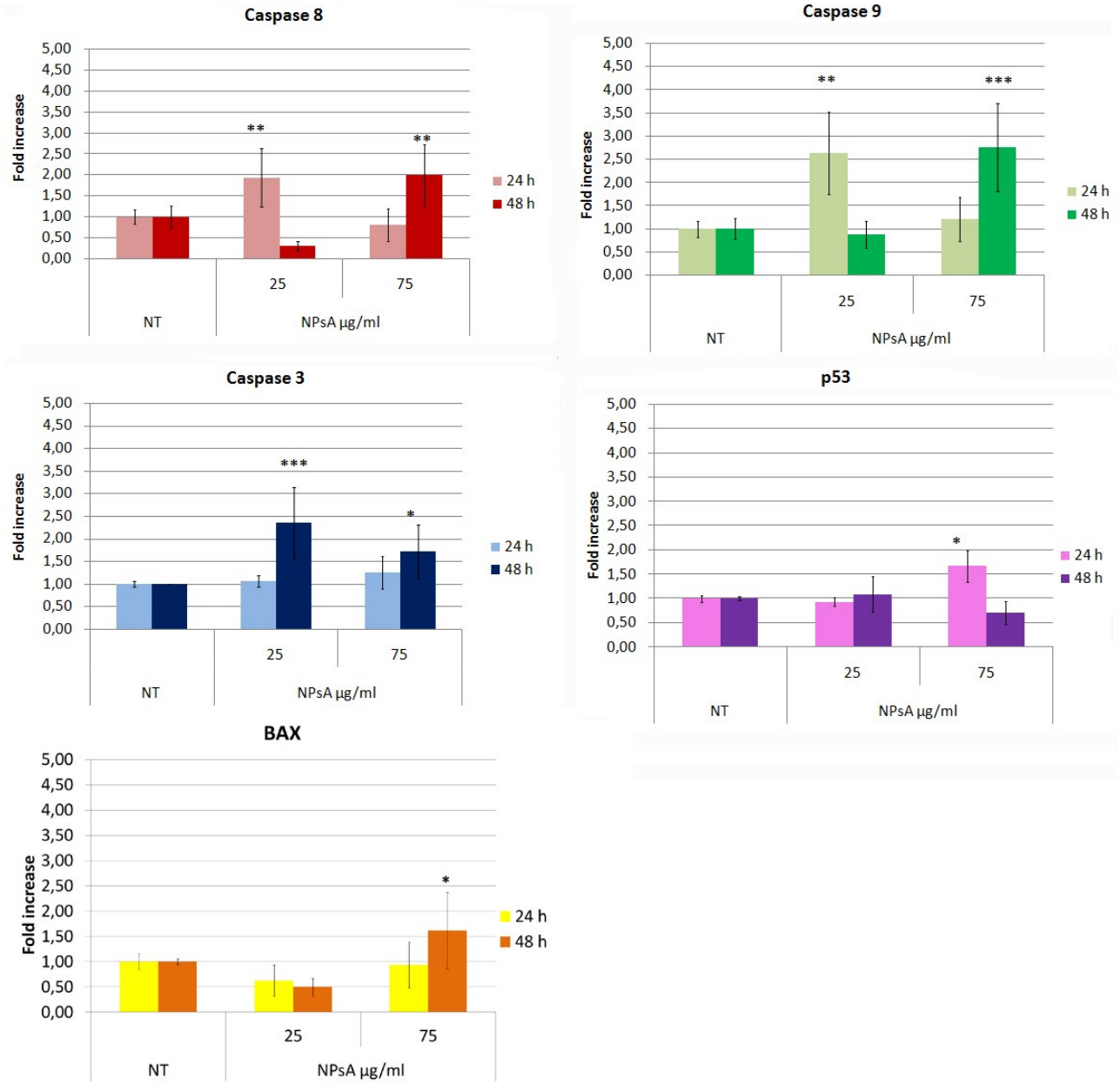

Fig. 4.10. Analyses of relative gene expression by RTqPCR on PC12 cells treated with NPsA, expressed as normalized fluorescence intensity with standard errors as bars. Asterisks indicate significant values in comparison to control (NT). * = $p<0.05$; **= $p<0.01$; ***=$p<0.001$).

The analyses of activated biochemical patterns by Western Blot allowed to quantitatively measure the expression of some key proteins related to cell stress and involved in the apoptosis process, such as phosphorylated extracellular signal regulated kinase (pERK), cleaved caspase 3 and cleaved poly ADP ribosome phosphorylase (PARP). The comparison of expression profiles of these proteins at the different NPsA concentrations yielded information about biochemical and molecular responses of PC12 cells. When PC12 cells were treated by NPsA, no significant dose dependent variation in comparison to control was detected in pERK at 24 hours, but the amount of this protein significantly decreased at 48 hours, remaining lower than at 24 hours (Fig. 4.11). The levels of caspase 3 and cleaved PARP did not significantly changed at the concentrations tested, supporting the hypothesis that cells were not initiating apoptosis. According to the results of protein markers in Fig. 4.11, the cell response appears only time dependent.

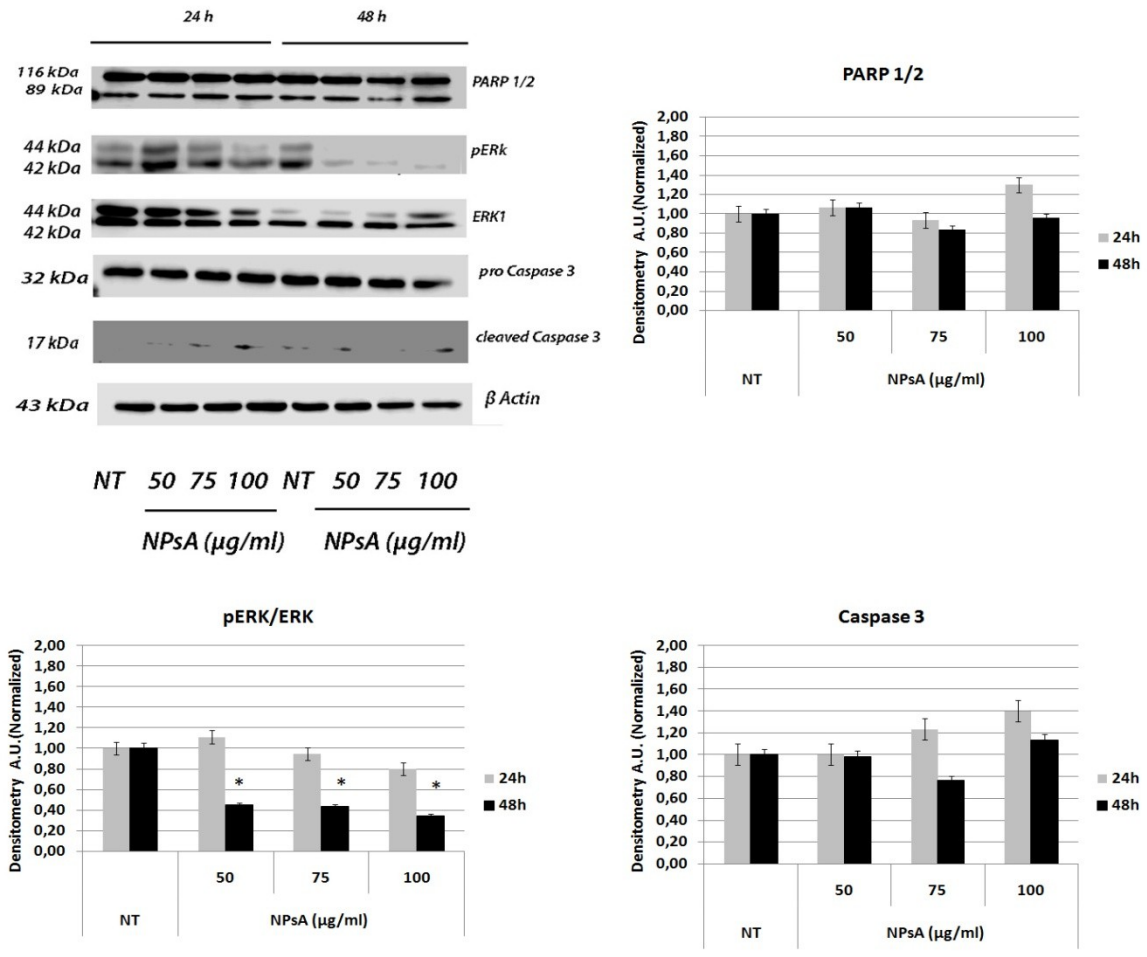

Fig. 4.11. Western Blot after SDS-PAGE and densitometric analysis of key proteins related to apoptosis (with β-actin as standard marker) in PC12 cells treated with NPsA (50, 75 and 100 µg/ml) for 24 and 48 hours. Bars represent standard errors. Asterisks indicate significant values in comparison to control (NT). * = $p<0.05$

The same series of analyses perfomed on PC12 cells to characterize the effects of NPsA was repeated on OC-k3 cells, in the same experimental conditions. These data allowed to evaluate the differences in NPs tolerance of two cell lines representative of inner ear cell populations.

The viability tests by MTS on OC-k3 cells (Fig. 4.12) revealed that NPsA induced a toxicity dose dependent, but not time dependent. The concentration limit after which there was a significant decrease of cell viability was 50 µg/ml ($p<0.001$), both at 24 and 48 hours of treatment. Concentrations above 100 µg/ml caused a cell mortality higher than 80%.

These results are very different from those obtained in PC12 cells: the effects of NPsA may therefore depend on the type of cell line used. It was therefore decided to employ for the other tests on OC-k3 a narrower concentration range of NPsA, 10-50 µg/ml.

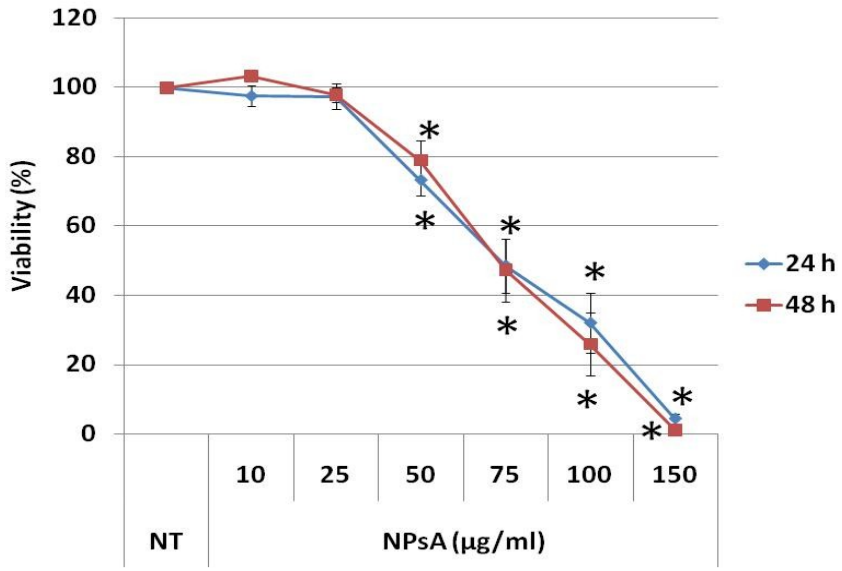

Fig. 4.12. *In vitro* toxicity of NPsA on OC-k3 cells, expressed as percentage of cell viability vs. NPsA concentration. Bars represent the standard errors. Asterisks indicate significant differences in comparison to untreated controls (NT) (* = $p<0.001$).

The cell viability data were compared to those obtained by flow cytometry in OC-k3 cells exposed to NPsA for 24 and 48 hours, at a concentration range not causing any significant cell toxicity. Generally, the treatment with NPsA did not cause a significant variation of the cell population in each phase of the cell cycle (Fig. 4.13). Even at the limit concentration of 50 µg/ml no significant increase of the hypodiploid cell number was observed. However, there was a trend in reduction of cell population in S and G2/M and an increase in G0/G1, more evident at 48 hours of treatment.

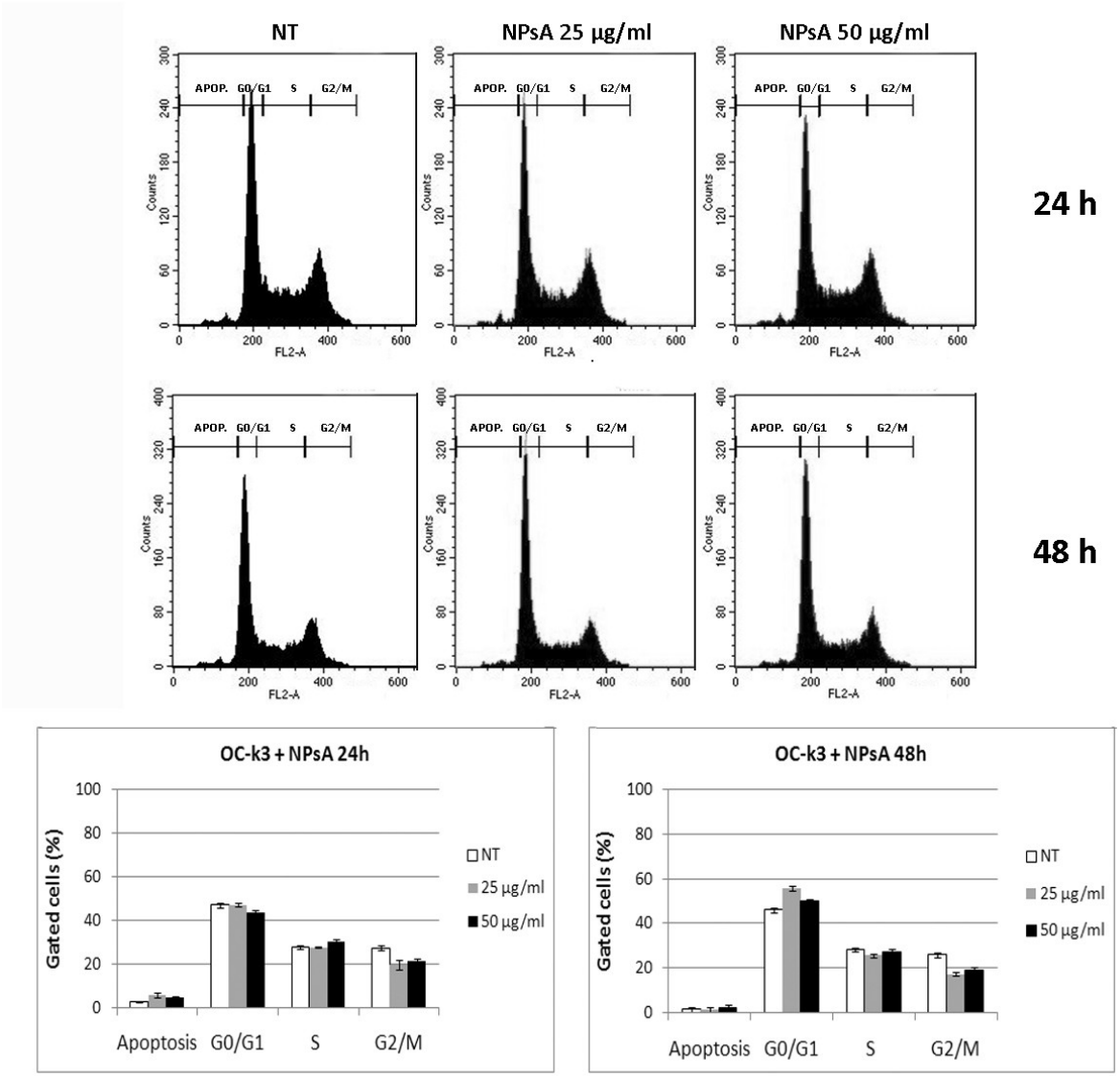

Fig. 4.13. Analyses by flow cytometry of OC-k3 cells treated with NPsA at 25 and 50 µg/ml for 24 and 48 hours. A, B. Number of cells (expressed as counts) in each phase of the cell cycle. For each experimental condition, about 20000 events were analysed. NT, untreated control. APOP, apoptosis. C, D. Distribution of cells expressed as percentage of gated cells ± standard error in each cell cycle phase.

As for PC12 cells, the morphological analyses by phase contrast optical microscopy on OC-k3 cells treated with NPsA showed the presence of intracellular vesicles in the perinuclear region: their number and size increased with increasing concentrations of NPsA (Fig. 4.14). As previously observed for PC12 cells, this dose dependent effect was related to uptake of NPsA inside the cell, thus probably related to a response to the osmotic stress caused by NPs treatment; however, the type

and role of these vesicles is still unclear. At the NPsA concentrations tested, the size and shape of OC-k3 cells was not altered.

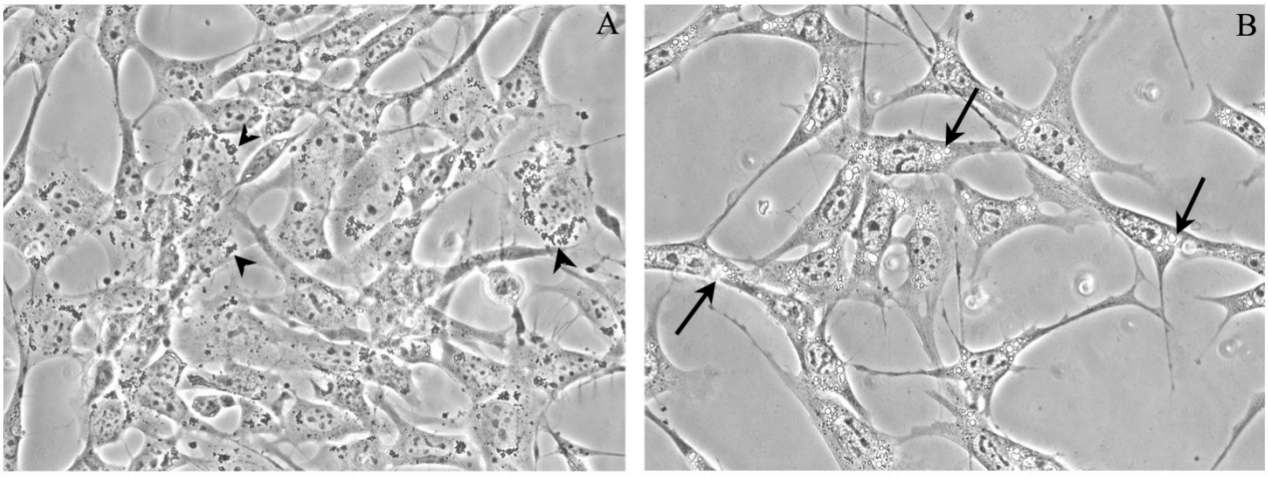

Fig. 4.14. Phase contrast images of OC-k3 cells treated with NPsA. Magnification 40x. A. 25 µg/ml: arrow heads indicate small perinuclear vesicles. B. 50 µg/ml: arrows indicate large vesicles.

The analyses by fluorescence microscopy of OC-k3 cells treated with NPs conjugated with rhodamine B at concentrations 25 and 50 µg/ml for 2, 4, 24 and 48 hours confirmed the fast internalization of NPs: the signal was clearly visible at 4 hours of treatment (Fig. 4.15). No significant differences in internalization times were detected at the two concentrations of NPs plus rhodamine B tested. Although a quantitative analysis of fluorescence was not performed, the signals resulted more intense at increasing NPs concentration and reached a peak at 24 hours, decreasing at 48 hours. As observed for PC12 cells, the NPs apparently localized in the perinuclear region but not in the positions corresponding to vesicles.

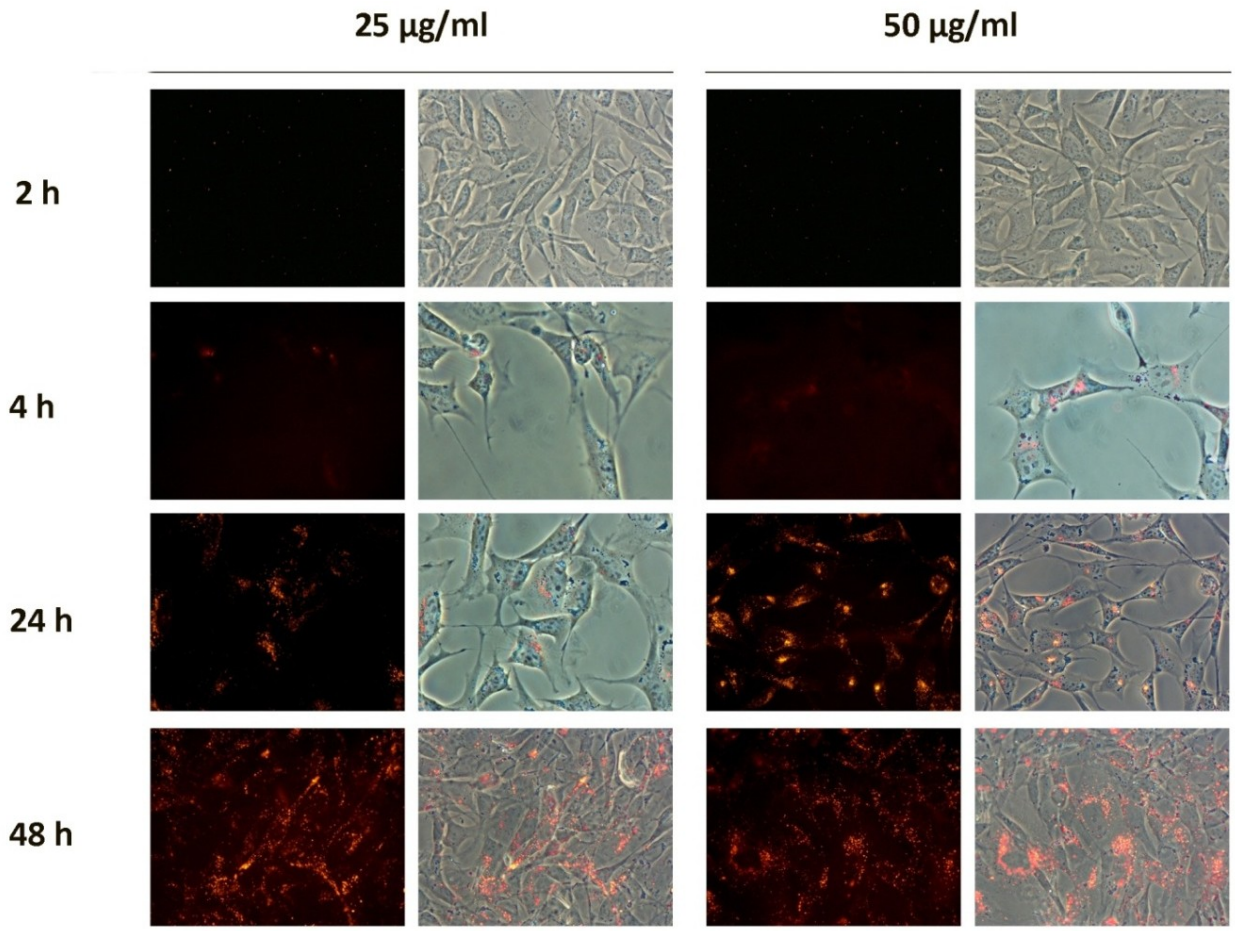

Fig. 4.15. Fluorescent microscope images and colour-combined (phase contrast plus fluorescence) images of OC-k3 cells treated with 25 and 50 µg/ml NPs conjugated with rhodamine B for 2, 4, 24 and 48 hours. Magnification 40x.

The results of morphological tests by annexin V-FITC and PI indicated that NPsA up to the concentration of 50 µg/ml did not cause cell death by apoptosis (green-red double signal) in OC-k3 cells treated for 24 and 48 hours, in comparison to untreated controls and to the number of cells still adhering to culture flasks after treatment (Fig. 4.16). Cells exhibiting the double signal were in low number and almost all detached. The number of cells undergoing apoptosis was not significantly different from that of control populations. However, the number of adhering cells progressively reduced with increasing concentrations of NPsA. Similarly, the tests with DAPI and phalloidin-TRITC on OC-k3 cells did not reveal any sign of apoptosis at the NPsA concentration tested (Fig. 4.17). The cells appeared normal in shape, withouth any significant alterations of cytoskeleton, the nuclei were not fragmented and the chromatin was not condensed, as expected in typical apoptotic events.

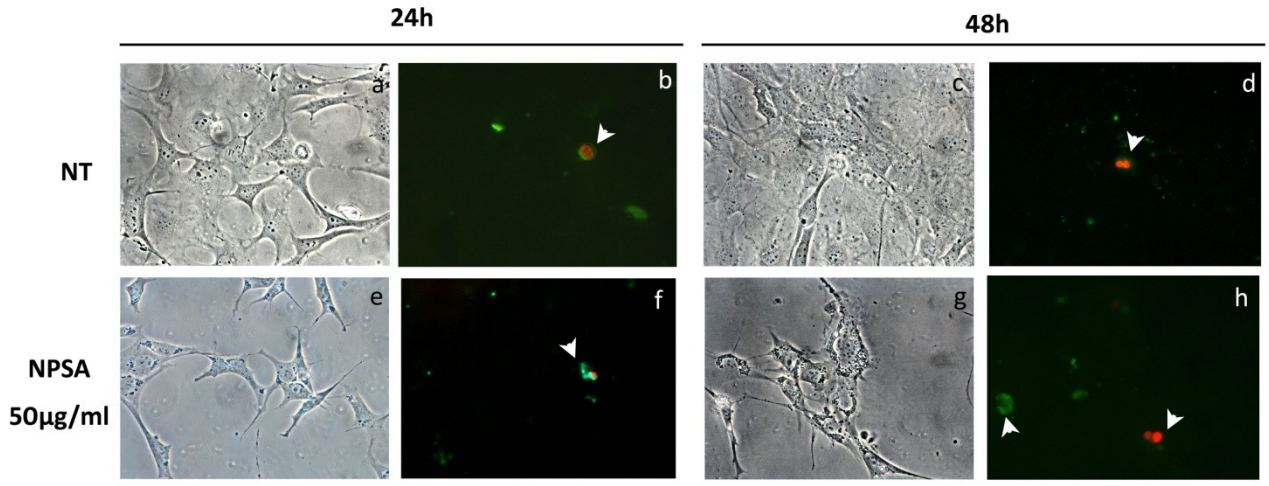

Fig. 4.16. Morphological investigations with annexin V-FITC (green) and PI (red) on OC-k3cells treated with NPsA 50 µg/ml at 24 and 48 hours. Images a, c, e, g are phase contrast. NT, untreated control. White arrows indicate cells in apoptosis or necrosis. Magnification 40x.

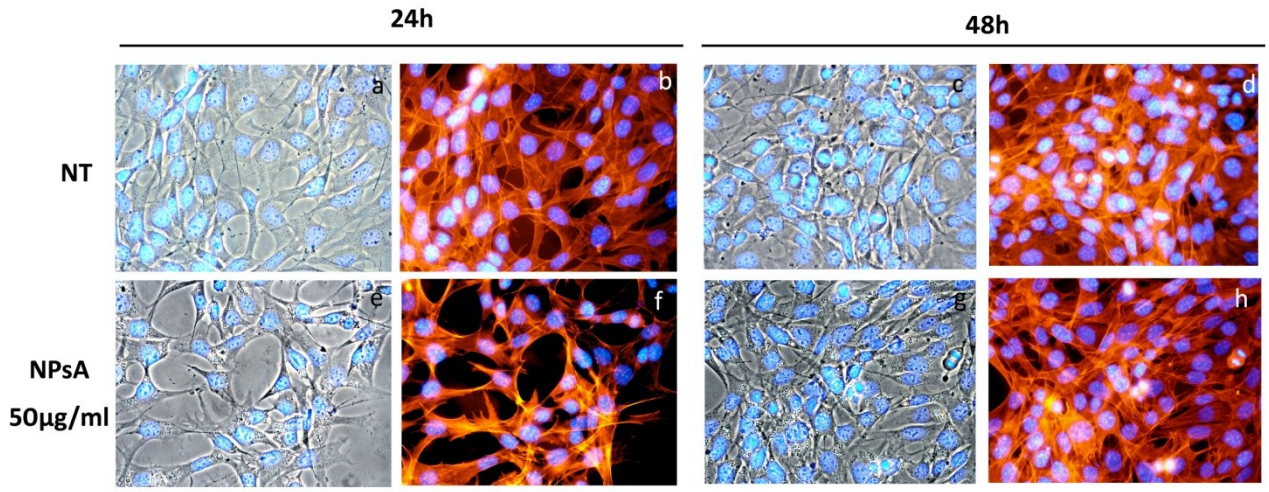

Fig. 4.17. Morphological investigations with DAPI(blue) and phalloidin-TRITC (red) on OC-k3 cells treated with NPsA 50 µg/ml at 24 and 48 hours. Images a, c, e, g are colour-combined DAPI-phase contrast. NT, untreated control. Magnification 40x.

Concerning gene expression profiles analysed by RTqPCR, the exposure of OC-k3 cells to NPsA at concentrations 10 and 25 µg/ml revealed a time dependent increase of gene expression of caspase 8, initiator of the extrinsic apoptotic, but a decrease in gene expression of caspase 9, initiator of the intrinsic pathway (Fig. 4.18). Genes such as the effector caspase 3 or p53 were overexpressed, again in time dependent way. The BAX and Bid genes, involved in the cell response at mitochondrial level, resulted significantly overexpressed after 48 hours of treatment.

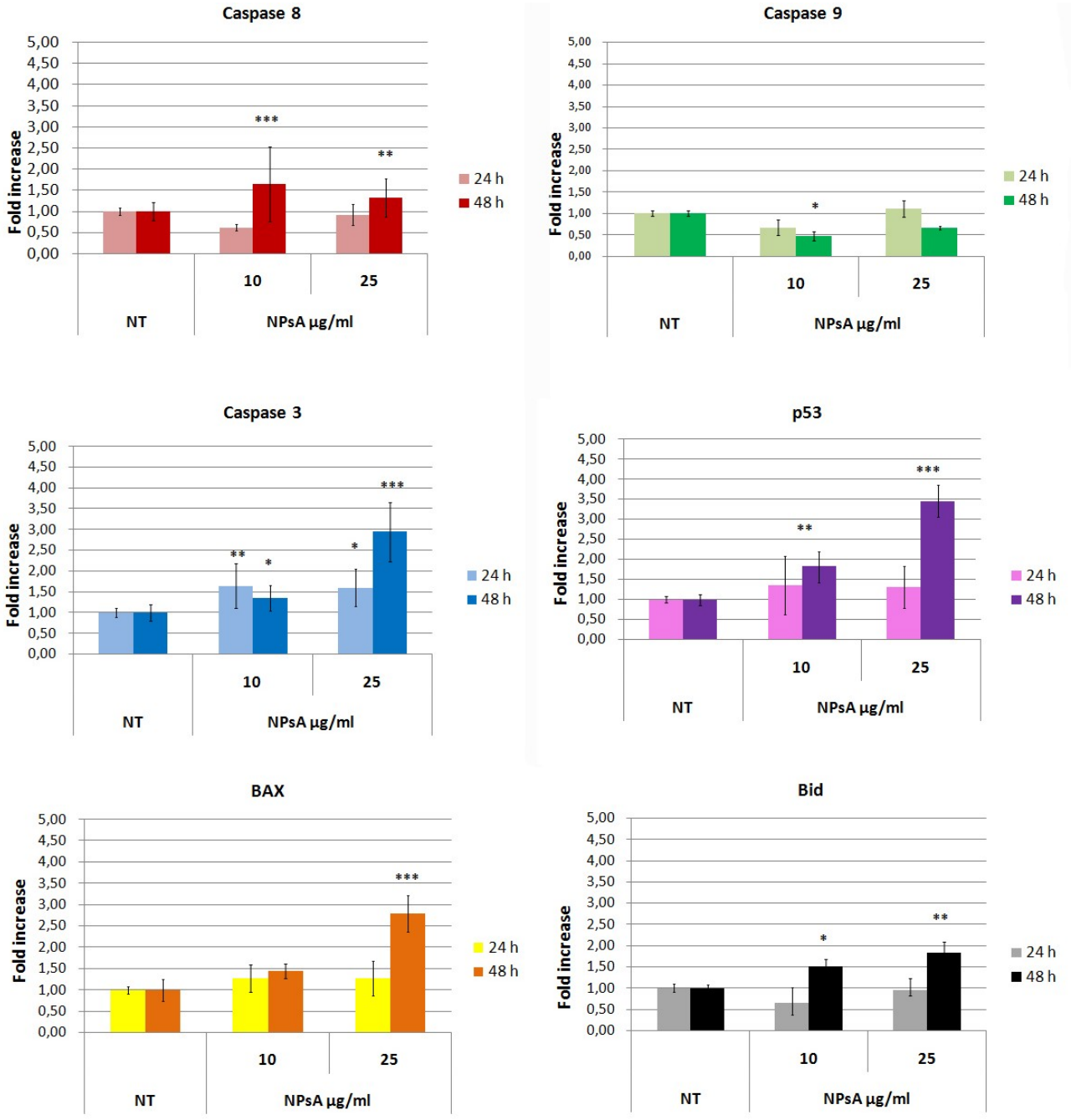

Fig. 4.18. Analyses of relative gene expression by RTqPCR on OC-k3 cells treated with NPsA, expressed as normalized fluorescence intensity with standard errors as bars. Asterisks indicate significant values in comparison to control (NT). * = $p<0.05$; **= $p<0.01$; ***=$p<0.001$).

The analyses of activated biochemical patterns by Western Blot on OC-k3 did not show any increase in expression of protein markers related to apoptosis up to the concentration of 25 µg/ml of NPsA, in comparison to untreated controls (Fig.4.19). The level of pERK decreased in a dose and time dependent way in comparison to controls; that of cleaved caspase 3 increased only at NPsA 50

µg/ml for 48 hours, a concentration which resulted toxic for OC-k3 cells according to the viability tests. The same significant trend ($p<0.001$) was observed for the levels of cleaved PARP.

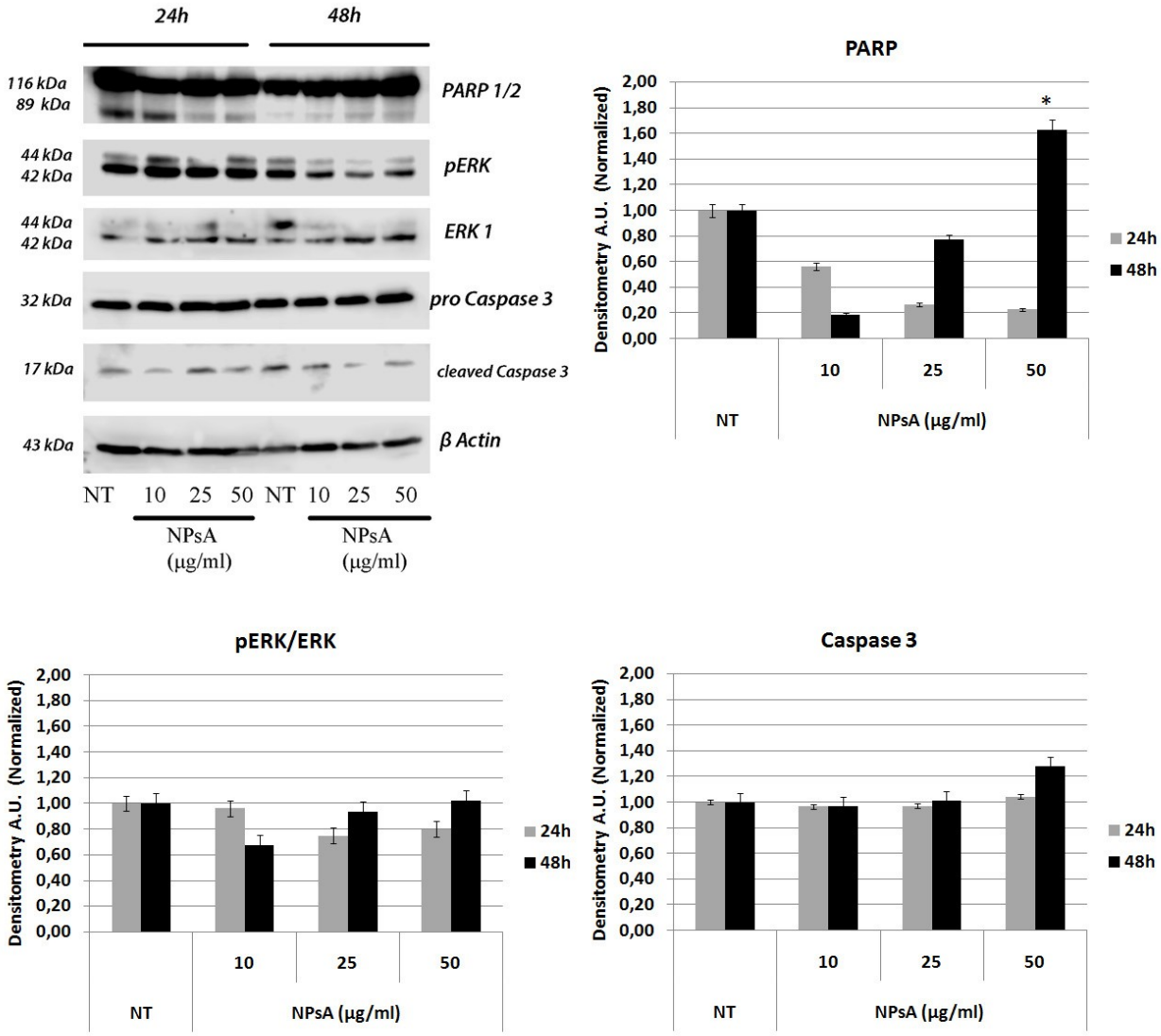

Fig. 4.19. Western Blot after SDS-PAGE and densitometric analysis of key proteins related to apoptosis (with β-actin as standard marker) in PC12 cells treated with NPsA (10, 25 and 50 µg/ml) for 24 and 48 hours. Bars represent standard errors. Asterisks indicate significant values in comparison to control (NT). * = $p<0.001$.

4.2.2 Characterization of NPsQ

The *in vitro* analyses performed on NPsQ alone had the aim to verify possible differences in comparison to NPsA. Since the two types of nanoparticles have similar physical chemical properties, the hypothesis was that the cell response could be affected by the presence of coenzyme Q conjugated to NPs.

In PC12 cells, the treatment with NPsQ at 24 and 48 hours induced an increase of cell viability even at high concentrations (Fig. 4.32). The increase in cell viability became significant at 50 µg/ml ($p<0.05$) at 24 and 48 hours and up to 120 µg/ml an increase in cell viability was observed. No cell toxicity was observed at doses lower than 150 µg/ml. However, comparing the results at 24 and 48 hours, the trends appeared rather different, with a slight increase (although not significant) at 48 hours. Based on the above data, the concentration range chosen for all analyses conducted on NPsQ was 25 - 100 µg/ml.

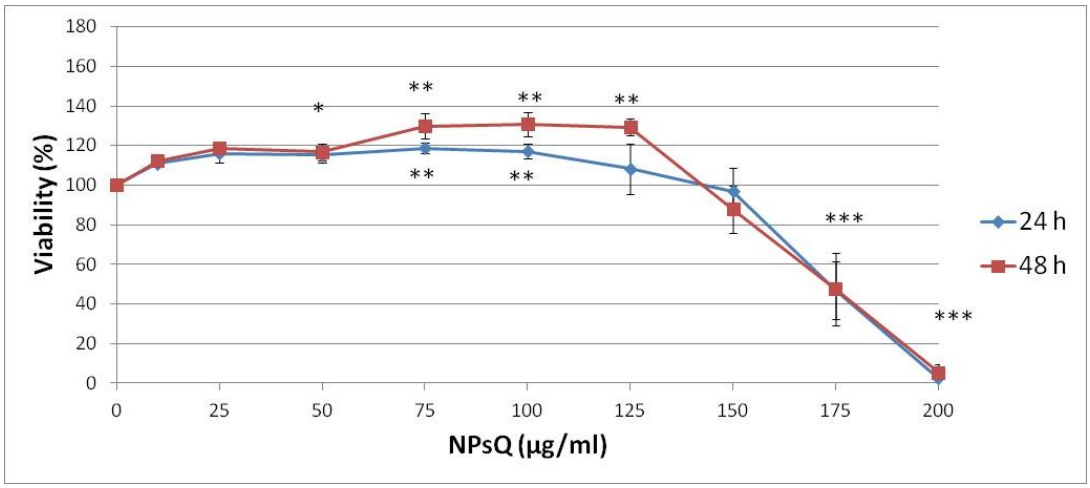

Fig. 4.32. *In vitro* toxicity of NPsQ on PC12 cells, expressed as percentage of cell viability vs. NPsQ concentration (µg/ml) at 24 and 48 hours. Bars represent the standard errors. The asterisks indicate significant differences in comparison to untreated controls (* = $p<0.05$; ** = $p<0.01$; *** = $p<0.001$).

The analyses of cell cycle by flow cytometry indicated that the PC12 cell populations treated with NPsQ had a distribution similar to untreated controls, both at 24 and 48 hours (Fig. 4.33). At 24 hours and 75-100 µg/ml NPsQ the PC12 cell populations showed a slight significant increase

(p<0.05) in S phase. For other NPsQ concentrations a progressive decrease in G2/M was observed at 24 hours, while at 48 hours a progressive (but not significant) increase was observed at 48 hours. No significant increase in hypodiploid population was detected when NPsQ doses or time of exposure were increased.

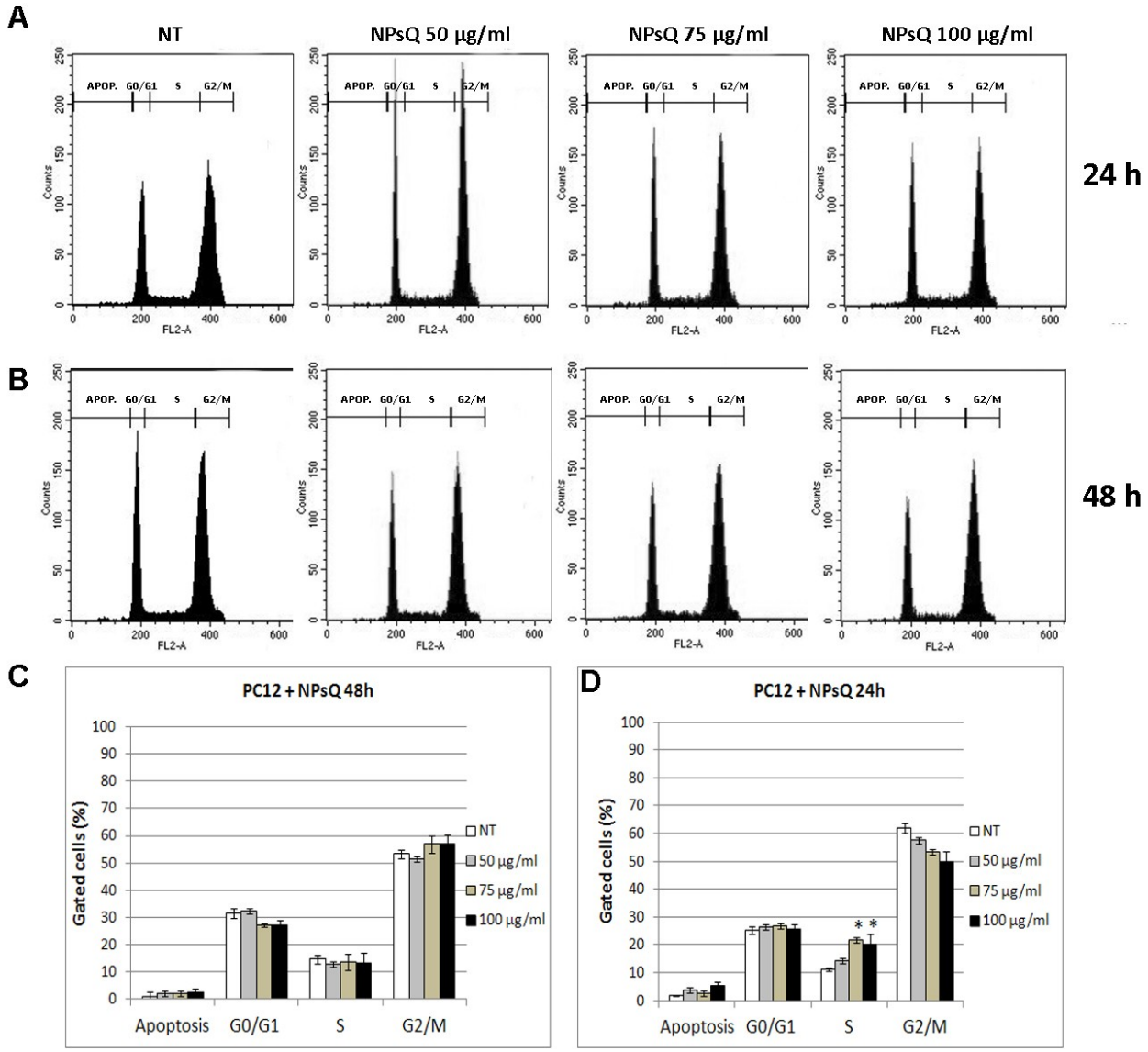

Fig. 4.33. Analyses by flow cytometry of PC12 cells treated with NPsQ (50, 75 and 100 µg/ml) for 24 and 48 hours. A, B. Number of cells (expressed as counts) in each phase of the cell cycle. For each experimental condition, about 20000 events were analysed. NT, untreated control. APOP, apoptosis. C, D. Distribution of cells expressed as percentage of cells ± standard error in each cell cycle phase. The asterisks indicate significant differences in comparison to untreated controls (*=p<0.05).

The morphological analyses by annexin V-FITC and PI confirm that at the NPsQ concentrations examined (up to 100 µg/ml) no evident apoptosis was detected by fluorescence microscopy (Fig. 4.34). The PC12 cells treated with NPsQ (Fig. 4.34 F-H) did not show any green stain characterizing the initial apoptotic process in comparison to controls where few stained cells are detected within a high number of cells (Fig. 4.34 B-D).

The PC12 cells treated with NPsQ and stained by DAPI and phallodin-TRITC showed a normal nucleus and cytoskeleton, very similar to untreated controls (Fig. 4.35). The condition of cytoskeleton was not clearly visible because of PC12 cell morphology, but the cell shape was preserved at high NPsQ concentration (Fig. 4.35 F-H) at 24 and 48 hours; moreover, nuclei appeared roundish and undistorted (Fig. 4.35 E-G).

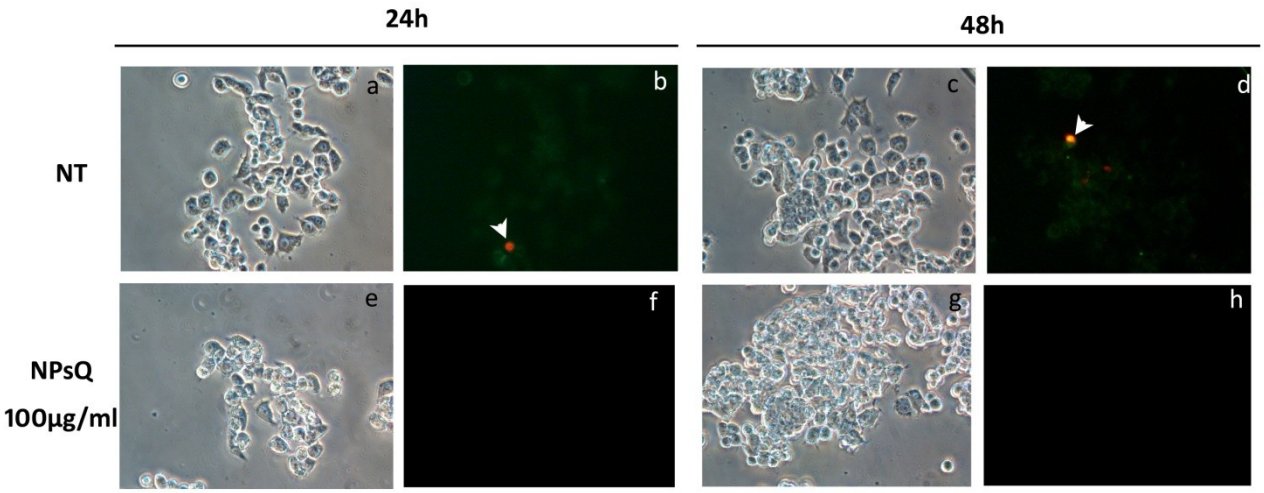

Fig. 4.34. Morphological investigations with annexin V-FITC (green) and PI (red) on PC12 cells treated with NPsQ (100 µg/ml) at 24 and 48 hours. Images a, c, e, g are phase contrast. NT, untreated control. Magnification 40x.

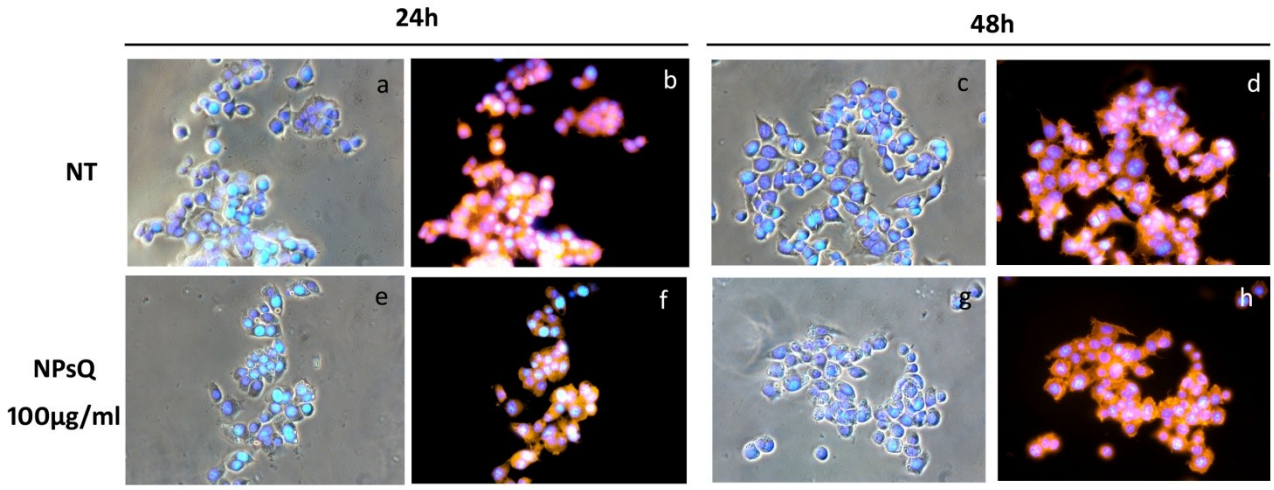

Fig. 4.35. Morphological investigations with DAPI (blue) and phalloidin-TRITC (red) on PC12 cells treated with NPsQ (100 µg/ml) at 24 and 48 hours. Images a, c, e, g are colour-combined DAPI-phase contrast. NT, untreated control. Magnification 40x.

The analyses on gene expression profiles by RTqPCR showed that the treatment of PC12 cells with NPsQ increased the transcription of some apoptosis-related genes (Fig. 4.36). The interaction of NPsQ with cells induced an increase in initiatior caspases, especially caspase 9: the levels of caspase 9 transcripts increased in a significant way ($p<0.001$) at 48 hours. After the activation of caspase 9, other transcription factors involved in apoptosis, such as BAX ans caspase 3, are slightly (but not significantly) overexpressed. The expression of these genes was lower at 48 hours.

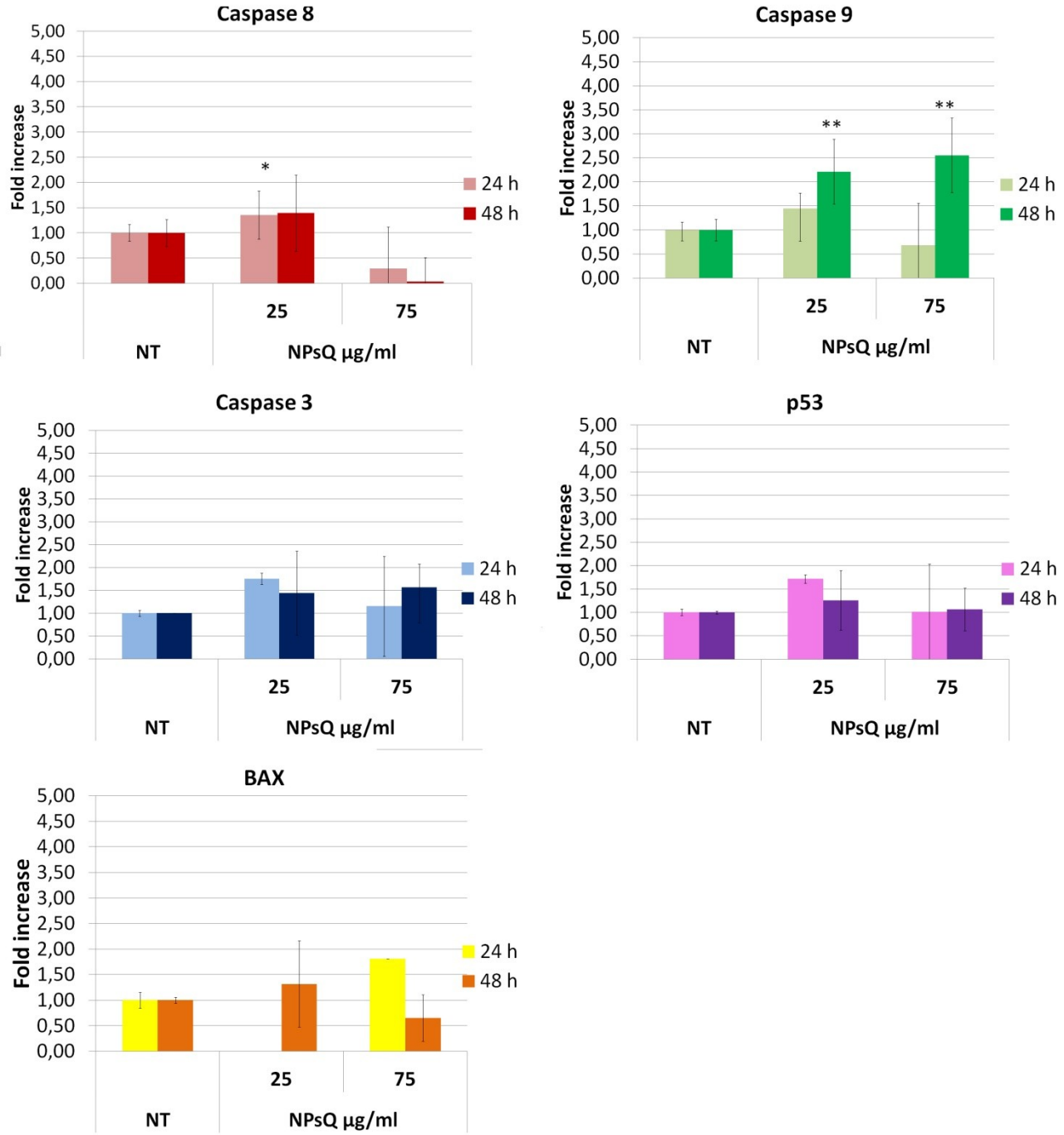

Fig. 4.36. Analyses of relative gene expression by RTqPCR on PC12 cells treated with NPsQ (25 and 75 µg/ml) at 24 and 48 hours, expressed as normalized fluorescence intensity with standard errors as bars. Asterisks indicate significant values in comparison to control (NT). (* = $p<0.05$; **= $p<0.01$).

The results of protein expression measured by Western blot were in agreement with the previous ones: the apoptotic marker proteins were not significantly overexpressedand were neither dose nor

time dependent (Fig. 4.37). The level of cleaved PARP significantly decreased in comparison to untreated controls at 24 hours and NPsQ 100 µg/ml ($p<0.01$) and at 48 hours from 50 µg/ml onwards ($p<0.05$). The levels of pERK also decreased in a dose and time dependent way.

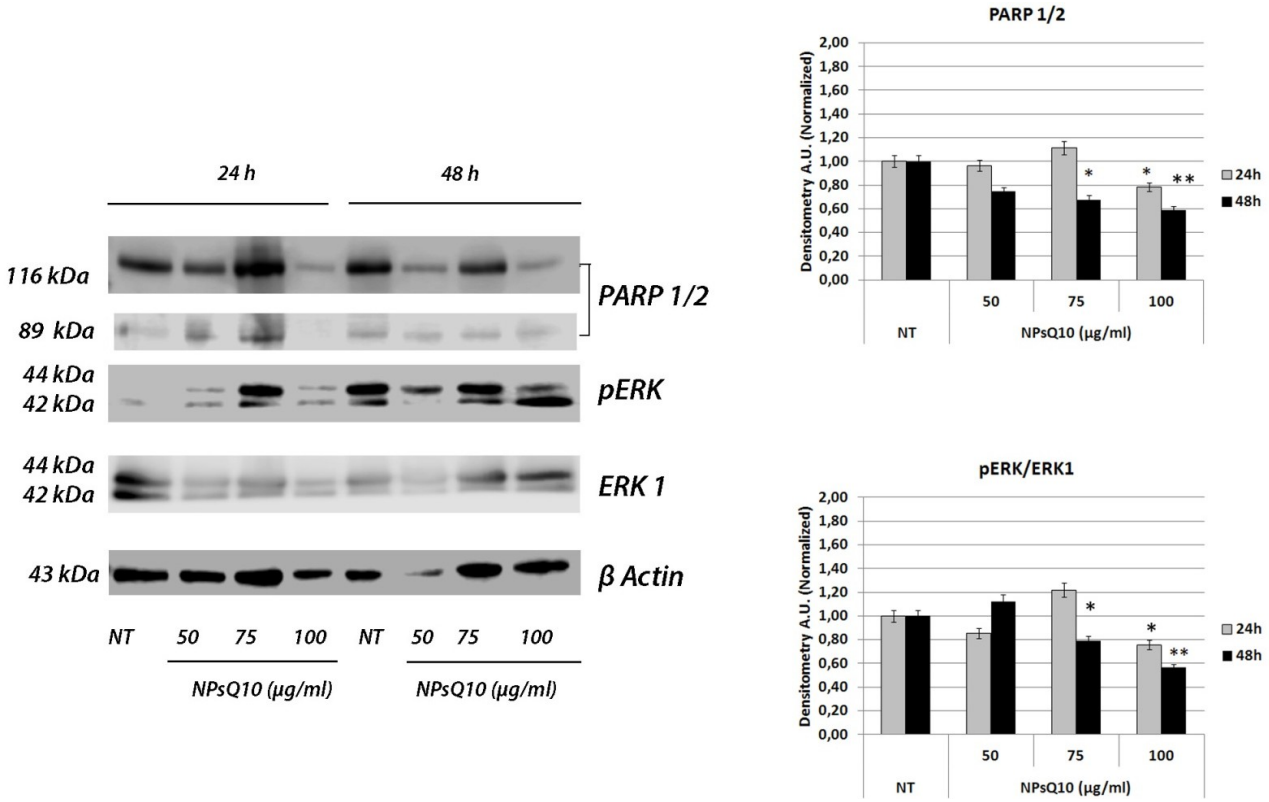

Fig. 4.37. Western Blot after SDS-PAGE and densitometric analysis of key proteins related to apoptosis (with β-actin as standard marker) in PC12 cells treated with NPsQ (50, 75 and 100 µg/ml) for 24 and 48 hours. Bars represent standard errors. Asterisks indicate significant values in comparison to control (NT). (* = $p<0.05$; ** = $p<0.01$).

On OC-k3 cells the NPsQ induced a toxicity dose dependent but not time dependent. The concentration causing a first toxic effect on OC-k3 cells treated with NPsQ at 24 and 48 hours was 50 µg/ml ($p<0.001$): a 20% decrease in cell viability was detected (Fig. 4.38). Increasing the NPsQ concentration to 75 µg/ml, the cell viability decreased to 40% for both 24 and 48 hours ($p<0.001$) and at 100 µg/ml the decrease reached 80%.

Based on cell viability tests, a concentration range of NPsQ between 10 and 75 µg/ml was chosen for the molecular analyses: this range was the best to verify the possible effects of the conjugated compound.

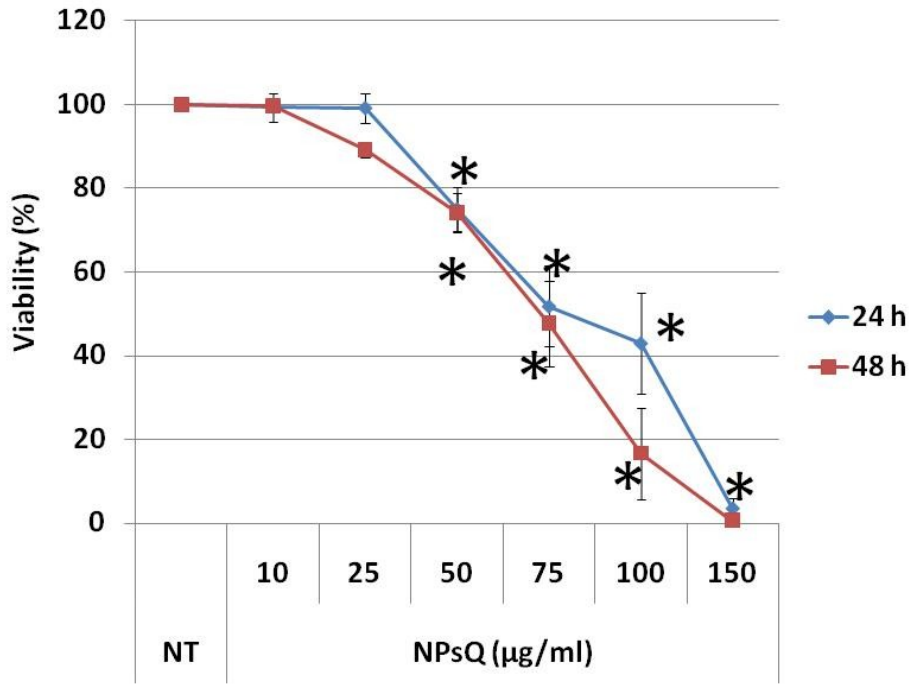

Fig. 4.38. *In vitro* toxicity of NPsQ on OC-k3 cells, expressed as percentage of cell viability vs. NPsQ concentration (µg/ml) at 24 and 48 hours. Bars represent the standard errors. The asterisk indicates significant differences in comparison to untreated controls (* = $p<0.001$).

The analyses of cell cycle by flow cytometry in OC-k3 cells at 24 and 48 hours was performed at NPsQ concentrations 0-50 µg/ml. The results confirmed that NPsQ did not cause apoptosis in OC-k3 cells and no significant variations were detected in comparison to untreated controls (Fig. 4.39). At 24 hours, a slight dose dependent decrease in cell population number in G0/1 and G2/M was detected, together with an increase in S. At 48 hours a slight increase was detected in G0/1 and a decrease in S and G2/M.

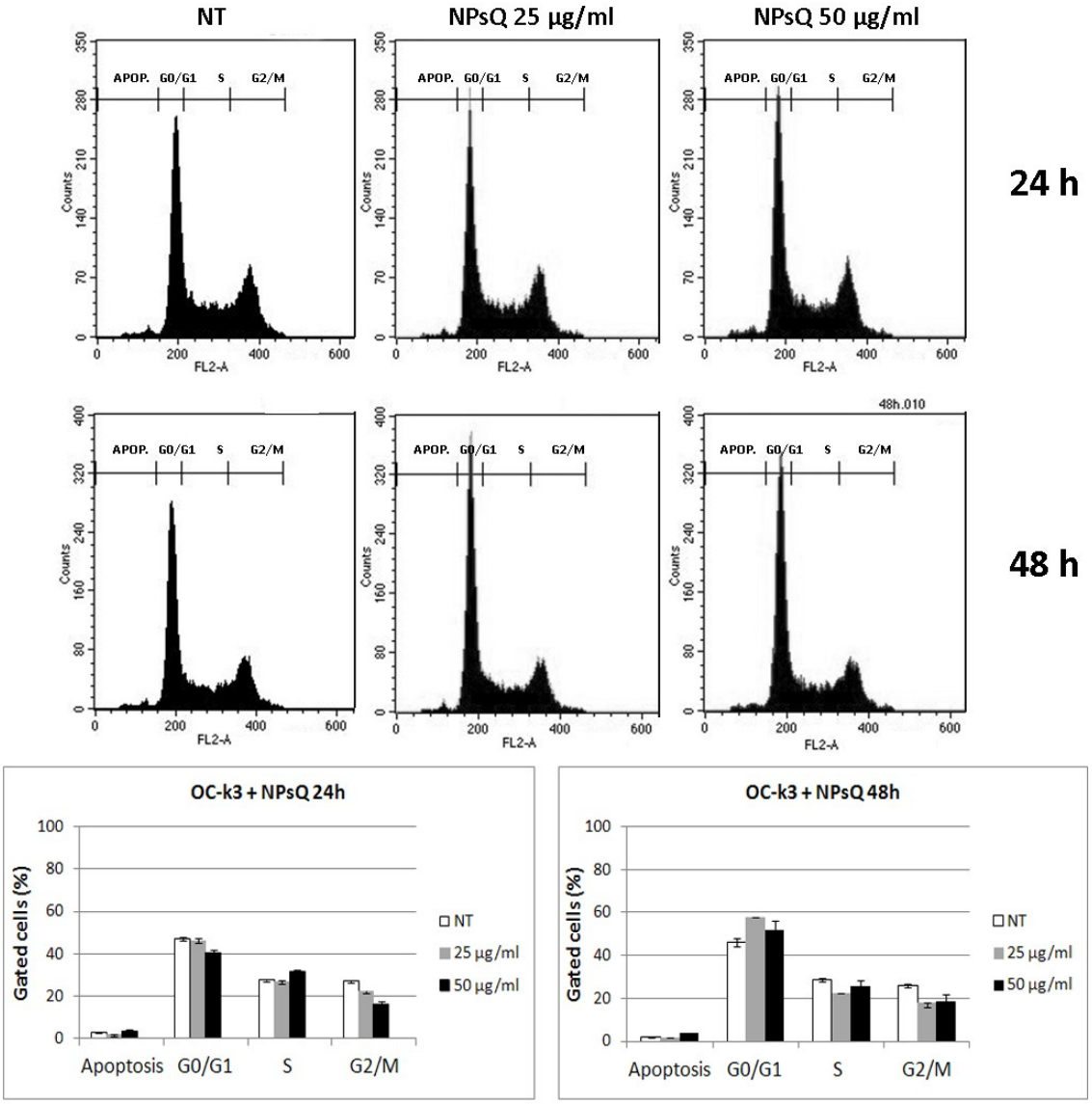

Fig. 4.39. Analyses by flow cytometry of OC-k3 cells treated with NPsQ (25 and 50 µg/ml) for 24 and 48 hours. A, B. Number of cells (expressed as counts) in each phase of the cell cycle. For each experimental condition, about 20000 events were analysed. NT, untreated control. APOP, apoptosis. C, D. Distribution of cells expressed as percentage of cells ± standard error in each cell cycle phase.

The morphological analyses by annexin V-FITC (Fig. 4.40) and PI revealed that NPsQ did not induce cell death by apoptosis. There was no evident difference between the number of treated cells showing the double stain with annexin V-FITC and PI in comparison to untreated controls (Fig. 4.39). The stain with DAPI (Fig. 4.41) did not show any evident chromatin condensation or nuclei fragmentation, typical of the apoptotic process. However, the number of cells adhering to the

substrate was markedly reduced at NPsQ concentration 100 µg/ml (Fig 4.41 E-G). The cell shape was preserved and cytoskeleton was not apparently altered by the treatment (Fig. 4.41 F-H).

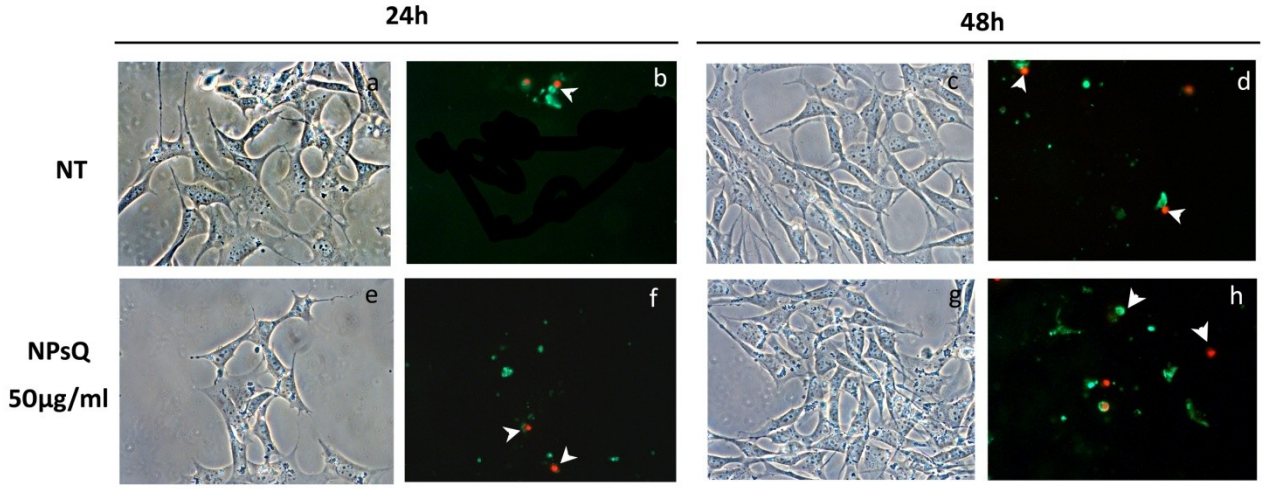

Fig. 4.40. Morphological investigations with annexin V-FITC (green) and PI (red) on OC-k3 cells treated with NPsQ (50 µg/ml) at 24 and 48 hours. White arrowheads indicate cells in apoptosis. Images a, c, e, g are phase contrast. NT, untreated control. Magnification 40x.

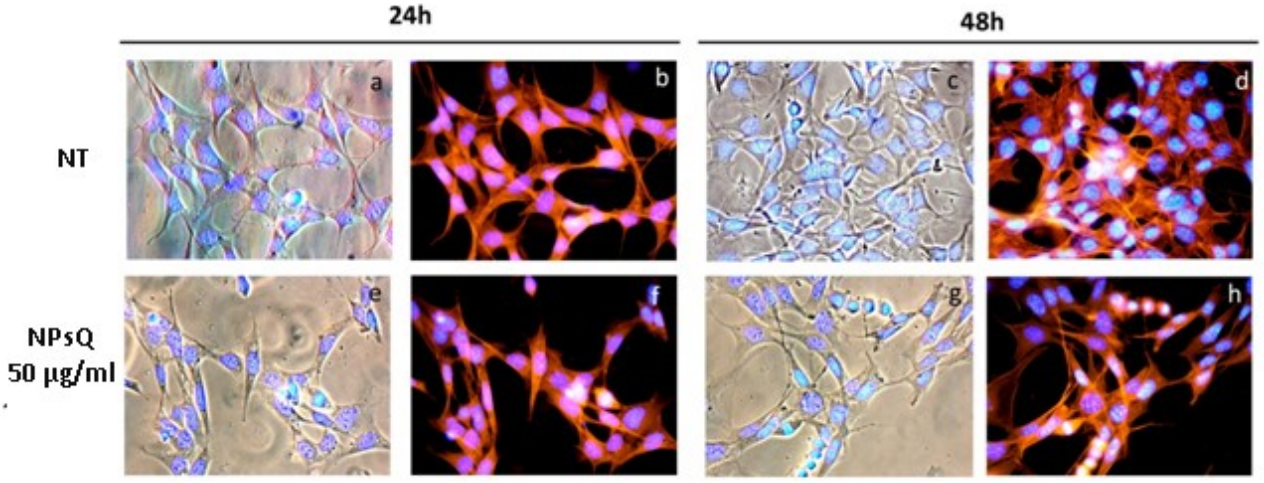

Fig. 4.41. Morphological investigations with DAPI (blue) and phalloidin-TRITC (red) on OC-k3 cells treated with NPsQ (50 µg/ml) at 24 and 48 hours. Images a, c, e, g are colour-combined DAPI-phase contrast. NT, untreated control. Magnification 40x.

For analyses of OC-k3 cells by RTqPCR the NPsQ concentration range employed was 10-25 µg/ml (Fig 4.42). Generally, the level of analysed transcripts increased in a dose and time dependent way. The level of caspase 8 did not increase significantly, except at 25 µg/ml and 48 hours; the

expression of caspase 9 remained similar to the untreated controls. Concerning the genes transcribed after the activation of caspase 8 and 9, BAX and Bid followed a similar path, increasing in a dose dependent way, significant only at 25 µg/ml and 48 hours. The expression of initiator caspase and that of genes regulating the next apoptotic phases appeared in good agreement. Among the genes investigated, the most expressed one was the effector caspase 3, significantly expressed after 48 hours ($p<0.001$) at both doses tested.

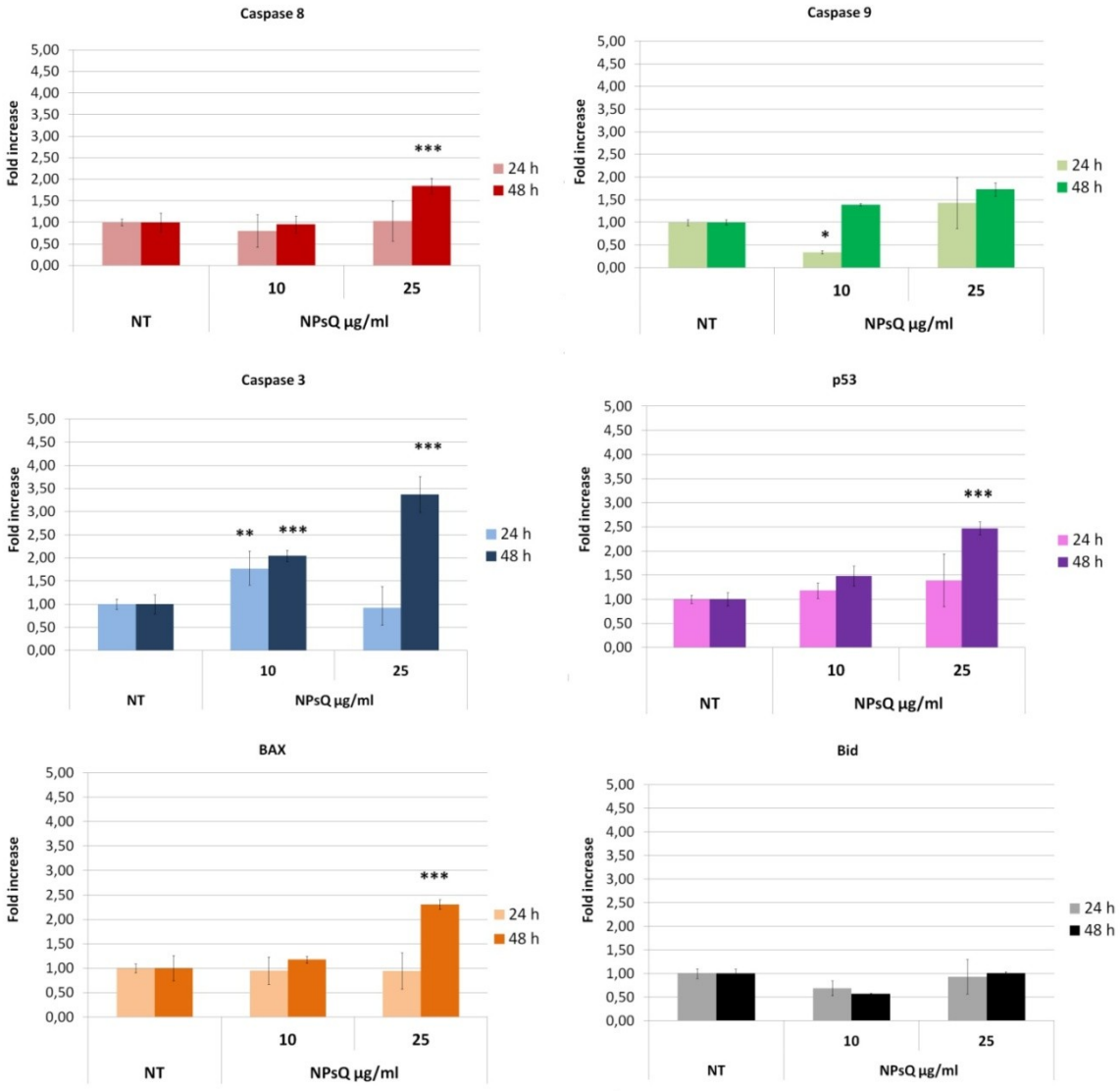

Fig. 4.42. Analyses of relative gene expression by RTqPCR on OC-k3 cells treated with with NPsQ (100 µg/ml) at 24 and 48 hours, expressed as normalized fluorescence intensity with standard errors as bars. Asterisks indicate significant values in comparison to control (NT). (* = $p<0.05$; ** = $p<0.01$; ***=$p<0.001$).

In analyses by Western blot on OC-k3 cells a range of NPsQ concentration 25-75 µg/ml was employed. At that range, the results indicated that proteins involved in apoptosis were not overexpressed (Fig. 4.43). The level of pERK is more or less similar to untreated controls and that of cleaved caspase 3 showed a slight (but not significant) time dependent increase. The same trend is observed for cleaved PARP at 24 hours, but a significant increase at 75 µg/ml NPsQ ($p<0.001$) was detected at 48 hours.

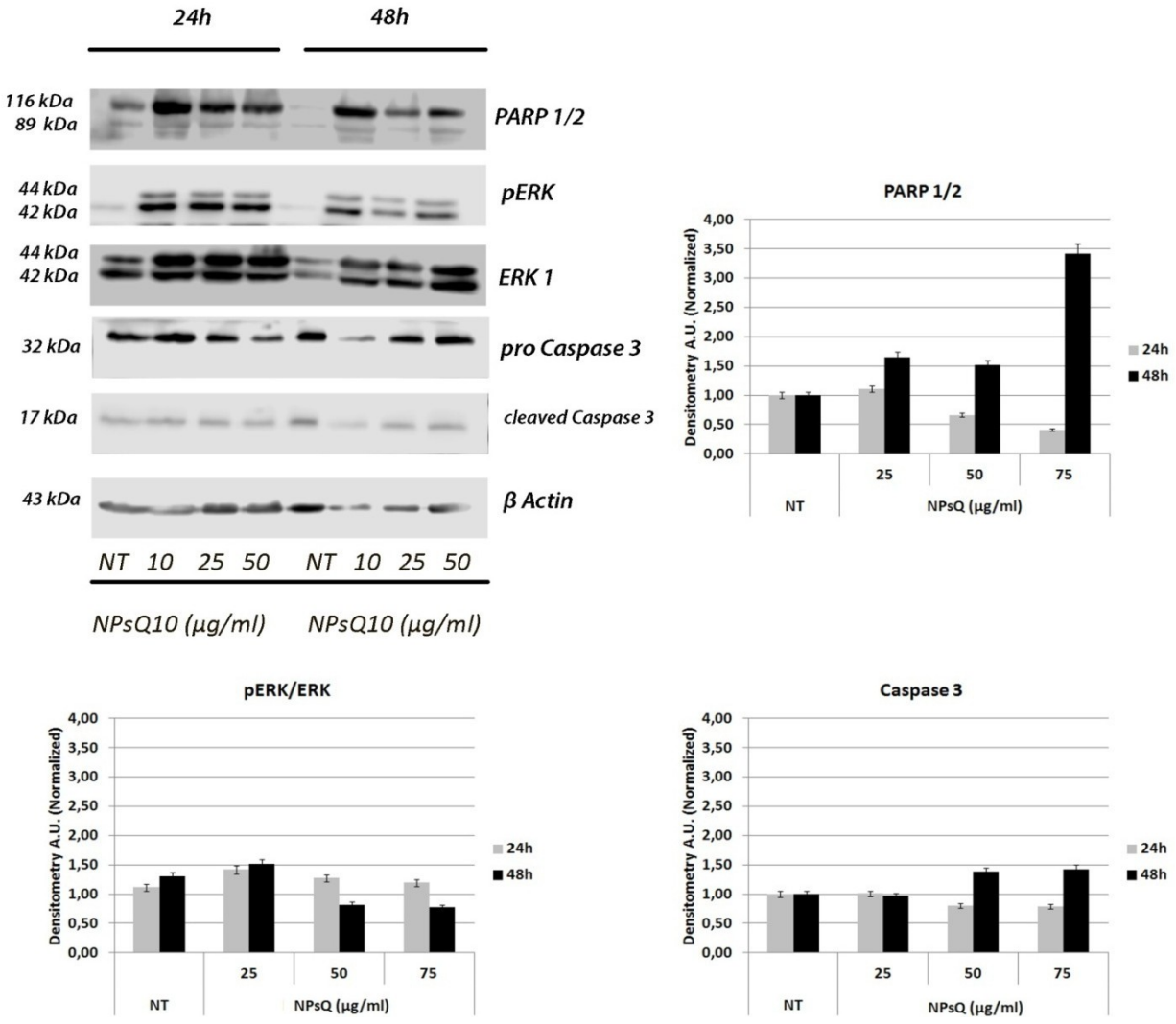

Fig. 4.43. Western Blot after SDS-PAGE and densitometric analysis of key proteins related to apoptosis (with β-actin as standard marker) in OC-k3 cells treated with NPsQ (25, 50 and 75 µg/ml) for 24 and 48 hours. Bars represent standard errors. Asterisks indicate significant values in comparison to control (NT). (**= $p<0.01$; *** = $p<0.001$).

4.2.3 Characterization of NPsD

The same analyses performed on NPSQ were conducted for NPsD with the aim to verify the effects of dexamethasone conjugated to NPs in comparison to NPsA, and in order to calculate the range of tolerance of these nanoparticles in PC12 and OC-k3 cells for protection tests. However, unlike for the other two types of NPs, the effects of NPsD were quite different according to the cell line tested.

When PC12 were treated with NPsD at different concentrations, a significant toxic effect on cell viability was detected at concentrations as low as 10 and 25 µg/ml at 24 hours ($p<0.05$) (Fig. 4.44). This toxic effect was followed by a recovery, restoring the viability at control levels at100 µg/ml. The NPsD toxicity apparently reduced in a dose dependent way from 25 to 100 µg/ml for both times of exposure. At 48 hours, it increased in a highly significant way ($p<0.001$) when cells were treated from 10 to 75 µg/ml: again, a recovery occurred at 100 µg/ml, but beyond this concentration limit the toxicity increased again for both 24 and 48 hours.

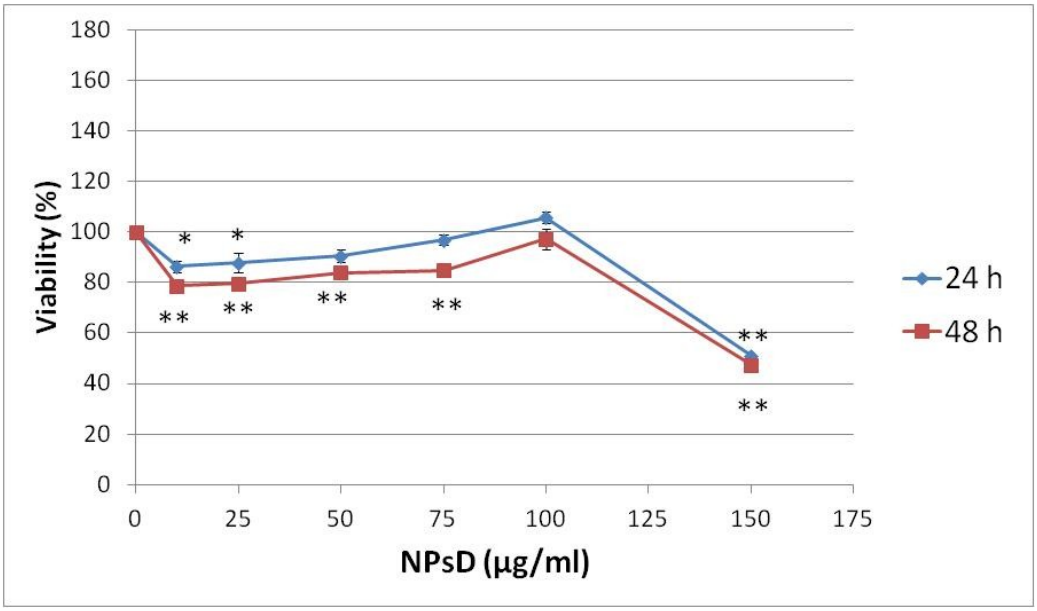

Fig. 4.44. *In vitro* toxicity of NPsD on PC12 cells, expressed as percentage of cell viability vs. NPsD concentration (µg/ml) at 24 and 48 hours. Bars represent the standard errors. The asterisks indicate significant differences in comparison to untreated controls (* = $p<0.05$;** = $p<0.001$).

The preliminary morphological investigations (by annexin V-FITC and PI, and by DAPI and phalloidin-TRITC) and the molecular ones (cell cycle by flow cytometry, gene expression by RTqPCR and protein expression by Western blot) confirmed the toxic effect of NPsD on PC12 cells

even at low concentrations. Based on these data, the protections tests on PC12 cells with CDDP (highly toxic at low concentrations for this cells line) were not performed with NPsD.

In OC-k3 cells the NPsD affect cell viability in a similar way to NPsA and NPsQ, but with a higher time dependent toxic effect (Fig. 4.45). At 24 hours, NPsD were not significantly toxic up to 50 µg/ml: at this concentration a 20% decrease in cell viability was detected in comparison to controls ($p<0.001$). The toxicity of NPsD increased in a significant way ($p<0.001$) at higher concentrations. At 48 hours, from 50 µg/ml the toxicity showed a sharper increase in comparison to 24 hours ($p<0.001$), inducing a 70% vitality decrease at the concentration 75 µg/ml NPsD.

Based on these results, for the next molecular analyses on OC-k3 the range of NPsD concentrations used was 25-75 µg/ml, with the aim to convey a higher drug amounts within the cells and verify their effects. The lower NPsD concentrations were excluded because of the very low amount of conjugated drug.

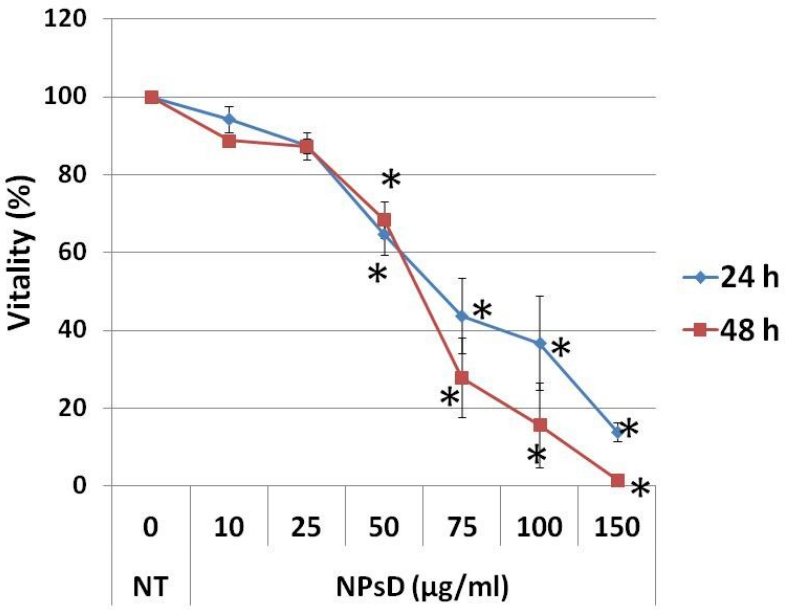

Fig. 4.45. *In vitro* toxicity of NPsD on OC-k3 cells, expressed as percentage of cell viability vs. NPsD concentration (µg/ml) at 24 and 48 hours. Bars represent the standard errors. The asterisk indicates a significant difference in comparison to untreated controls (* = $p<0.001$).

For the analyses of cell cycle by flow cytometry on OC-k3 cells, the range of NPsD concentrations examined was wide (25-75 µg/ml), but no significant variations were detected in the distribution of

cell populations in the different phases of the cell cycle (Fig. 4.46). At 24 and 48 hours a slight dose dependent increase of hypodiploid cells and a decrease of cells in G2/M was noticed, and a slight recovery was observed at 48 hours in G2/M.

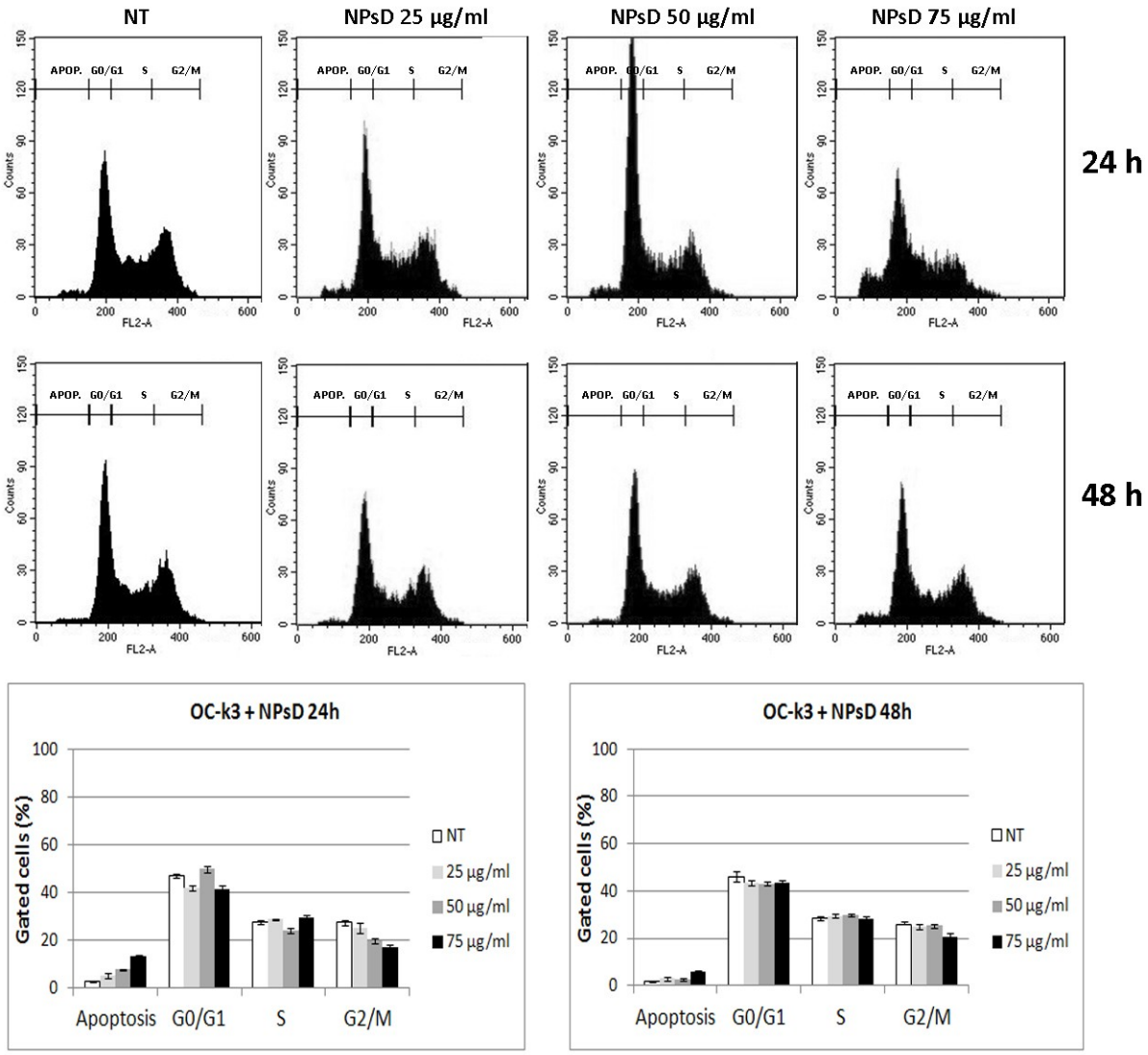

Fig. 4.46. Analyses by flow cytometry of OC-k3 cells treated with NPsD (25, 75 and 50 µg/ml) for 24 and 48 hours. A, B. Number of cells (expressed as counts) in each phase of the cell cycle. For each experimental condition, about 20000 events were analysed. NT, untreated control. APOP, apoptosis. C, D. Distribution of cells expressed as percentage of cells ± standard error in each cell cycle phase.

According to morphological analyses with annexin V-FITC and PI (Fig. 4.47) up to NPsD concentration 50 µg/ml, at 24 hours the number of cells exhibiting the double staining (green-red)

was not apparently different in comparison to untreated controls (Fig.4.47 F-H). The number of cells stained in green-red increased with time, but the differences in comparison to controls were hardly visible. At 48 hours, the number of cells undergoing cell division was higher in comparison to 24 hours.

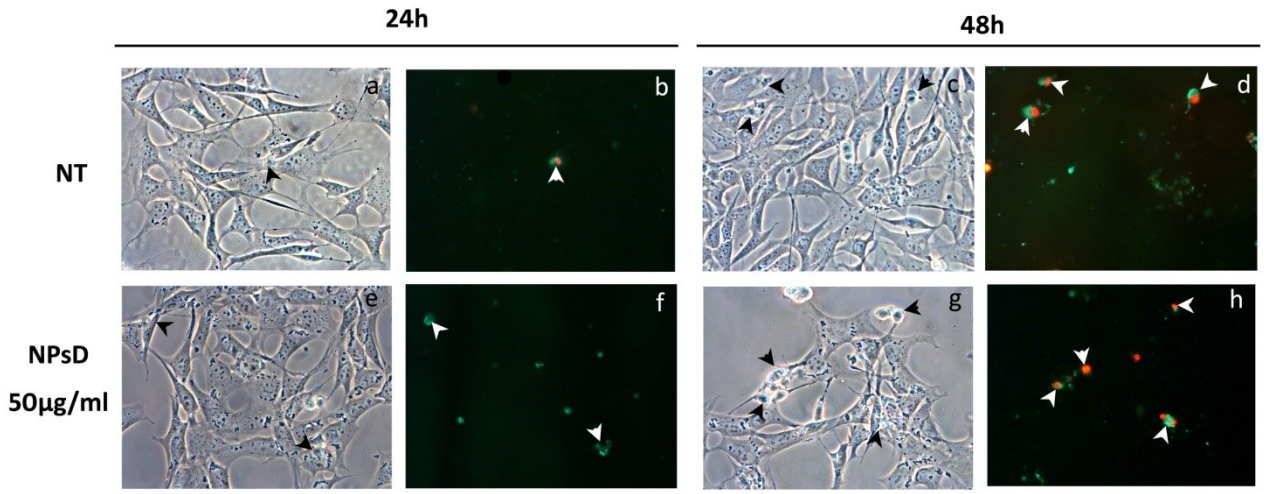

Fig. 4.47. Morphological investigations with annexin V-FITC (green) and PI (red) on OC-k3 cells treated with NPsD (50 µg/ml) at 24 and 48 hours. White arrowheads indicate cells in apoptosis. Images a, c, e, g are phase contrast. NT, untreated control. Magnification 40x.

The morphological investigations by DAPI and phalloidin-TRITC did not reveal any difference in the aspect of cytoskeleton and/or nucleus (Fig. 4.48). At 50 µg/ml NPsD the cells maintained their normal shape and the cytoskeleton fibres appeared long and intact. No chromatin condensation or enlargement of nuclei was visible, thus cells did not show any sign of apoptosis even at high NPsD doses.

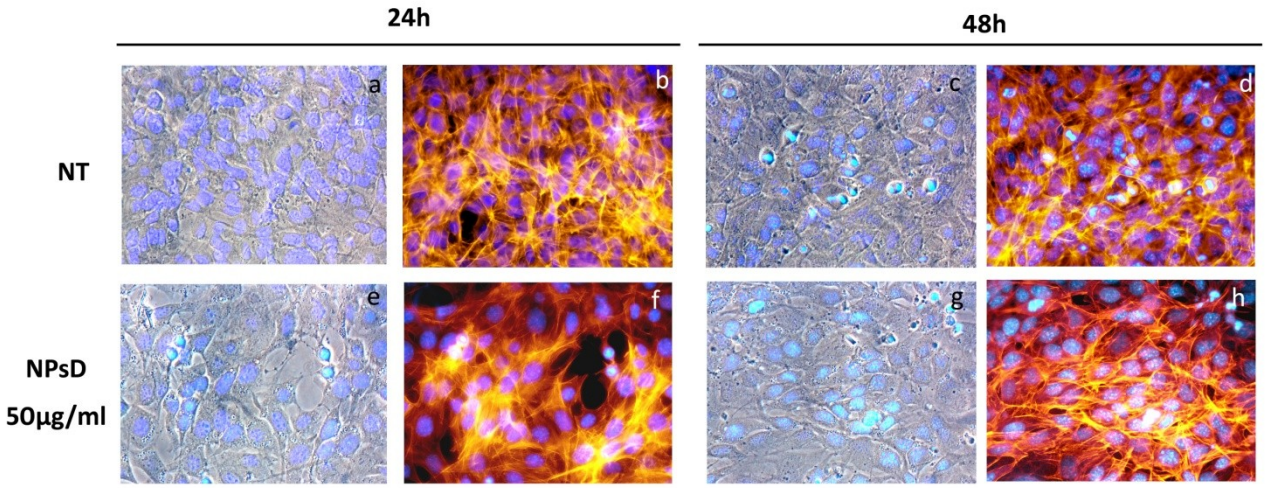

Fig. 4.48. Morphological investigations with DAPI (blue) and phalloidin-TRITC (red) on OC-k3 cells treated with NPsD (50 µg/ml) at 24 and 48 hours. Images a, c, e, g are colour-combined DAPI-phase contrast. NT, untreated control. Magnification 40x.

When gene expression profiles were analysed by RTqPCR in OC-k3 cells exposed to NPsD, all transcripts examined closely followed the levels of controls for both NPsD concentrations analysed (25 and 50 µg/ml) and for both exposure times, 24 and 48 hours (Fig. 4.48).Only caspase 3 resulted significantly overexpressed at 24 hours ($p<0.05$): all other genes had a lower time dependent expression in comparison to controls.

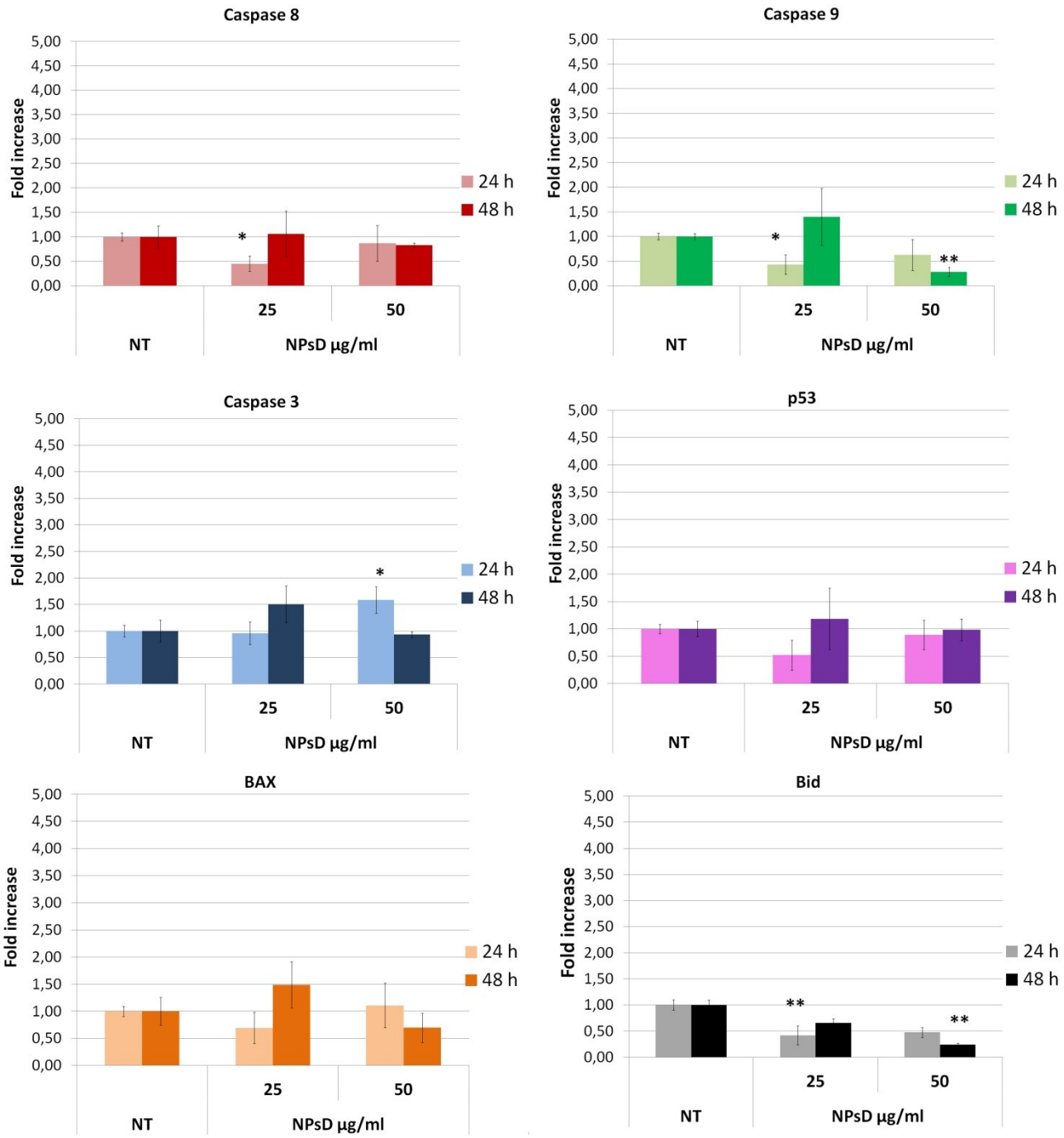

Fig. 4.49. Analyses of relative gene expression by RTqPCR on OC-k3 cells treated with NPsD (25 and 50 µg/ml) at 24 and 48 hours, expressed as normalized fluorescence intensity with standard errors as bars. Asterisks indicate significant values in comparison to control (NT). (* = $p<0.05$; **= $p<0.01$).

The densitometric analyses of Western blot of apoptotic markers in OC-k3 cells treated with NPsD confirmed the results obtained by RTqPCR: the expression of proteins directly involved in the apoptotic process, such as cleaved caspase 3 and PARP, was significantly reduced in a dose and

time dependent way, in comparison to controls. However, the level of pERK increased at 48 hours and at higher NPsD doses.

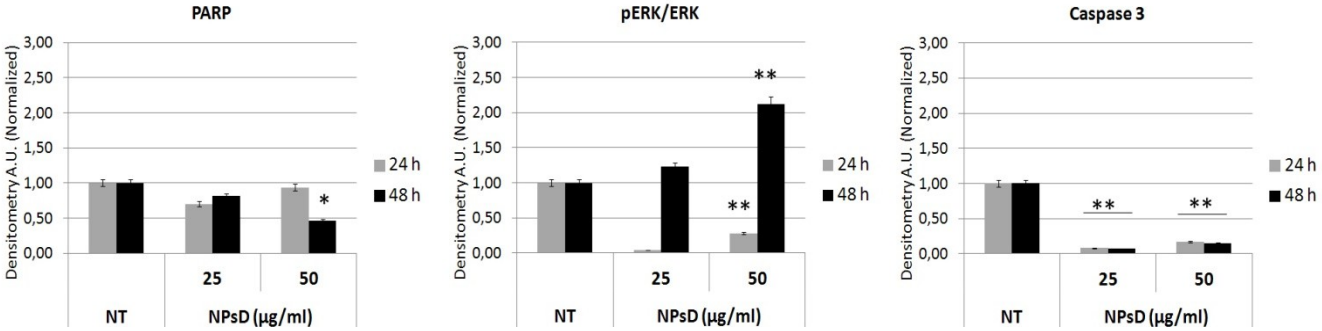

Fig. 4.50. Densitometric analysis of Western blot of key proteins related to apoptosis in OC-k3 cells treated with NPsD (25 and 50 µg/ml) for 24 and 48 hours. Bars represent standard errors. Asterisks indicate significant values in comparison to control (NT). (* = $p<0.05$; ** = $p<0.001$).

4.3 Characterization of cisplatin *in vitro*

The PC12 cells resulted very sensitive to treatment with CDDP. A significant 20% decrease ($p<0.001$) in cell viability was detected at concentration 5 µM for 24 hours, and more than 70% ($p<0.001$) at 25 µM. When the exposure time was increased to 48 hours, the toxicity increased to 60% at 5 µM and reached a highly significant peak of 89% ($p<0.001$) at 25 µM. Therefore CDDP induced a dose and time dependent toxicity on PC12 cells.

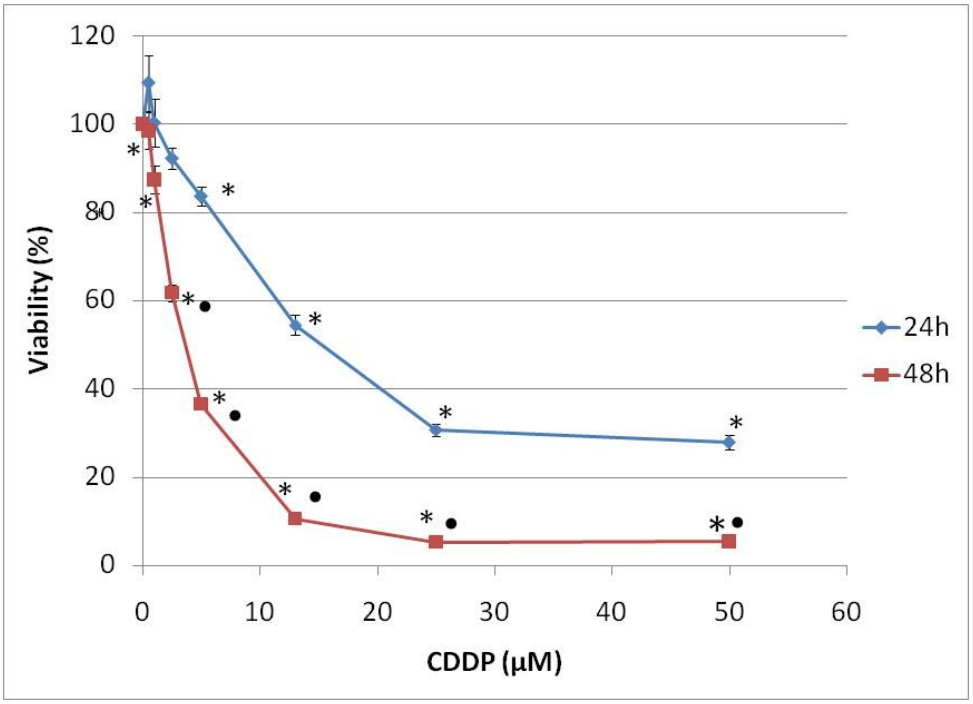

Fig. 4.20. *In vitro* toxicity of CDDP on PC12 cells, expressed as percentage of cell viability vs. CDDP concentration (µM). Bars represent the standard errors. The asterisk indicates significant differences in comparison to untreated controls (* = $p<0.001$). The dot indicates significant differences between 48 and 24 hours of exposure (• = $p<0.05$).

The analyses of cell cycle by flow cytometry in PC12 cells treated with CDDP at 24 an 48 hours (Fig. 4.21) showed alterations in the distribution of cell populations in comparison to controls. At 24 hours of treatment, for low CDDP concentrations (2.5 and 5 µM) a progressive increase in the number of cells in S and a decrease of those in G2/M was detected. For concentrations from 13 µM on, the number of cells in S sharply decreased while a significant increase since the concentration 5 µM of hypodiploid cells was observed. After 48 hours there is a significant decrease ($p<0.001$) in S and G2/M cell population from the CDDP concentration 13 µM onward and a significant increase in the number of hypodiploid cells ($p<0.001$).

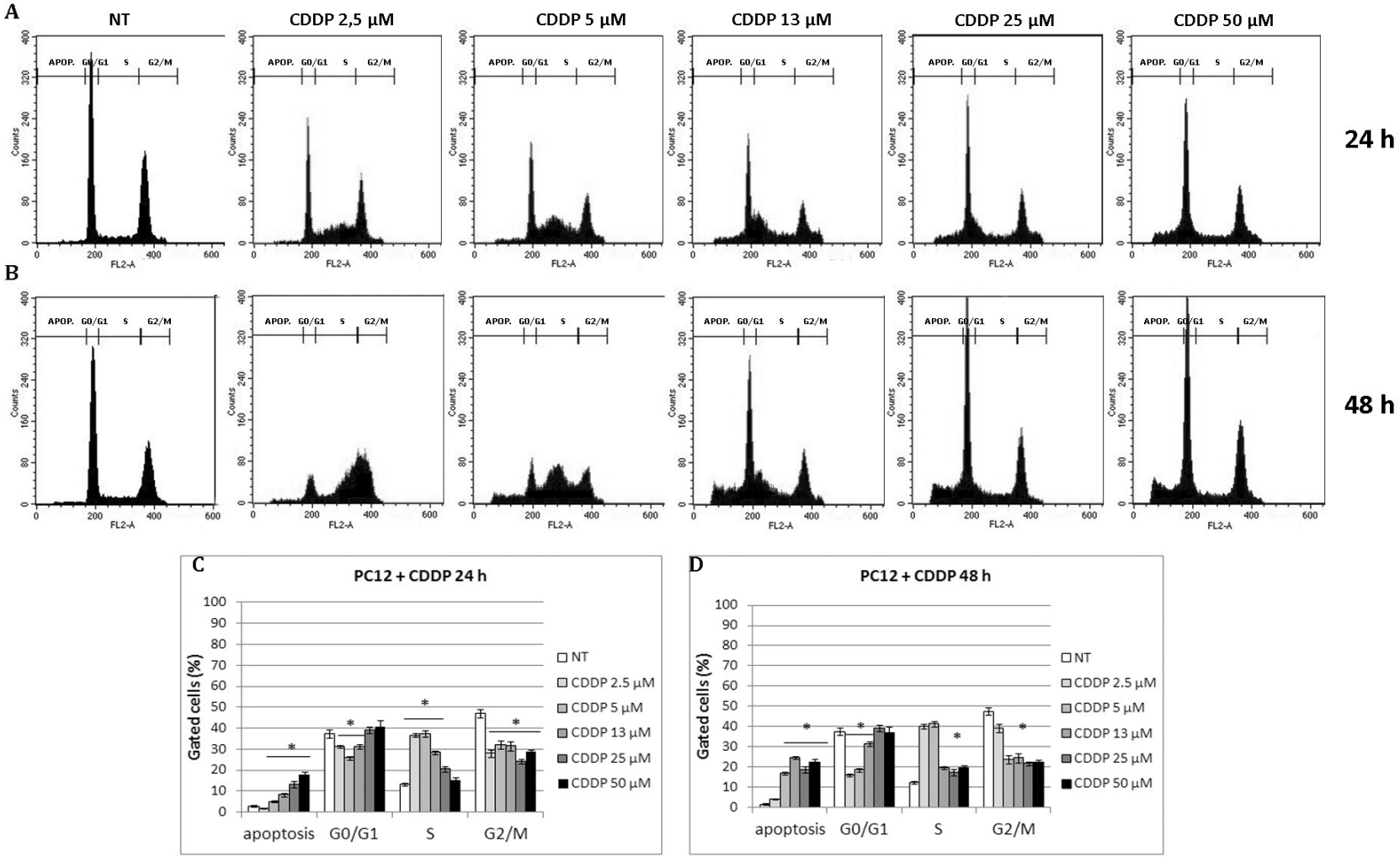

Fig. 4.21. Analyses by flow cytometry of PC12 cells treated with CDDP from 2.5 to 50 µM for 24 and 48 hours. A, B. Number of cells (expressed as counts) in each phase of the cell cycle. For each experimental condition, about 20000 events were analysed. NT, untreated control. APOP, apoptosis. C, D. Distribution of cells expressed as percentage of cells ± standard error in each cell cycle phase. The asterisk indicates significant differences in comparison to untreated controls (* = $p<0.001$).

The induction of apoptotic process by CDDP in PC12 cells was confirmed in morphological tests.

The results of morphological tests by annexin V-FITC and PI on PC12 cells exposed to CDDP 5 µM for 24 hours showed that most adhering cells were stained in green because of binding of annexin V to phosphatidylserine exposed on the cell membrane in the early phases of apoptosis (Fig. 4.22). PC12 are cells that easily detatch from the culture flask if exposed to a high stress condition. Therefore the higher cytotoxicity experiments are usually performed after slide fixation. For this reason after 48 hours of treatment with higly cytotoxic doses of CDDP (13 and 25 µM) it was really difficult to obtain images of the cells treated and they are not reported in Fig. 4.22.

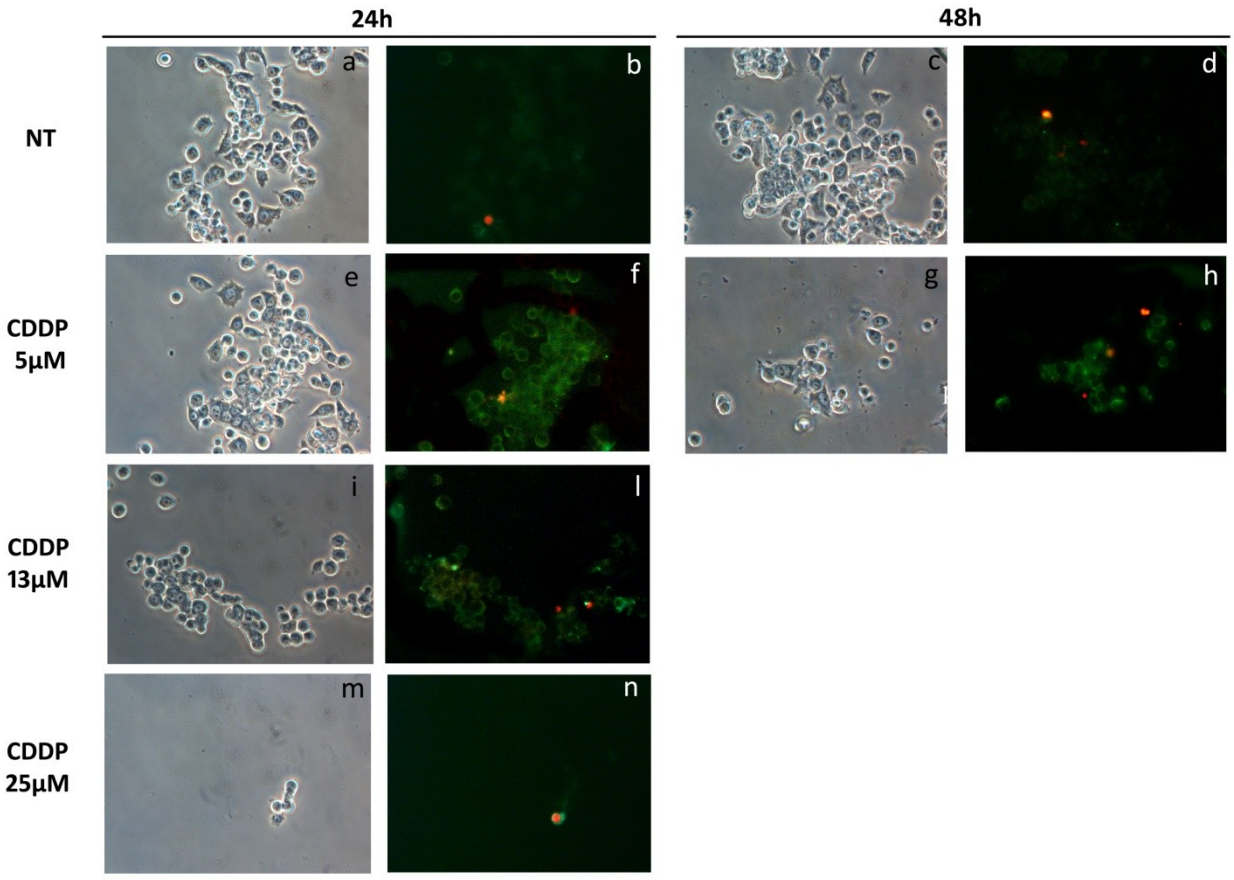

Fig. 4.22. Morphological investigations with annexin V-FITC (green) and propidium iodide (PI) (red) on PC12 cells treated with CDDP (from 5 to 25 µM) at 24 and 48 hours. Images a, c, e, g, i, m are phase contrast. NT, untreated control. Magnification 40x.

The tests with DAPI and phalloidin-TRITC on PC12 cells at the same CDDP concentrations and time of exposure showed a shrinkage in the few cells still adhering to the substrate, a reduction in cytoskeleton and a highly reduced cytoplasm, hardly visible around the nucleus (Fig. 4.23). Several

nuclei appeared fragmented and multi-lobed, showing a chromatin condensation typical of the apoptotic process. At increasing CDDP concentration the number of adhering cells sharply decreased and the last identifiable cells had highly reduced cytoplasms and condensed nuclei.

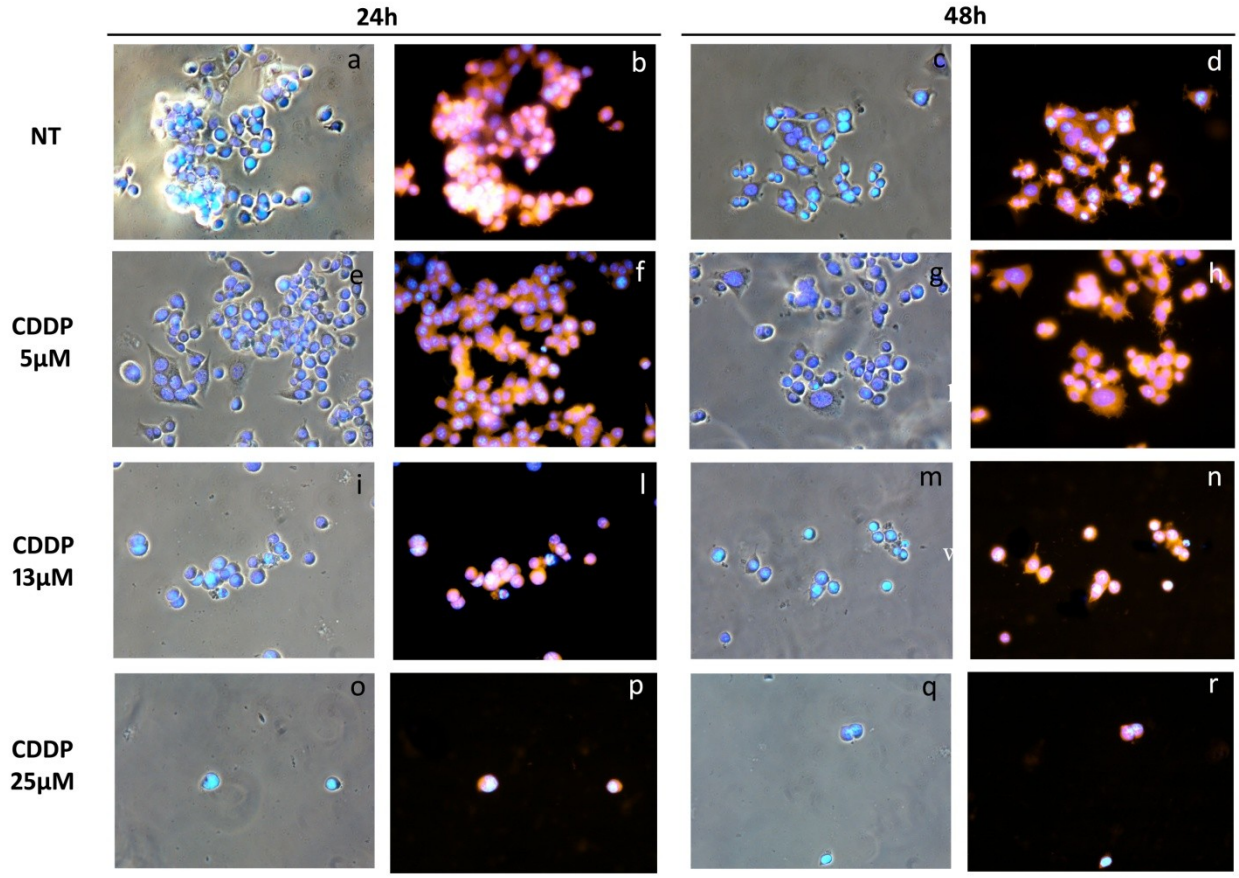

Fig. 4.23. Morphological investigations with DAPI (blue) and phalloidin-TRITC (red) on PC12 cells treated with CDDP(5, 13 and 25 µM) at 24 and 48 hours. Images a, c, e, g, i, m, o, q are colour-combined DAPI-phase contrast. NT, untreated control. Magnification 40x.

In the analysis of gene expression the same genes previously examined for NPsA were investigated for CDDP in PC12 cells: the expression of these transcripts significantly increased in a dose and time dependent way (Fig. 4.24). At the lowest CDDP concentration tested (5 µM) the increased gene expression was significant ($p<0.05$) at 48 hours for almost all genes examined. At higher CDDP concentrations, a significant increase in gene expression was detected, also time dependent. The markers of early apoptotic process, such as caspase 8 and 9, at CDDP 5 µM after 48 hours were significantly overexpressed ($p<0.05$). Caspase 3 was significantly overexpressed already at 5 µM and 24 hours. The levels of p53 increased in a dose and time dependent way, but the increase was significant ($p<0.001$) only at 25 µM after 24 hours. The transcript of BAX was significantly

expressed since the CDDP concentration 5 µM at 24 h ($p<0.05$) onwards in a dose and time dependent way.

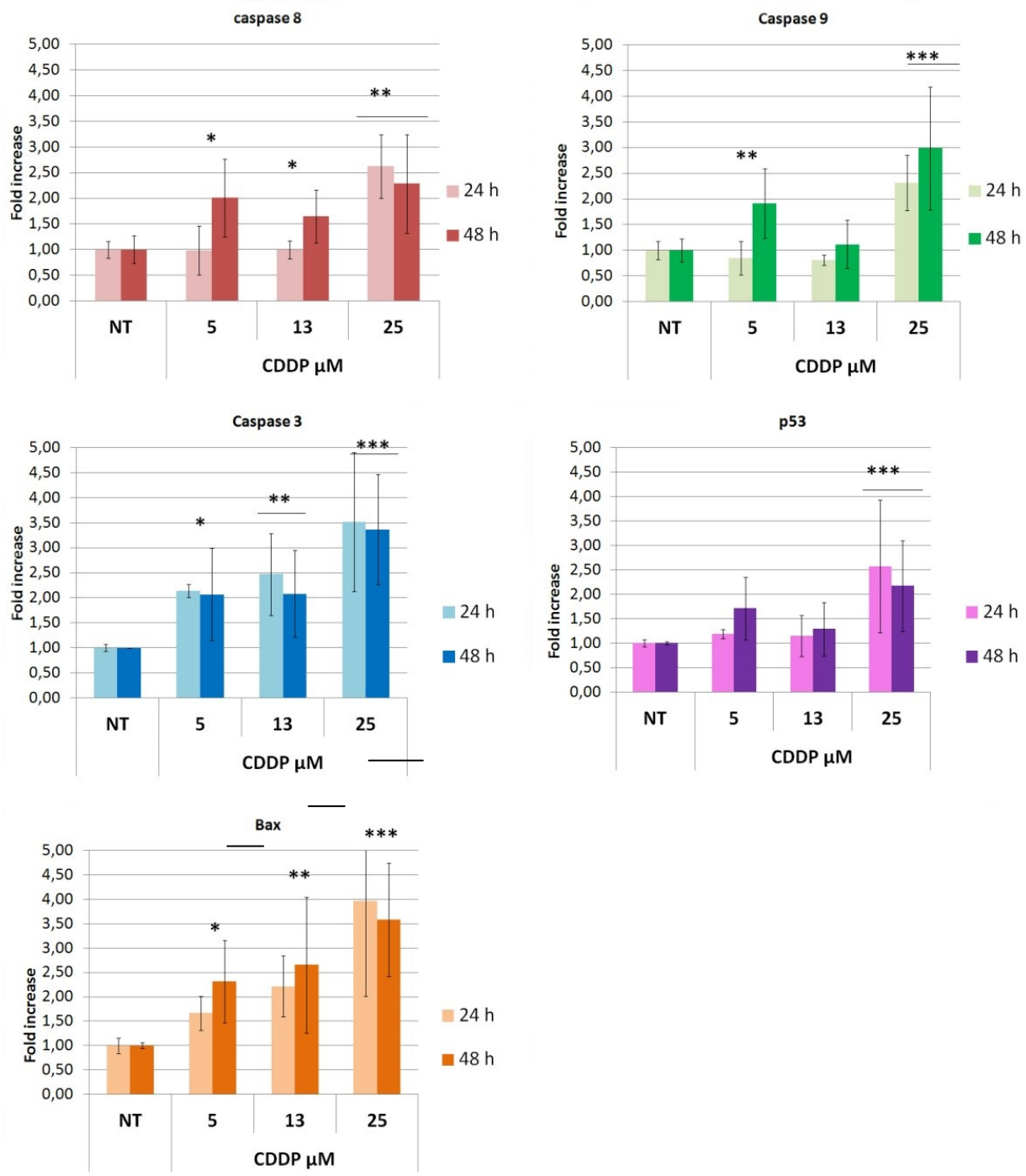

Fig. 4.24. Analyses of relative gene expression by RTqPCR on PC12 cells treated with CDDP (5-25 µM, expressed as normalized fluorescence intensity with standard errors as bars. Asterisks indicate significant values in comparison to control (NT). * = $p<0.05$; **= $p<0.01$; ***=$p<0.001$).

The data of relative gene expression by RTqPCR agreed with those obtained by Western blot: all proteins analysed were overexpressed at all CDDP concentrations and time of exposure examined. The level of expression of PARP, marker of DNA damage, after CDDP treatment, resulted significantly higher in comparison to controls only at 13 µM ($p<0.01$); the level of caspase 3 was also significantly higher since CDDP 5 µM and 48 hours ($p<0.05$) onwards. The level of pERK protein was significantly overexpressed ($p<0.001$) for all the CDDP concentration tested at 24 hours. after 48 hours the levels of pERK decreased compared to the same values at 24 hours, but its expression remain higher than the untreated control (NT).

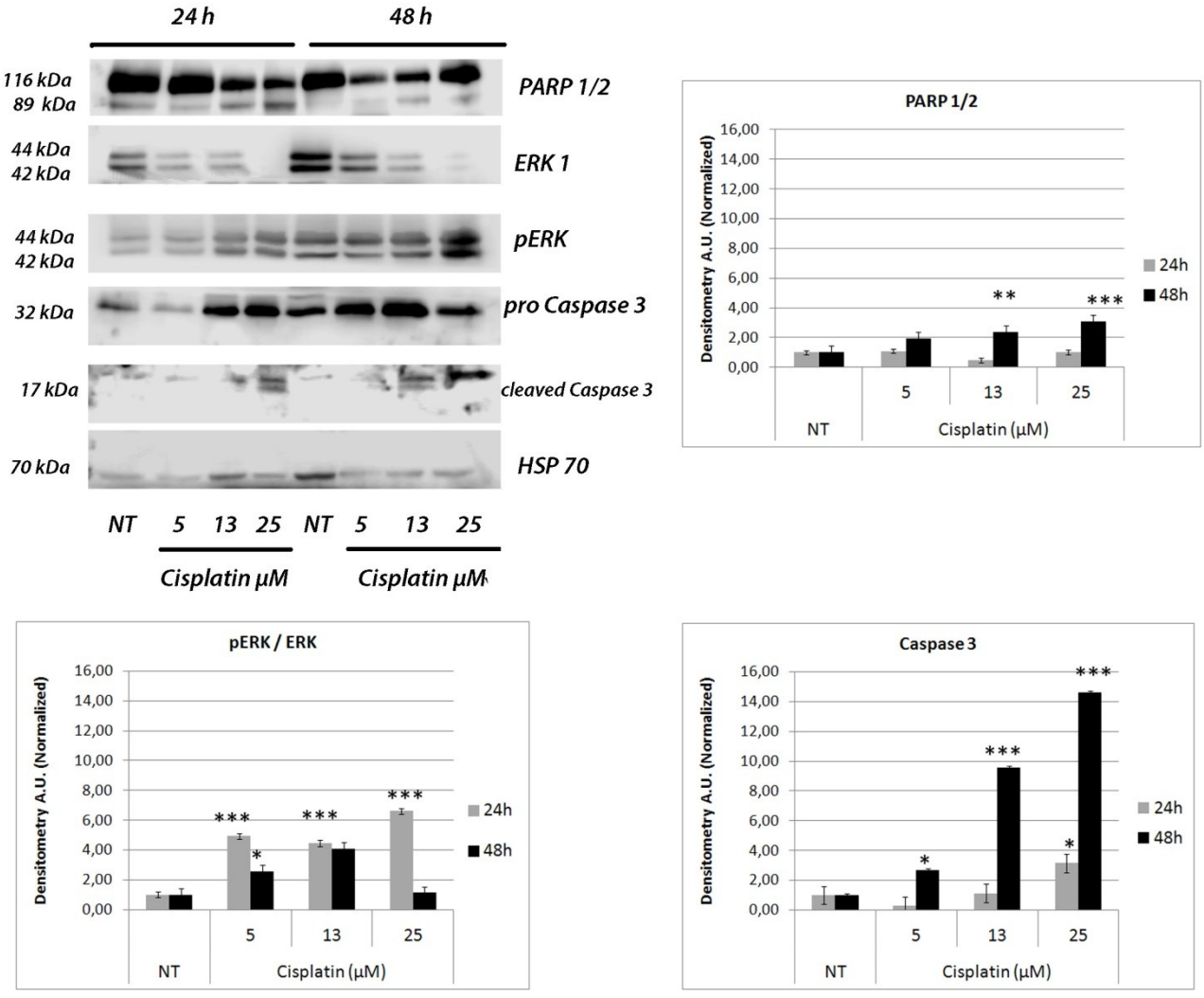

Fig. 4.25. Western Blot after SDS-PAGE and densitometric analysis of key proteins related to apoptosis (with β-actin as standard marker) in PC12 cells treated with CDDP (5, 13 and 25 µM) for 24 and 48 hours. Bars represent standard errors. Asterisks indicate significant values in comparison to control (NT). (* = $p<0.05$;**=$p<0.01$; ***=$p<0.001$).

In OC-k3 cells the exposure to CDDP caused a toxicity dose and time dependent: CDDP was already significantly toxic at 13 µM, causing a 12% decrease of cell viability ($p<0.001$). The toxic effect increased along with CDDP concentrations (Fig. 4.26). At 48 hours the toxicity was significant at 5 µM, with a 12% decrease of cell viability ($p<0.001$) and a 60% decrease at 13 µM a 48 ore ($p<0.001$).

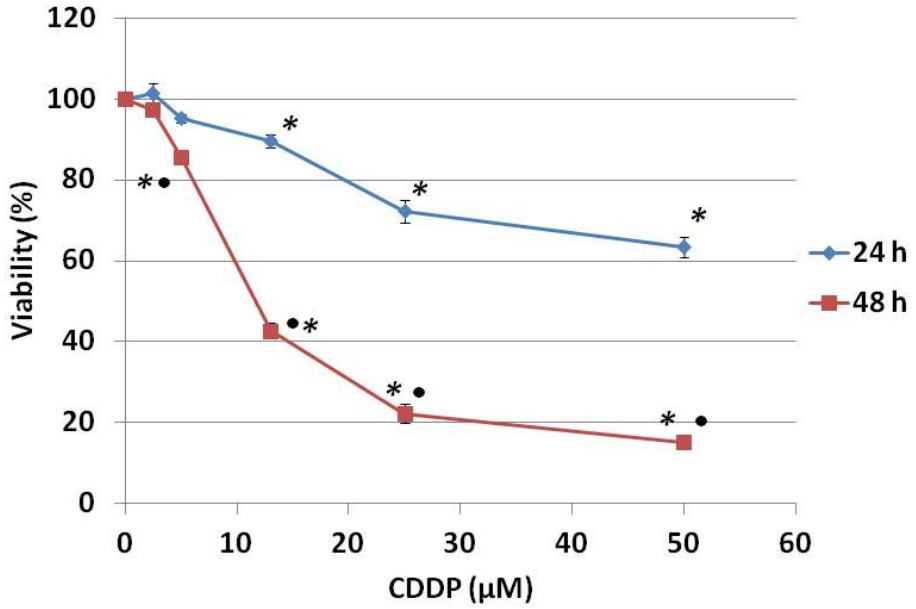

Fig. 4.26. *In vitro* toxicity of CDDP on OC-k3 cells, expressed as percentage of cell viability vs. CDDP concentration (µM). Bars represent the standard errors. The asterisk indicates significant differences in comparison to untreated controls (* = $p<0.001$). The dot indicates significant differences at 48 hours of exposure (• = $p<0.05$).

The analyses of cell cycle by flow cytometry in OC-k3 cells treated with CDDP showed a significant increase of the hypodiploid population at 5 µM and 24 hours (Fig. 4.27), increasing in a dose and time dependent way. At 48 hours the number of cells in G0/G1 phase significantly decrease at the concentrations 2.5 – 25 µg/ml ($p<0.001$), while at the same concentration there is an increase of the S phase cell ($p<0.001$). In G2/M phase a general decrease in cell number was observed from the 13 µM. At 24 hours the increase in hypodiploid cell population (thus undergoing apoptosis) was significant since the CDDP concentration 13 µM ($p<0.001$) onwards; at 48 hours the increase of hypodiploid population is significant ($p<0.001$) since the concentration 2.5 µM of CDDP.

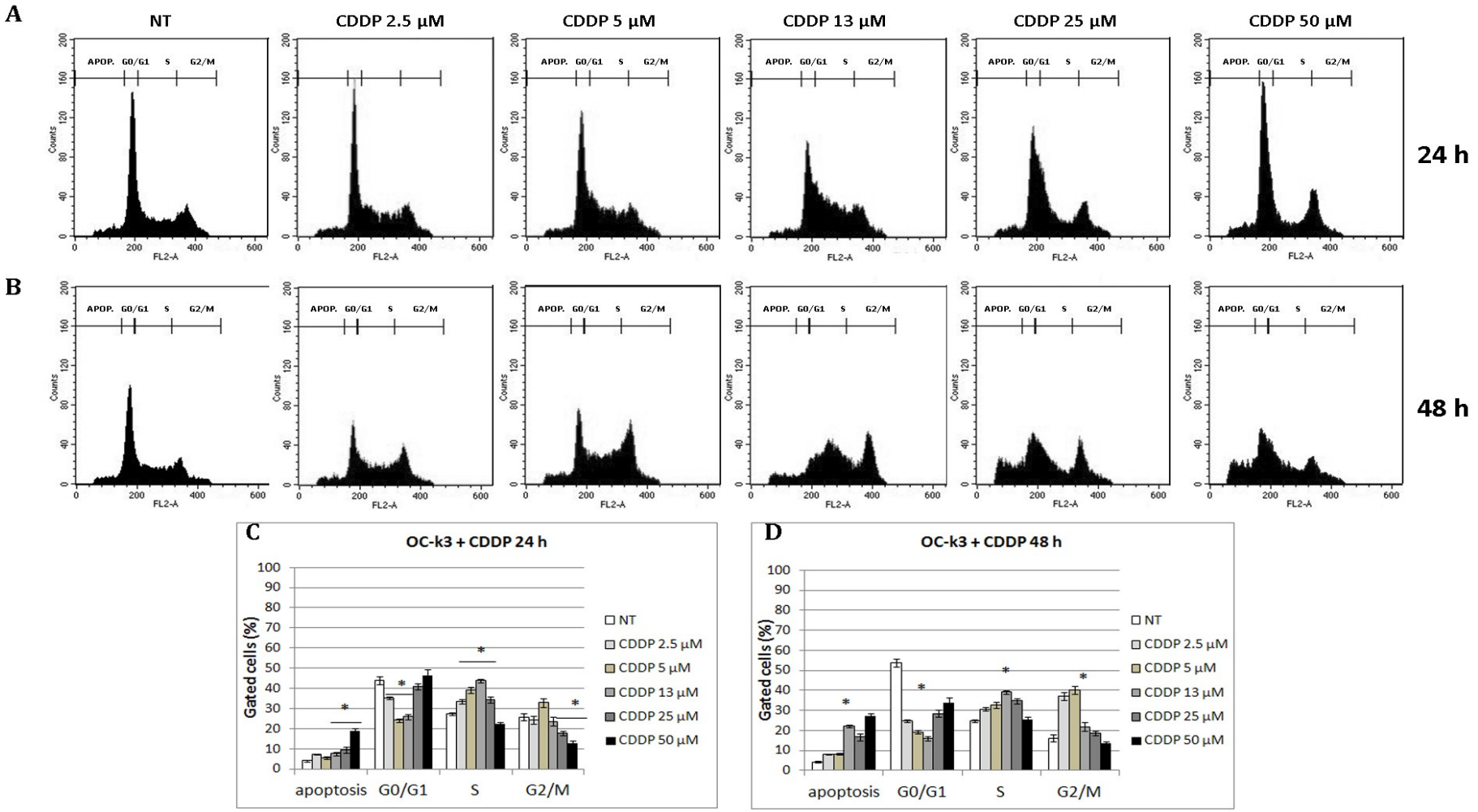

Fig. 4.27. Analyses by flow cytometry of OC-k3 cells treated with CDDP from 2.5 to 50 µM for 24 and 48 hours. A, B. Number of cells (expressed as counts) in each phase of the cell cycle. For each experimental condition, about 20000 events were analysed. NT, untreated control. APOP, apoptosis. C, D. Distribution of cells expressed as percentage of cells ± standard error in each cell cycle phase. The asterisk indicates significant differences in comparison to untreated controls (* = $p<0.001$).

The results of morphological tests by annexin V-FITC and PI on OC-k3 cells exposed to CDDP show a cell death dose and time dependent by apoptosis or necrosis. In controls, a few cells were positive to annexin V-FITC and PI treatment: at 5 µM and 24 hours few cells were positive to annexin V-FITC and PI (Fig. 4.28). The signal increased with CDDP concentration: at 24 hours, a diffused green staining at 13 µM indicated that most cells were entering apoptosis, and at 25 µM most cells were dying and detaching from substrate: the few still adhering showed a double stain (green and red), indicating that the cell membrane was breaking apart and cell death was under way. A remarkable worsening of these conditions at 48 hours, with a low number of adhering cells and a higher number showing annexin V-FITC green signals at low concentrations (Fig. 4.28 J).

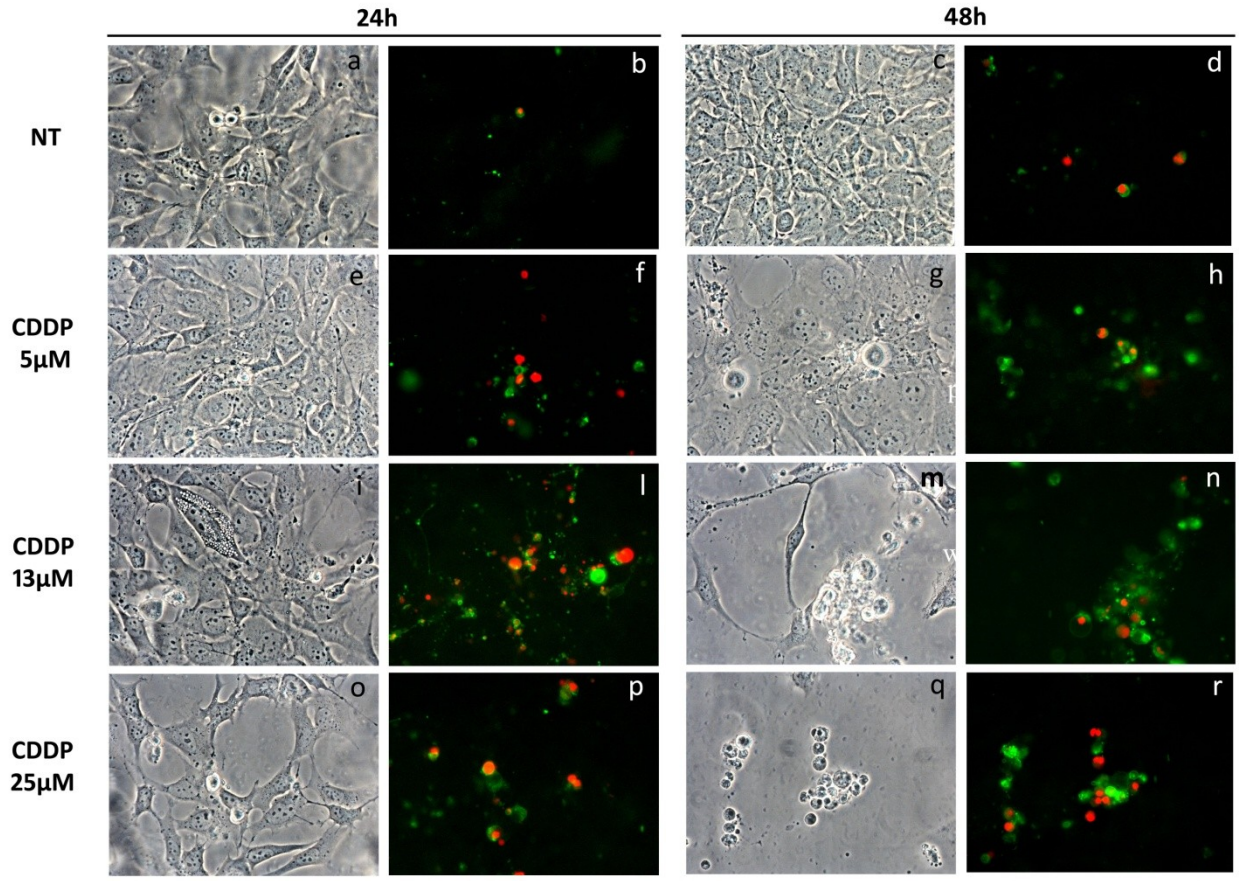

Fig. 4.27. Morphological investigations with annexin V-FITC (green) and PI (red) on OC-k3 cells treated with CDDP (5, 13 and 25 µM) at 24 and 48 hours. Images a, c, e, g, i, m, o, q are phase contrast. NT, untreated control. Magnification 40x.

The effects of CDDP treatment on OC-k3 cells were visible also on cytoskeleton, morphologically analysed by DAPI and phalloidin TRITC: marked alterations were observe in cytoskeleton as well

as in cell nuclei (Fig. 4.29). At 24 hours the normal shape of OC-k3 cells, long and narrow with long microtubules (Fig. 4.29B), was altered at 5 µM, the lowest CDDP concentration: cells appeared enlarged and roundish, with swollen nuclei (Fig. 4.29F). At 13 µM and 24 hours, or at 48 hours, these effects were more evident: the cytoskeleton fibers were shorter and thicker, and chromatin appeared fragmented within the nuclei (Fig.4.29 H-L). At increasing concentration and time of exposure the few adhering cells were completely distorted, with scarce cytoplasm and multi-lobed nuclei (Fig.4.29 N-P).

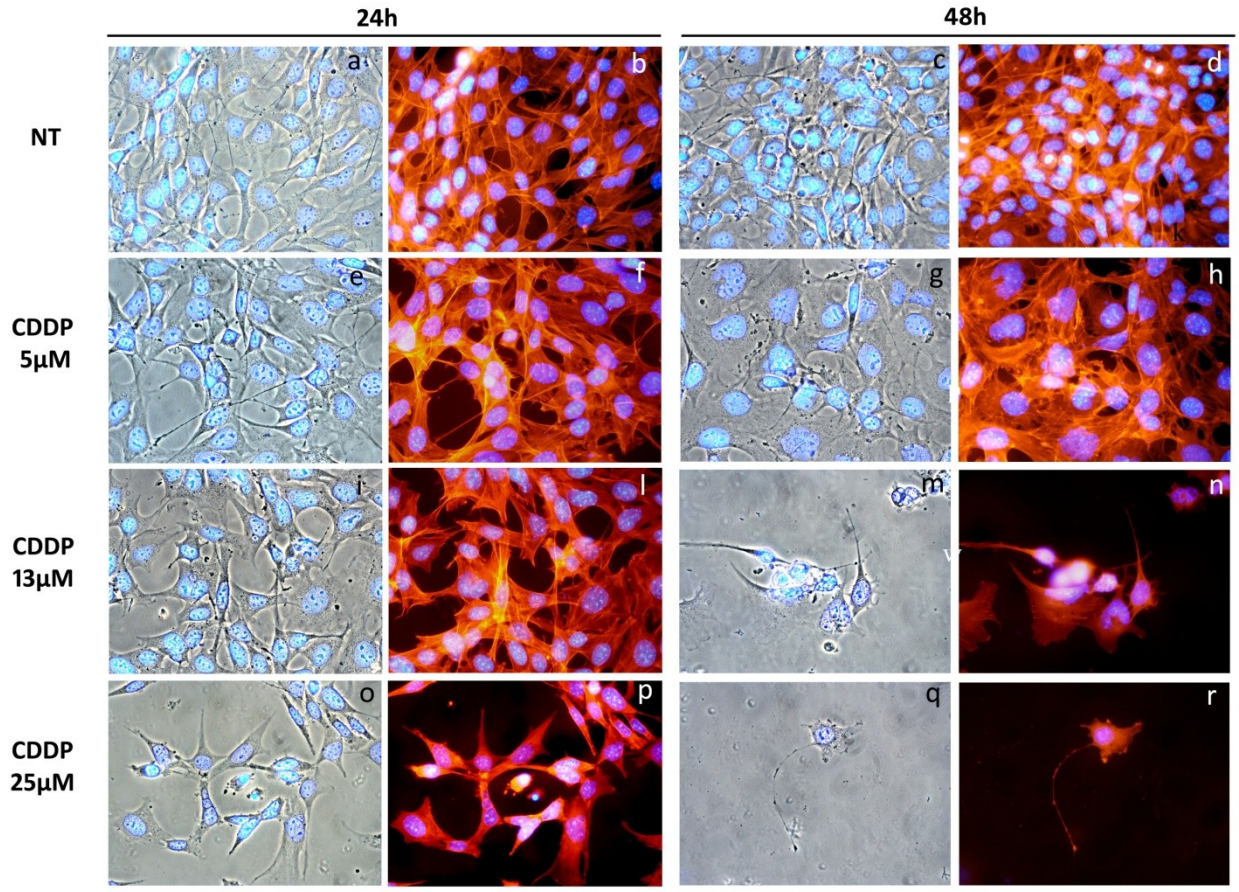

Fig. 4.29. Morphological investigations with DAPI (blue) and phalloidin-TRITC (red) on OC-k3 cells treated with CDDP (5, 13 and 25 µM) at 24 and 48 hours. Images a, c, e, g, i, m, o, q are colour-combined DAPI-phase contrast. NT, untreated control. Magnification 40x.

As for PC12 cells, the analyses by RTqPCR showed that CDDP induced in OC-k3 cells an overexpression of genes related to apoptosis in a dose and time dependent way (Fig. 4.30). The gene expression profiles appeared homogeneous in their response to treatment, with a gradual increase in all analysed transcripts. In OC-k3 a higher activation of the extrinsic pathway to

apoptosis was initially observed, with a significant increase of caspase 8 levels at 5 µM ($p<0.05$), while the expression of caspase 9 was significantly higher only at 25 µM after 48 hours ($p<0.01$). Concerning the other genes involved in the late apoptotic process (p53, BAX, Bid and caspase 3) an overexpression was observed increasing the concentration of CDDP, reaching a high significance ($p<0.001$) at 25 µM and 24 hours.

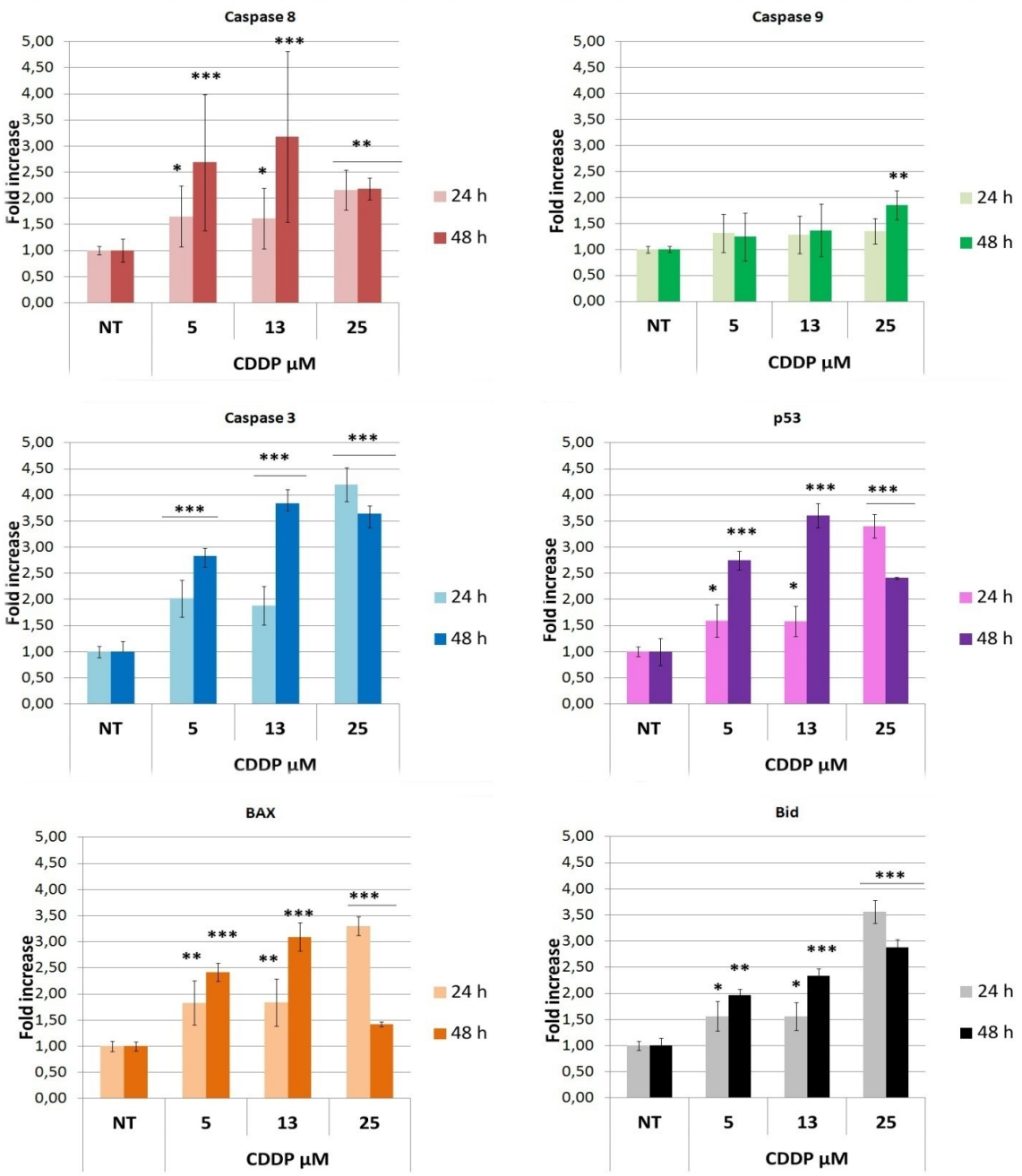

Fig. 4.30. Analyses of relative gene expression by RTqPCR on OC-k3 cells treated with CDDP (5, 13 and 25 µM) expressed as normalized fluorescence intensity with standard errors as bars. Asterisks indicate significant values in comparison to control (NT). (* = $p<0.05$; **= $p<0.01$; ***=$p<0.001$).

Also in OC-k3 cells the results of gene expression analyses agreed with those obtained by Western blot. The analyses of apoptotic markers at low CDDP concentration revealed a significant increase in pERK ($p<0.05$), caspase 3 ($p<0.01$) and PARP ($p<0.001$), in a dose and time dependent way (Fig. 4.31). The protein expression matched that of the transcripts examined by RTqPCR, indicating that cells entered apoptosis at low CDDP concentration. In detail, at 24 hours the level of cleaved caspase 3 was already significant at low CDDP concentration, indicating an advance apoptosis of a large number of cells. The cleaved PARP underwent a sharp increase at CDDP 25 µM at both 24 and 48 hours, indicating that DNA repair mechanisms were highly impaired by CDDP activity.

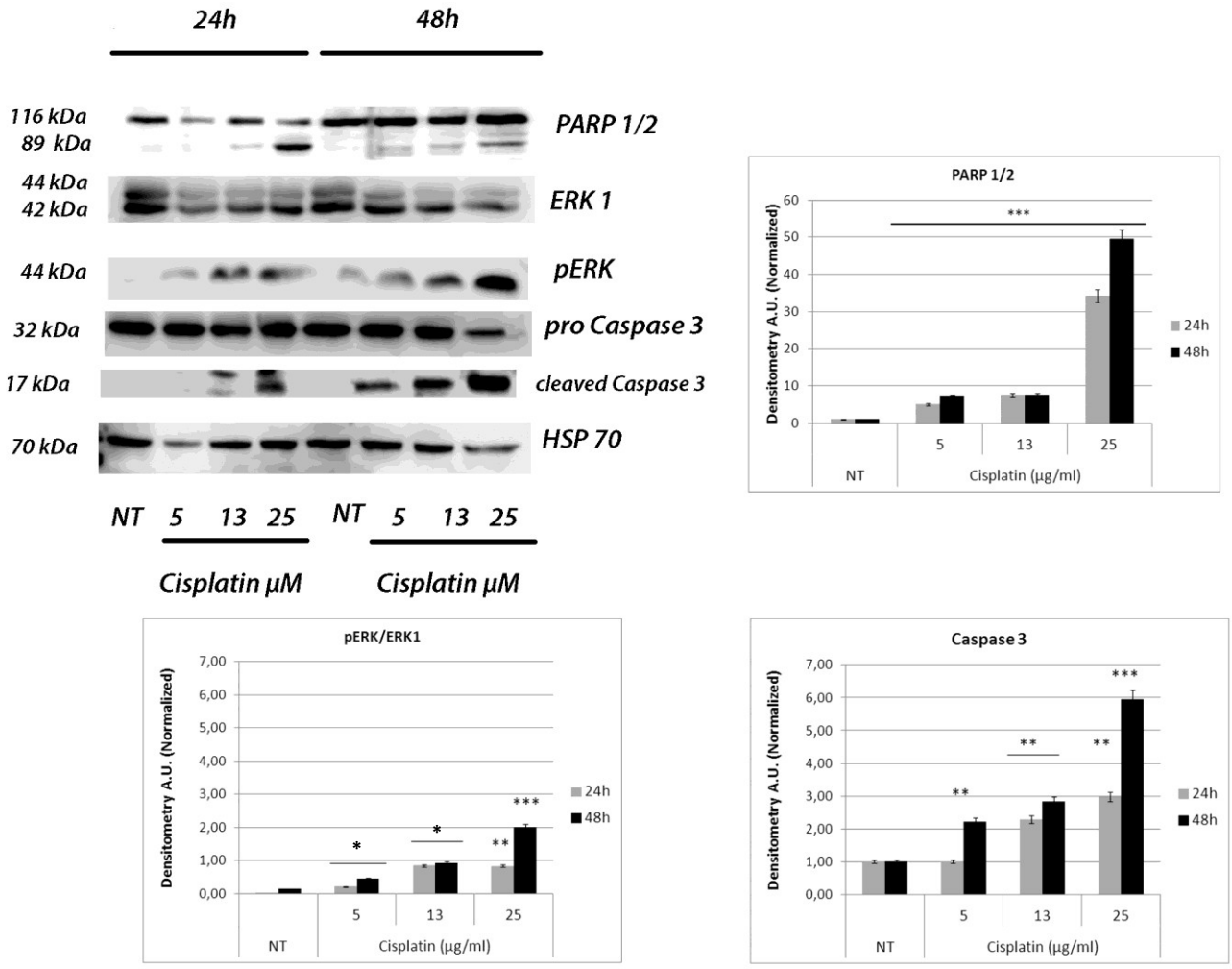

Fig. 4.31. Western Blot after SDS-PAGE and densitometric analysis of key proteins related to apoptosis (with HSP 70as standard marker) in OC-k3 cells treated with CDDP (5, 13 and 25 µM) for 24 and 48 hours. Bars represent standard errors. Asterisks indicate significant values in comparison to control (NT) (**=$p<0.01$; ***=$p<0.001$).

4.4 Protection analyses

For co-treatment tests of *in vitro* cell protection, cell lines were pre-treated for 24 hours with NPsQ or NPsD at different concentrations and afterwards with CDDP at different concentrations for 24 and 48 hours: the purpose was to obtain a full interaction between cells and NPs conjugated with pharmacological drugs, and therefore a maximum protection against CDDP cytotoxic effects. The only reported data were those concerning CDDP concentrations at which protective effects were detected in co-treatment with NPsD or NPsQ.

4.4.1 Experiments with NPsQ and CDDP

In co-treatment viability tests, the PC12 cells were pre-treated for 24 hours with NPsQ (25-100 µg/ml), then co-treated with CDDP 5 µM and the same NPsQ concentrations for 24 and 48 hours. A time dependent protective effect was detected, with an increase of cell viability in comparison to cells treated only with CDDP (Fig. 4.51). After 24 hours of co-treatment, from NPsQ 25 µg/ml onwards, a recovery of cell viability was observed which became significant at NPsQ 75-100 µg/ml ($p<0.05$), restoring the viability to values similar to controls. After 48 hours of co-treatment, CDDP 5 µM induced a 60% decrease in cell viability. The protective effect of NPsQ was observed from 25 µg/ml ($p<0.01$) and increased for higher NPsQ concentrations, 75-125 µg/ml ($p<0.001$). Data obtained at higher CDDP concentrations did not show any protective effect at all NPsQ concentrations tested (data not reported).

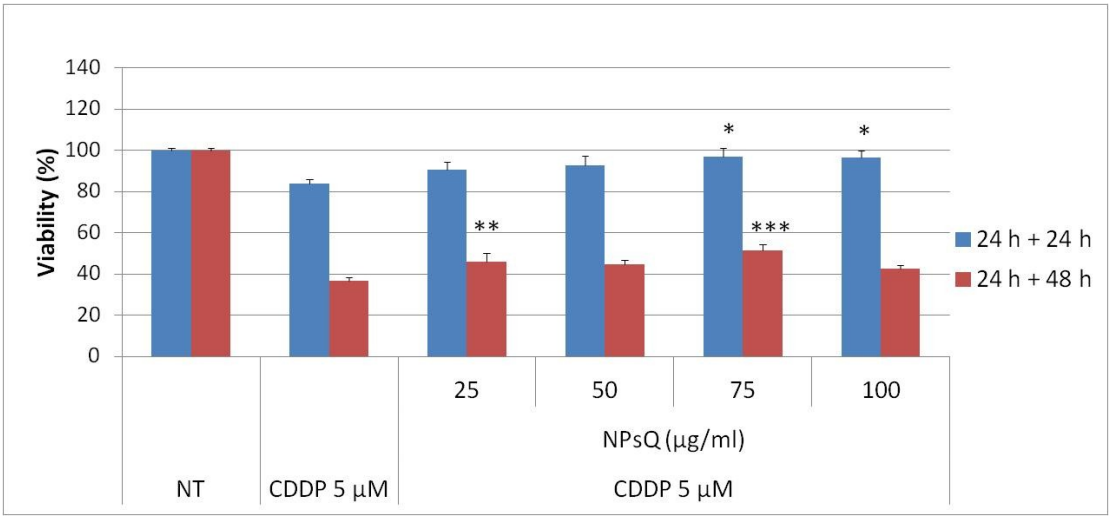

Fig. 4.51. Viability of PC12 cells pre-treated for 24 hours with NPsQ (25-100 µg/ml), then co-treated with CDDP 5 µM and the same NPsQ concentrations for 24 and 48 hours. Bars represent the standard errors. NT: untreated controls. Asterisks indicate significant differences in comparison to CDDP alone. (* = $p<0.05$; ** = $p<0.01$; ***=$p<0.001$).

The analyses of cell cycle by flow cytometry showed that CDDP 5 µM was able to impair the distribution of PC12 cell populations in the different phases of the cell cycle, while the co-treatment with NPsQ did not induce a significant recovery in comparison to untreated controls (Fig. 4.52). At 24 hours, CDDP alone induced an increase in hypodiploid cell population and of the number of cells in S, with a consequent decrease of the number of cells in G0 and G2/M. When PC12 cells were pre-treated with NPsQ 25 and 75 µg/ml, only a slight decrease of hypodiploid cell population was observed for NPsQ 25 µg/ml. At 48 hours, CDDP caused a further increase of the hypodiploid cell population and of the number of cells in G0 and G2/M. Again, at this time of exposure NPsQ were not apparently able to provide any protection against CDDP negative effects on PC12 cell cycle.

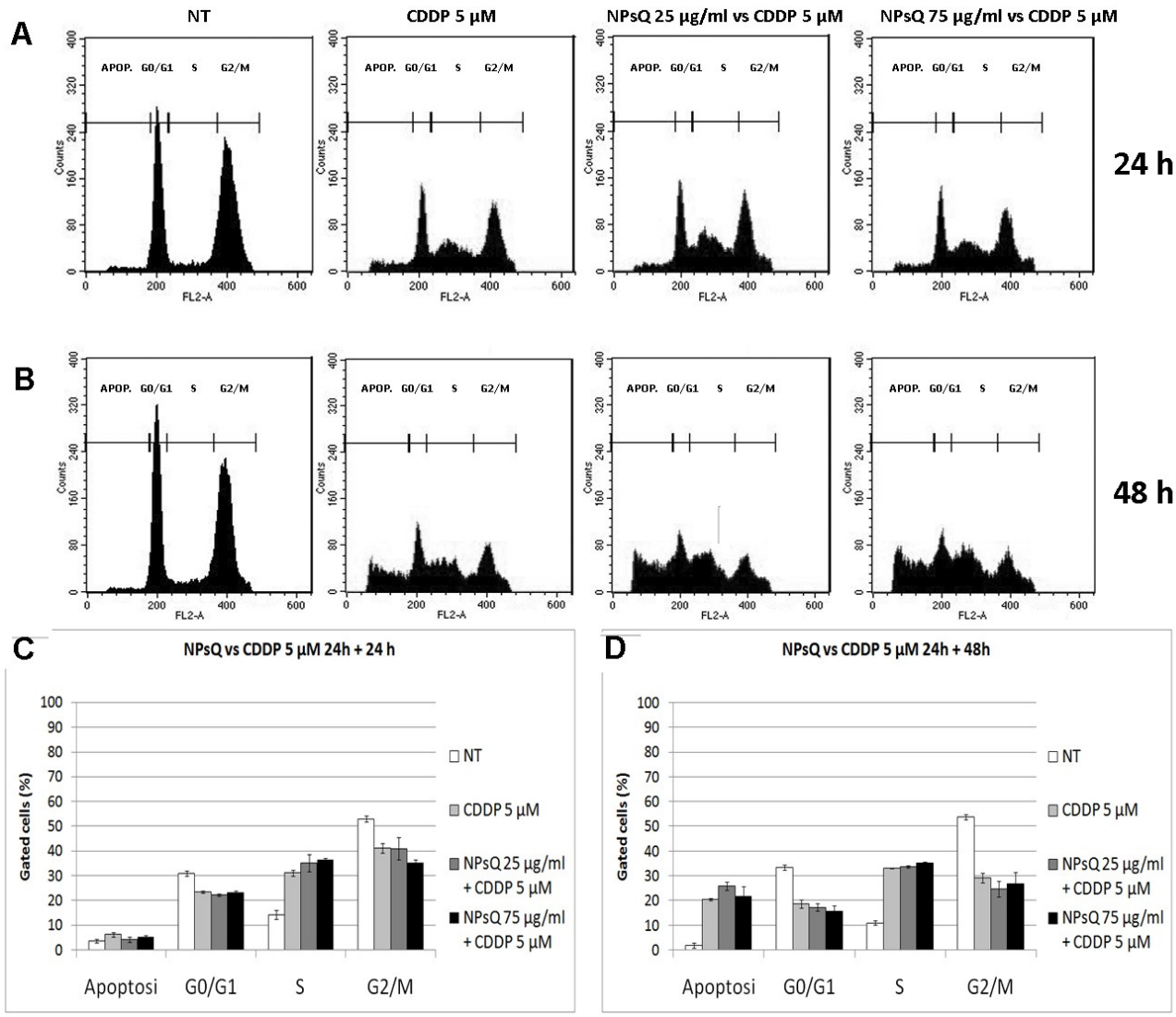

Fig. 4.52. Analyses by flow cytometry of PC12 cells pre-treated for 24 hours with NPsQ (25 and 75 µg/ml), then co-treated with CDDP 5 µM and the same NPsQ concentrations for 24 and 48 hours. A, B. Number of cells (expressed as counts) in each phase of the cell cycle. For each experimental condition, about 20000 events were analysed. NT, untreated control. APOP, apoptosis. C, D. Distribution of cells expressed as percentage of cells ± standard error in each cell cycle phase.

In treatments with CDDP 5 µM a sharp decrease in adhering cells was observed, more evident at 48 hours (Fig. 4.53). The number of adhering cells increased in co-treatments with NPsQ 75 µg/ml (Fig. 4.53 N-P).The normal shape of PC12 cells, roundish and flattened, changed after CDDP treatment and cells appeared smaller and round even in co-treatments. At 48 hours of co-treatment with NPsQ 75 µg/ml, in comparison to CDDP alone a lower number of multi-lobed nuclei was

observed in cells. The cytoskeleton and the amount of cytoplasm inside the cells appeared unchanged in co-treatments in comparison to CDDP alone.

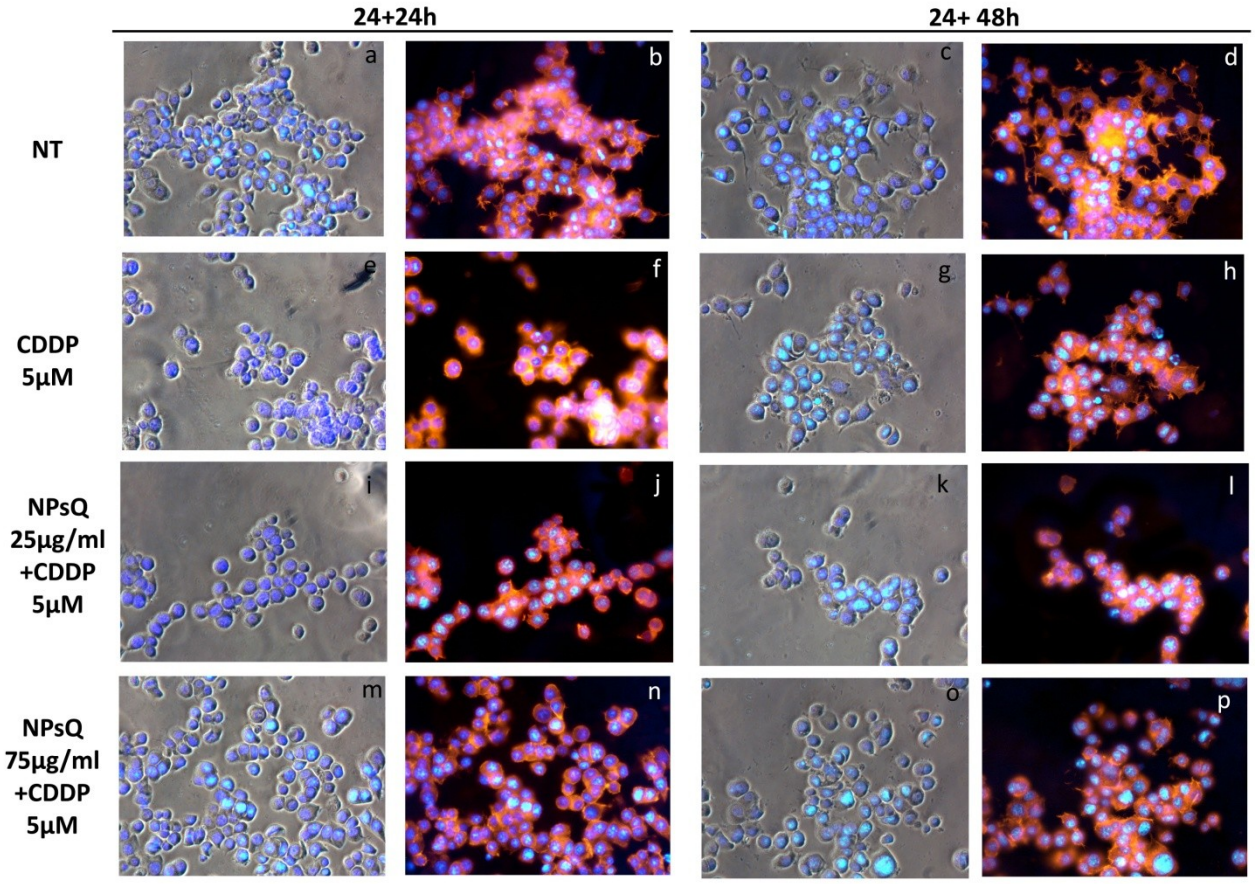

Fig. 4.53. Morphological investigations with DAPI (blue) and phalloidin-TRITC (red) on PC12 cells pre-treated for 24 hours with NPsQ (25 and 75 µg/ml), then co-treated with CDDP 5 µM and the same NPsQ concentrations for 24 and 48 hours. Images a, c, e, g, i, k, m, o are colour-combined DAPI-phase contrast. NT, untreated control. Magnification 40x.

The gene expression analyses by RTqPCR on PC12 cells pre-treated for 24 hours with NPsQ, then co-treated with CDDP 5 µM for 24 and 48 hours, did not reveal any protective effect of NPsQ against CDDP, but the cell response significantly changed in a time dependent way (Fig. 4.54). The treatment with CDDP 5 µM induced an increase in expression of all genes related to apoptosis, at both 24 and 48 hours. After 24 hours of co-treatment the expression of the analysed genes is similar or higher than that with CDDP alone. In co-treatment with NPsQ 25 µg/ml the caspase 8 caspase 9 genes were both overexpressed in comparison to CDDP alone. The BAX, p53 and caspase 3 further increased their overexpression in co-treatments with NPsQ 75 µg/ml. At 48 hours of co-treatment,

all analysed genes showed a marked decrease in expression in comparison to 24 hours and to CDDP alone, except for caspase 3. In co-treatments with NPsQ 25 and 75 µg/ml the expression of caspase 8 and BAX was even lower than in untreated controls ($p<0.001$).

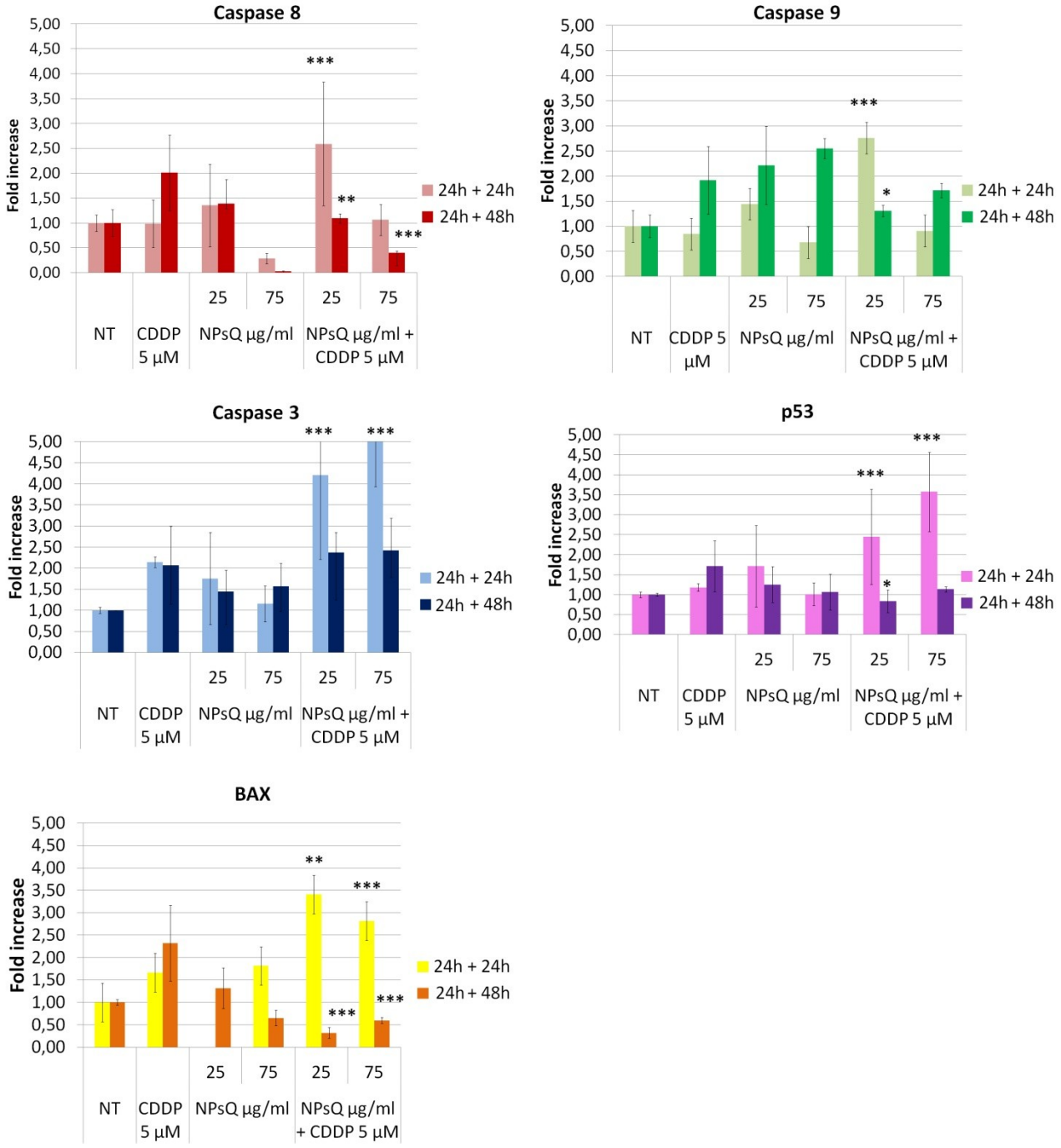

Fig. 4.54. Analyses of relative gene expression by RTqPCR on PC12 cells pre-treated for 24 hours with NPsQ (25 and 75 µg/ml), then co-treated with CDDP 5 µM and the same NPsQ concentrations for 24 and 48 hours, expressed as normalized fluorescence intensity with standard errors as bars. Asterisks indicate significant values in comparison to CDDP 5 µM (* = $p<0.05$; **= $p<0.01$; ***=$p<0.001$)

Data of protein expression markers related to apoptosis analysed by Western blot in PC12 cells pre-treated for 24 hours with NPsQ, then co-treated with CDDP and NPsQ for 24 and 48 hours indicated a time dependent cell response to co-treatments (Fig. 4.55). At both 24 and 48 hours CDDP induced a marked expression increase of the analysed proteins. At 24 hours of co-treatment the level of cleaved caspase 3 increased at increasing concentrations of NPsQ. The level of cleaved PARP decreased at 24 hours with significant values at the highest NPsQ concentration ($p<0.05$). The levels of pERK decreased at 24 hours at decreasing NPsQ concentrations ($p<0.01$). At 48 hours an improving of protection was detected in co-treatments, with levels of expression of all analysed proteins significantly lower than at 24 hours.

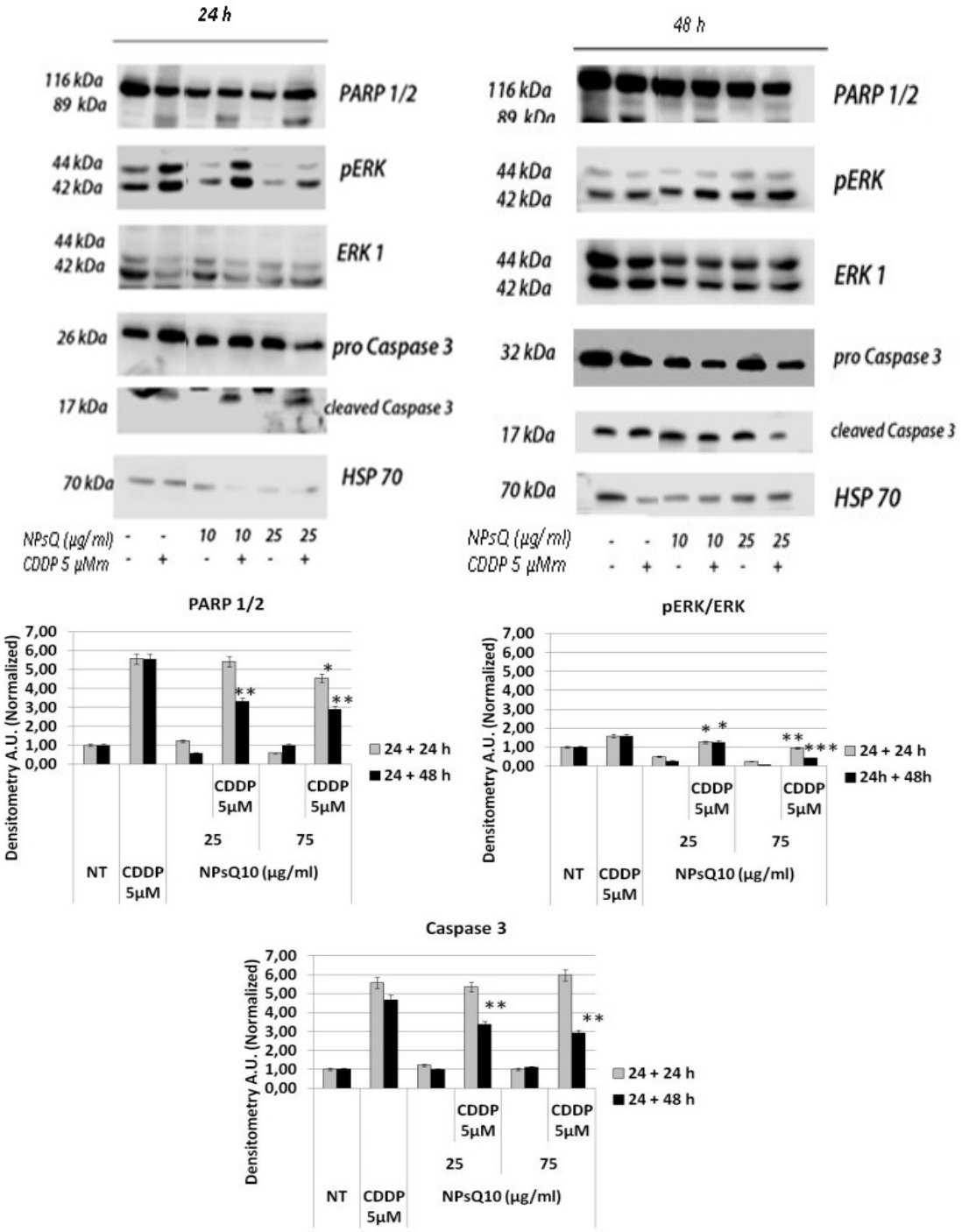

Fig. 4.55. Western Blot after SDS-PAGE and densitometric analysis of key proteins related to apoptosis (with HSP-70 as standard marker) inPC12 cells pre-treated for 24 hours with NPsQ (25 and 75 µg/ml), then co-treated with CDDP 5 µM and the same NPsQ concentrations for 24 and 48 hours. Bars represent standard errors. Asterisks indicate significant values in comparison to CDDP 5 µM (* = $p<0.05$; **=$p<0.01$; ***$p<0.001$).

Based on the results of viability assay with NPsQ on OC-k3 cells, it was decided to use the NPsQ concentration 10-25-50 µg/ml in the co-treatments, against the CDDP 5 and 13 µM.

On OC-k3 cells the co-treatments with NPsQ were protective only in comparison to CDDP 5 µM (Fig.4.56). At 24 hours of co-treatment a slight recovery of cell viability at NPsQ 10-25 µg/ml was observed. At NPsQ 50 µg/ml the cell viability decreased at lower levels in comparison to CDDP 5µM. At 48 hours CDDP was more toxic and in co-treatments a significant recovery was observed only at NPsQ 10 µg/ml ($p<0.05$). A further decrease in cell viability appeared at higher concentrations of CDDP, at both 24 and 48 hours, and co-treatments with NPsQ did not induce any significant recovery.

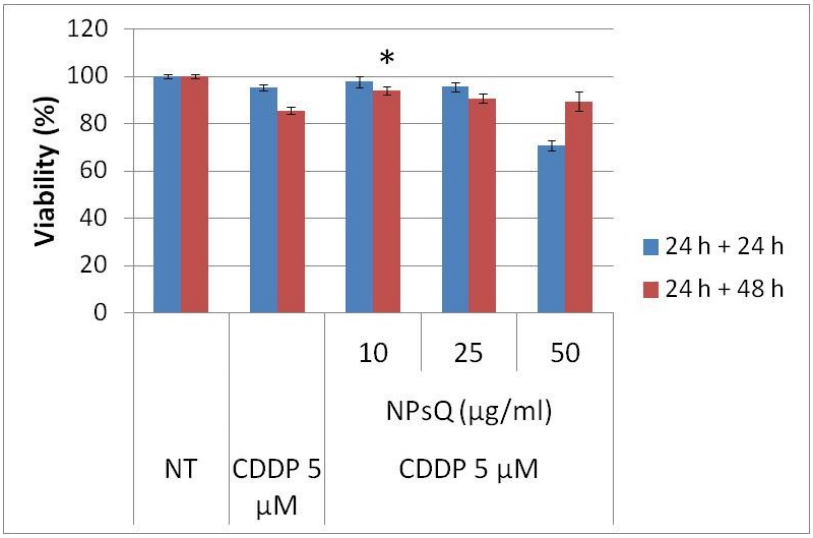

Fig. 4.56. Viability of OC-k3 cells pre-treated for 24 hours with NPsQ (NPsQ10) (10-50 µg/ml), then co-treated with CDDP 5 µM and the same NPsQ concentrations for 24 and 48 hours. Bars represent the standard errors. NT: untreated controls. Asterisks indicate significant differences in comparison to CDDP alone. (* = $p<0.05$).

The analyses by flow cytometry on OC-k3 co-treated cells showed that CDDP 5 µM induced a change in cell population distribution at 24 hours, with a significant decrease of the number of cells in G0 and an increase in S and G2 (Fig. 4.57). At 24 hours the effect of co-treatments is observed only at the NPsQ concentration 25 µg/ml, inducing a slight (although not significant) decrease in number of cells in S and an increase in G2/M compared to CDDP only. At 48 hours, CDDP 5 µM induced a sharp decrease in number of cells in G0 and S, and an increase in G2/M and hypodiploid cell population. No significant recovery of these adverse effects was detected in co-treatments with NPsQ.

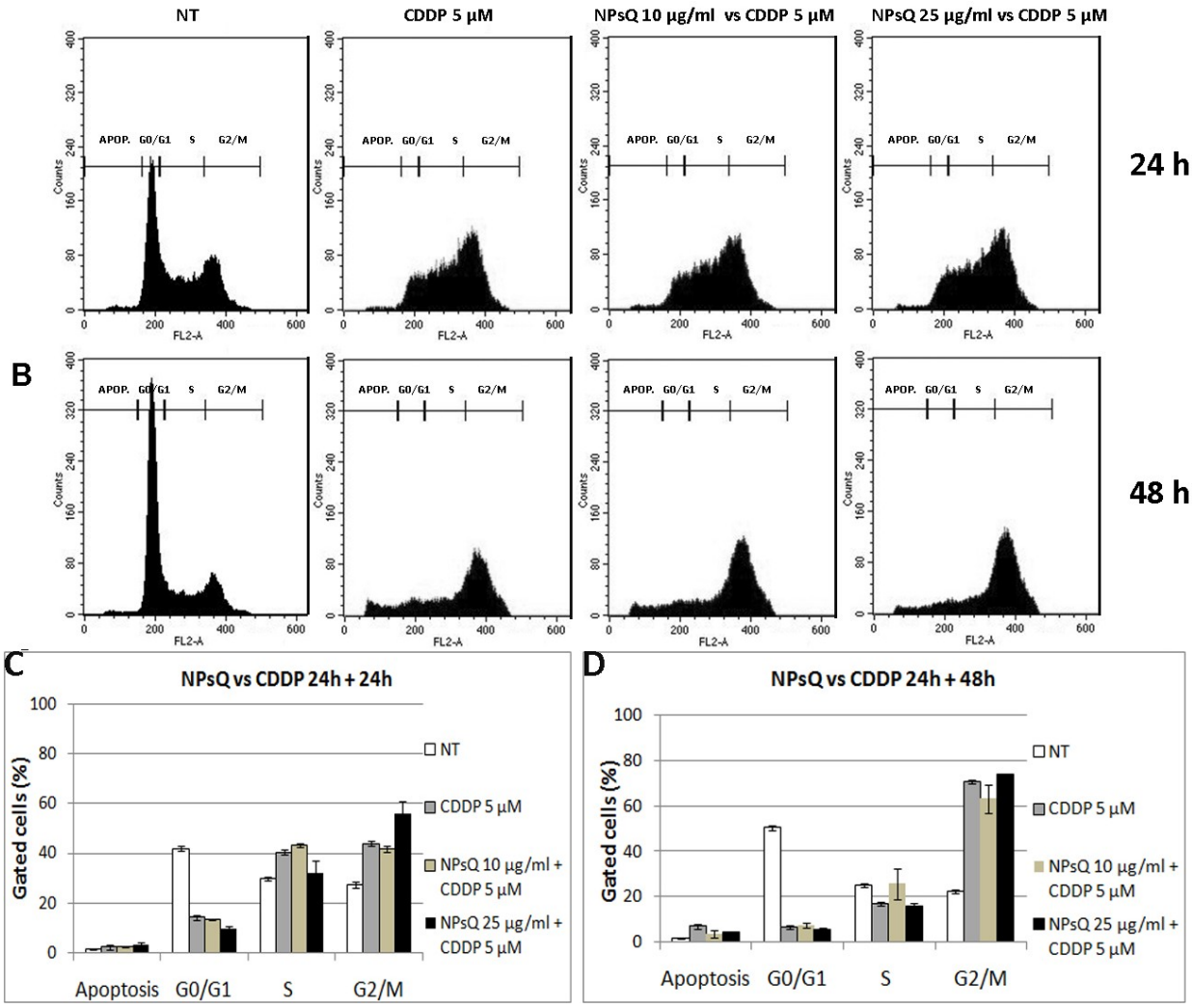

Fig. 4.57. Analyses by flow cytometry of OC-k3 cells pre-treated for 24 hours with NPsQ (10 and 25 µg/ml), then co-treated with CDDP 5 µM and the same NPsQ concentrations for 24 and 48 hours. A, B. Number of cells (expressed as counts) in each phase of the cell cycle. For each experimental condition, about 20000 events were analysed. NT, untreated control. APOP, apoptosis. C, D. Distribution of cells expressed as percentage of cells ± standard error in each cell cycle phase.

In morphological investigations with annexin V-FITC and PI on OC-k3 cells co-treated with NPsQ and CDDP, after 24 hours od co-treatment no significant differences were detected between untreated controls, CDDP 5 µM and co-treatments (Fig. 4.58). After 48 hours of exposure to CDDP most cells were positive to annexin V-FITC and PI, indicating an advanced apoptosis. In co-treatments a slight reduction of the cells in apoptosis, showing green or double stains (initial

apoptosis) was detected at NPsQ 10 µg/ml and 48 hours of co-treatment. At 25 µg/mlNPsQan increase of cells showing the double stain was observed.

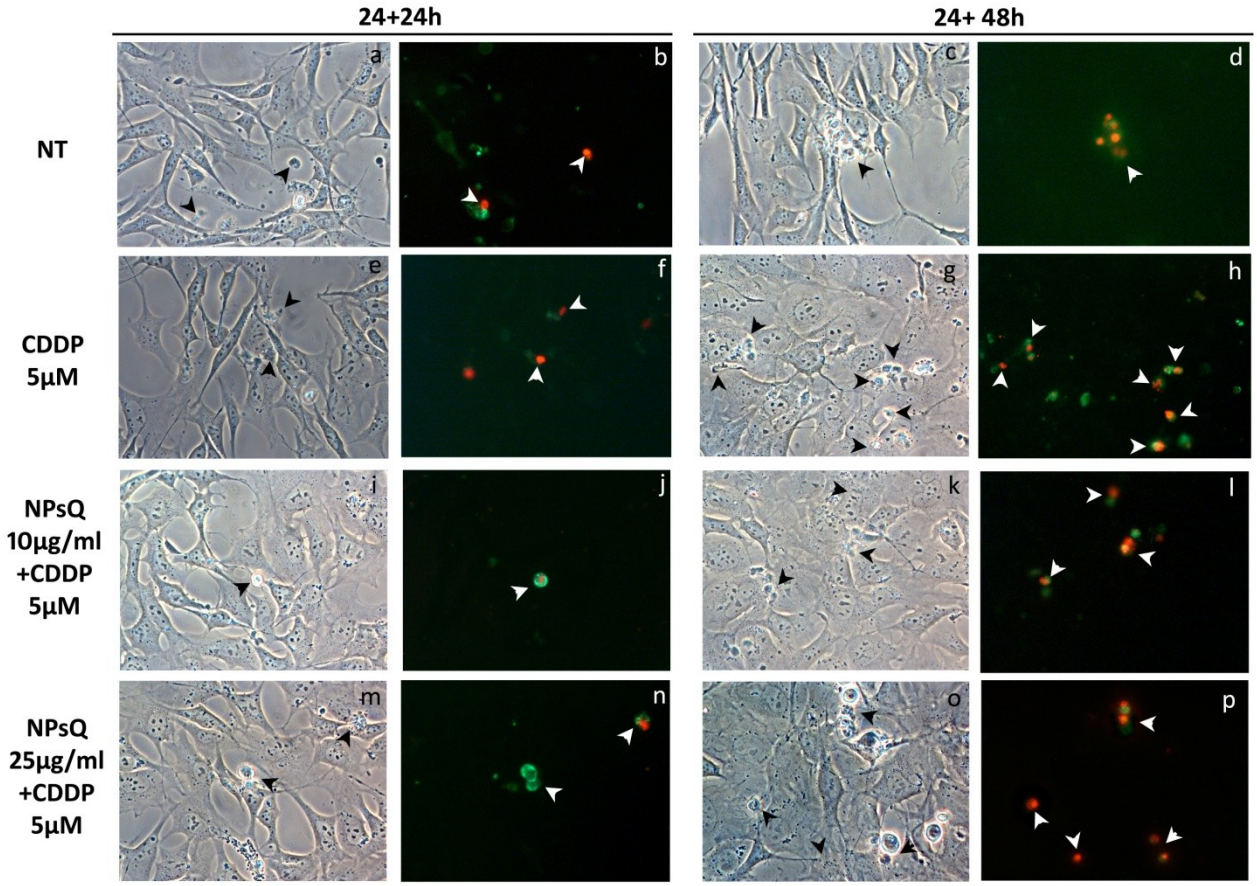

Fig. 4.58. Morphological investigations with annexin V-FITC (green) and PI (red) on OC-k3 cells pre-treated for 24 hours with NPsQ (10 and 25 µg/ml), then co-treated with CDDP 5 µM and the same NPsQ concentrations for 24 and 48 hours. White arrowheads indicate cells in apoptosis. Images a, c, e, g, i, k, m, o are phase contrast. NT, untreated control. Magnification 40x.

The morphological investigations with DAPI and phalloidin-TRITC revealed that co-treatments were not able to protect cells from alterations induced by CDDP (Fig. 4.59). The OC-k3 cells, either treated with CDDP or co-treated, appeared enlarged and flattened: the cytoskeleton fibres were shorter and nuclei were larger and multi-lobed. These alterations were more evident after 48 hours of co-treatment in comparison to 24 hours.

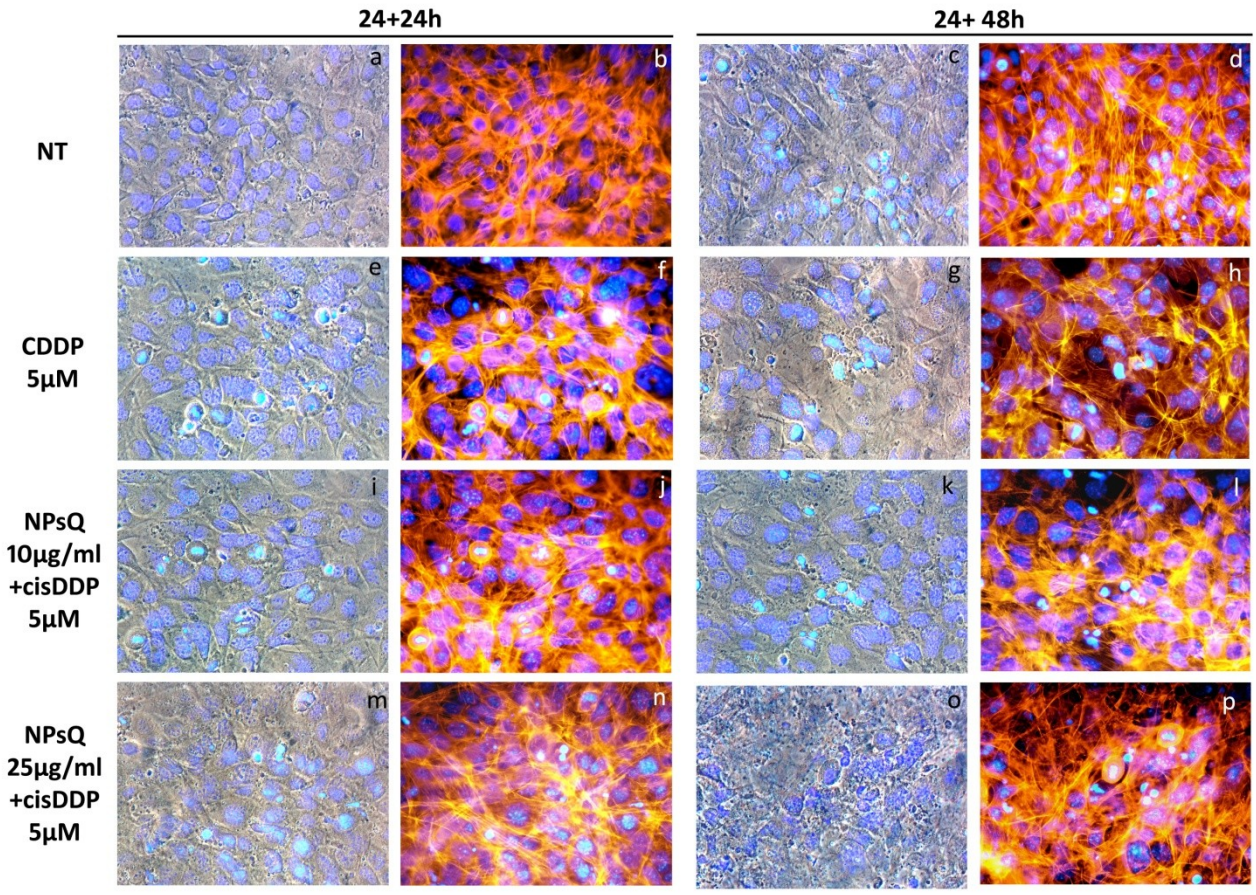

Fig. 4.59. Morphological investigations with DAPI (blue) and phalloidin-TRITC (red) on OC-k3 cells pre-treated for 24 hours with NPsQ (5 and 10 µg/ml), then co-treated with CDDP 5 µM and the same NPsQ concentrations for 24 and 48 hours. Images a, c, e, g, i, k, m, o are colour-combined DAPI-phase contrast. NT, untreated control. Magnification 40x.

The analyses of relative gene expression by RTqPCR on OC-k3 cells pre-treated with NPsQ, then co-treated with CDDP and NPsQ for 24 and 48 hours showed that co-treatments with NPsQ significantly reduced the expression of genes related to apoptosis at 24 hours in comparison to 48 hours (Fig. 4.60). The expression of transcripts of caspase 8 and 9 at 24 hours in co-treatments was significantly reduced ($p<0.01$) in comparison to CDDP alone. The same trend was observed for late apoptotic markers such as Bid ($p<0.05$), p53 ($p<0.05$) and BAX. For the caspase 3 gene, at 24 hours an increase of the expression level was instead observed, significant at NPsQ 25 µg/ml. At 48 hours all transcripts of genes related to apoptosis were generally expressed at a higher level than at 24 hours.

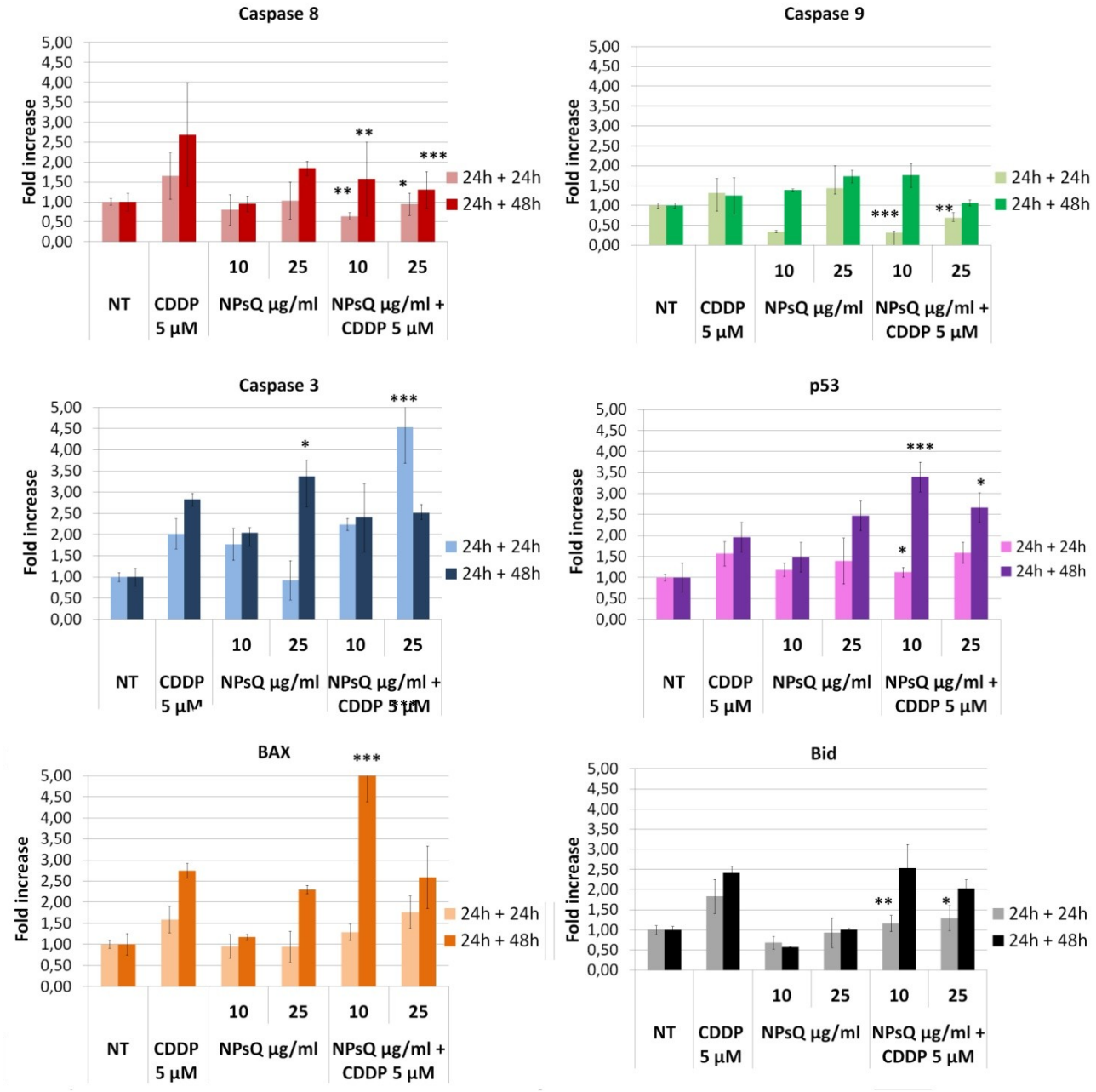

Fig. 4.60. Analyses of relative gene expression by RTqPCR on OC-k3 cells pre-treated for 24 hours with NPsQ (10 and 25 µg/ml), then co-treated with CDDP 5 µM and the same NPsQ concentrations for 24 and 48 hours, expressed as normalized fluorescence intensity with standard errors as bars. Asterisks indicate significant values in comparison to CDDP 5 µM (* = $p<0.05$; **= $p<0.01$; ***=$p<0.001$).

The results of analyses of protein expression markers related to apoptosis by Western blot in OC-k3 cells pre-treated for 24 hours with NPsQ, then co-treated with CDDP and NPsQ for 24 and 48 hours, at 24 hours CDDP did not induce an increase in cleaved caspase 3 or pERK in comparison to untreated controls (Fig. 4.61). In the same way, in co-treatments at 24 hours no increase of the cleaved protein is detected. At 48 hours the cleaved caspase 3 was significantly overexpressed with CDDP alone in comparison to untreated controls, but a decrease in expression dependent on NPsQ was observed in co-treatments The marker pERK was significantly overexpressed in co-treatments at 24 hours with NPsQ both 10 μg/ml ($p<0.01$) and 25 μg/ml ($p<0.001$). After 48 hours of treatment pERK was less expressed in comparison to 24 hours ($p<0.01$) and to CDDP alone ($p<0.01$). PARP level decreased in the co-treatments compared to the CDDP alone with NPsQ 25 μg/ml at 24 hours ($p<0.01$).

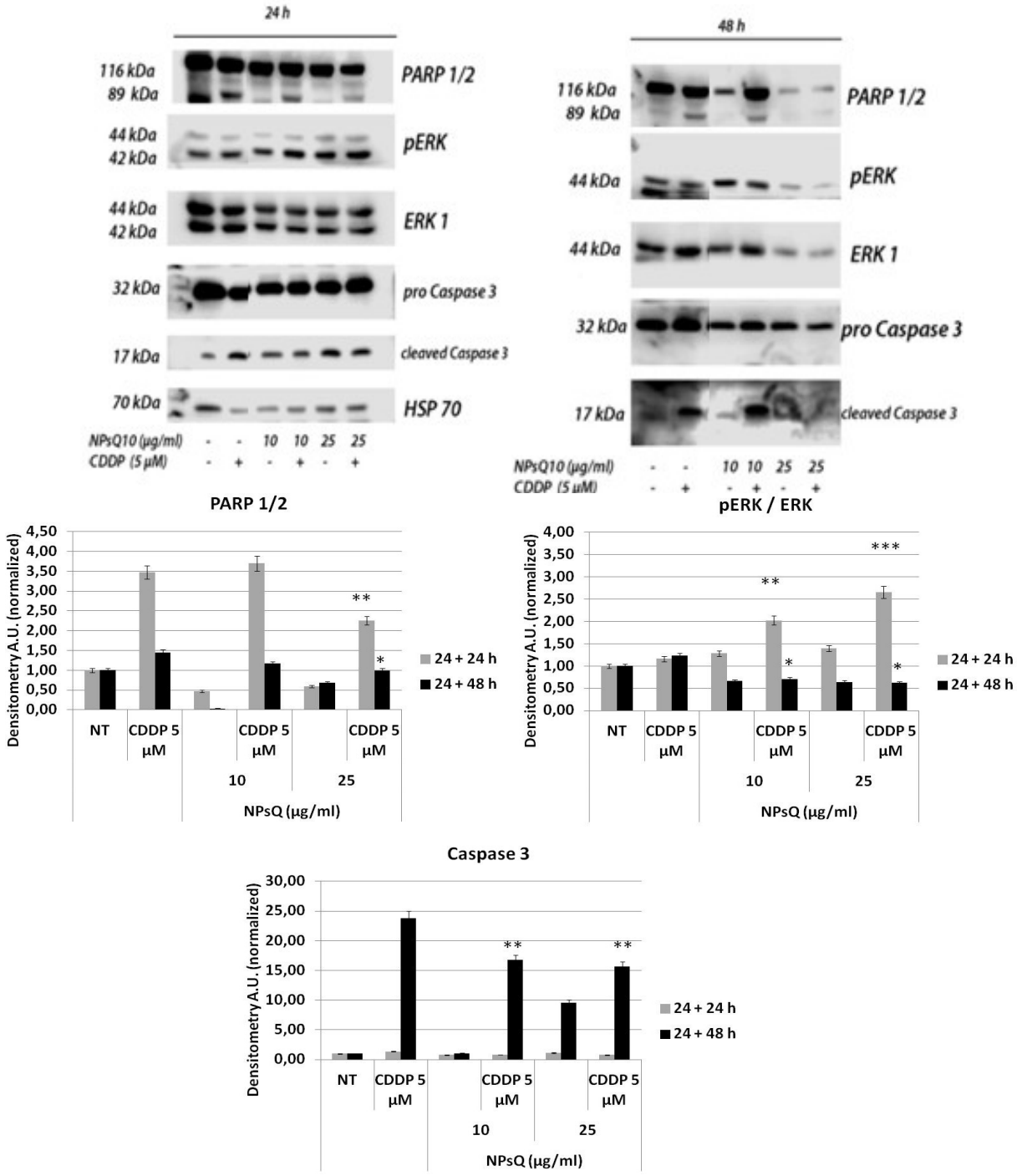

Fig. 4.61. Western Blot after SDS-PAGE and densitometric analysis of key proteins related to apoptosis (with HSP-70 as standard marker) in PC12 cells pre-treated for 24 hours with NPsQ (10 and 25 µg/ml), then co-treated with CDDP 5 µM and the same NPsQ concentrations for 24 and 48 hours. Bars represent standard errors. Asterisks indicate significant values in comparison to CDDP 5 µM (* = $p<0.05$; **=$p<0.01$; *** = $p<0.001$).

4.4.2 Experiments with NPsD and CDDP

In protection experiments, NPsD were able to exert a protective effect on OC-k3 cells against a highly toxic CDDP concentration, 13 µM. In viability tests, at 24 hours of co-treatment no significant recovery of cell viability was observed in comparison to CDDP alone: there was a slight (but not significant) decrease, dependent on NPsD concentration (Fig. 4.62). At 48 hours of co-treatment, a recovery of cell viability was observed from NPsD 10 µg/ml compared to the CDDP 13 µM alone, which became significant at NPsQ 25 and 50 µg/ml.

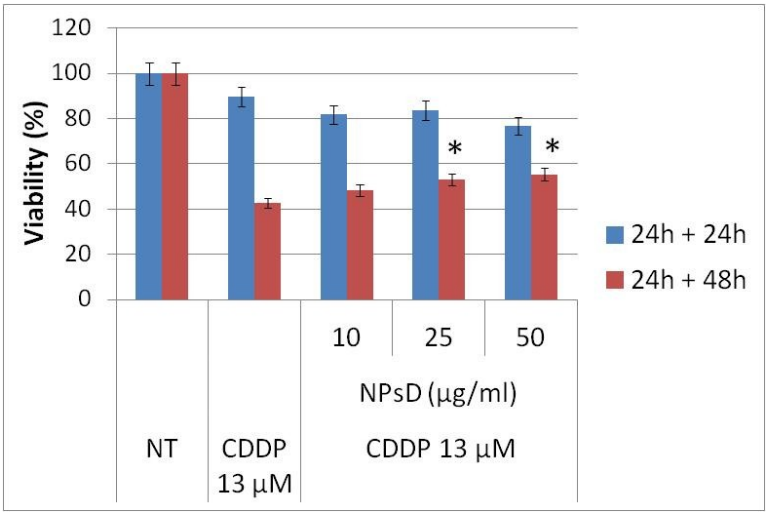

Fig. 4.62. Viability of OC-k3 cells pre-treated for 24 hours with NPsD (10, 25 and 50 µg/ml), then co-treated with CDDP 5 µM and the same NPsD concentrations for 24 and 48 hours. Bars represent the standard errors. NT: untreated controls. An asterisk indicates a significant difference in comparison to CDDP 13 µM (* = $p<0.001$).

The analysis of cell cycle by flow cytometry in OC-k3 cells pre-treated for 24 hours with NPsD and then co-treated with CDDP and the same NPsD concentrations for 24 and 48 hours confirmed the dose and time dependent response of cells to co-treatments (Fig.4.63). In the first 24 hours, CDDP induced a significant increase in the number of hypodiploid cells and of those in S, together with a decrease of those in G0. At 48 hours these effects were more evident, with a significant number of cells in apoptosis and a decrease of the number of cells in all other phases of the cell cycle. The co-treatment with NPsD from 10 µg/ml onwards induced a reduction in the number of hypodiploid cells, but this reduction was not significant at any time of exposure examined. With increasing

concentrations of NPsD a time dependent recovery of cells was observed in G2/M, which became highly significant at NPsD 25 and 50 µg/ml ($p<0.001$) at 48 hours of co-treatment.

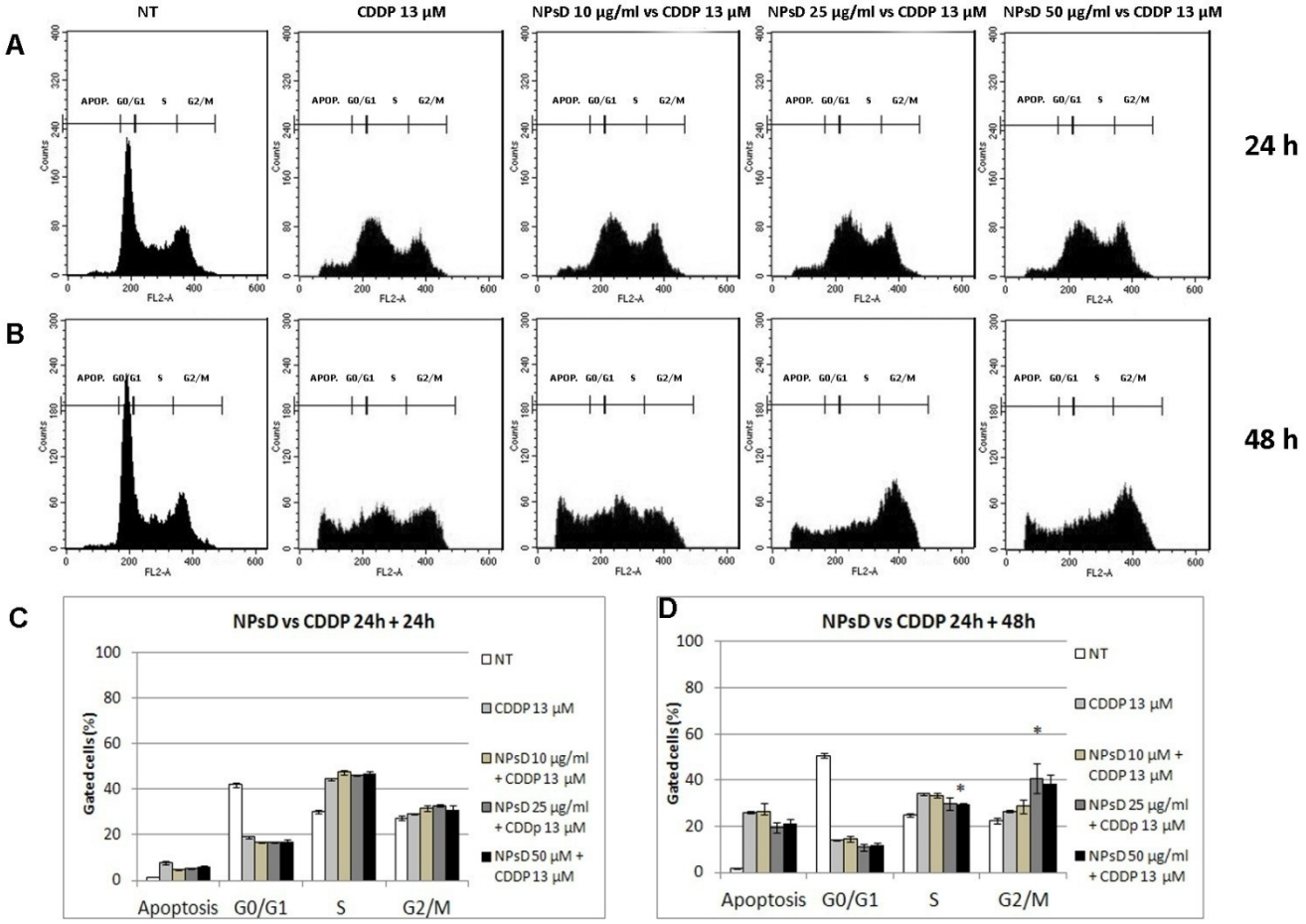

Fig. 4.63. Analyses by flow cytometry of OC-k3 cells pre-treated for 24 hours with NPsD (10 and 25 µg/ml), then co-treated with CDDP 5 µM and the same NPsD concentrations for 24 and 48 hours. A, B. Number of cells (expressed as counts) in each phase of the cell cycle. For each experimental condition, about 20000 events were analysed. NT, untreated control. APOP, apoptosis. C, D. Distribution of cells expressed as percentage of cells ± standard error in each cell cycle phase. An asterisk indicates a significant difference in comparison to CDDP 13 µM (* = $p<0.05$).

The morphological investigations with annexin V-FITC and PI on OC-k3 cells pre-treated for 24 hours with NPsD, then co-treated with CDDP and NPsQ for 24 and 48 hours, revealed a marked time dependent improvement of cell conditions in comparison to CDDP. After 24 hours of treatment with CDDP 13 µM, OC-k3 cells appeared deformed and enlarged: many of them were positive to annexin V-FITC and PI (Fig. 4.64). At the same time of exposure in co-treatments with NPsD 25 and 50 µg/ml a decrease in the number of double stained cells was detected. At 48 hours

of treatment with CDDP 13 µM, the number of cells entering apoptosis increased. In co-treatments the OC-k3 cells were more numerous and similar to untreated controls. However, the majority of cells appeared elongated and adhering to the substrate: only the roundish ones appeared double stained, depending on NPsD increasing concentrations.

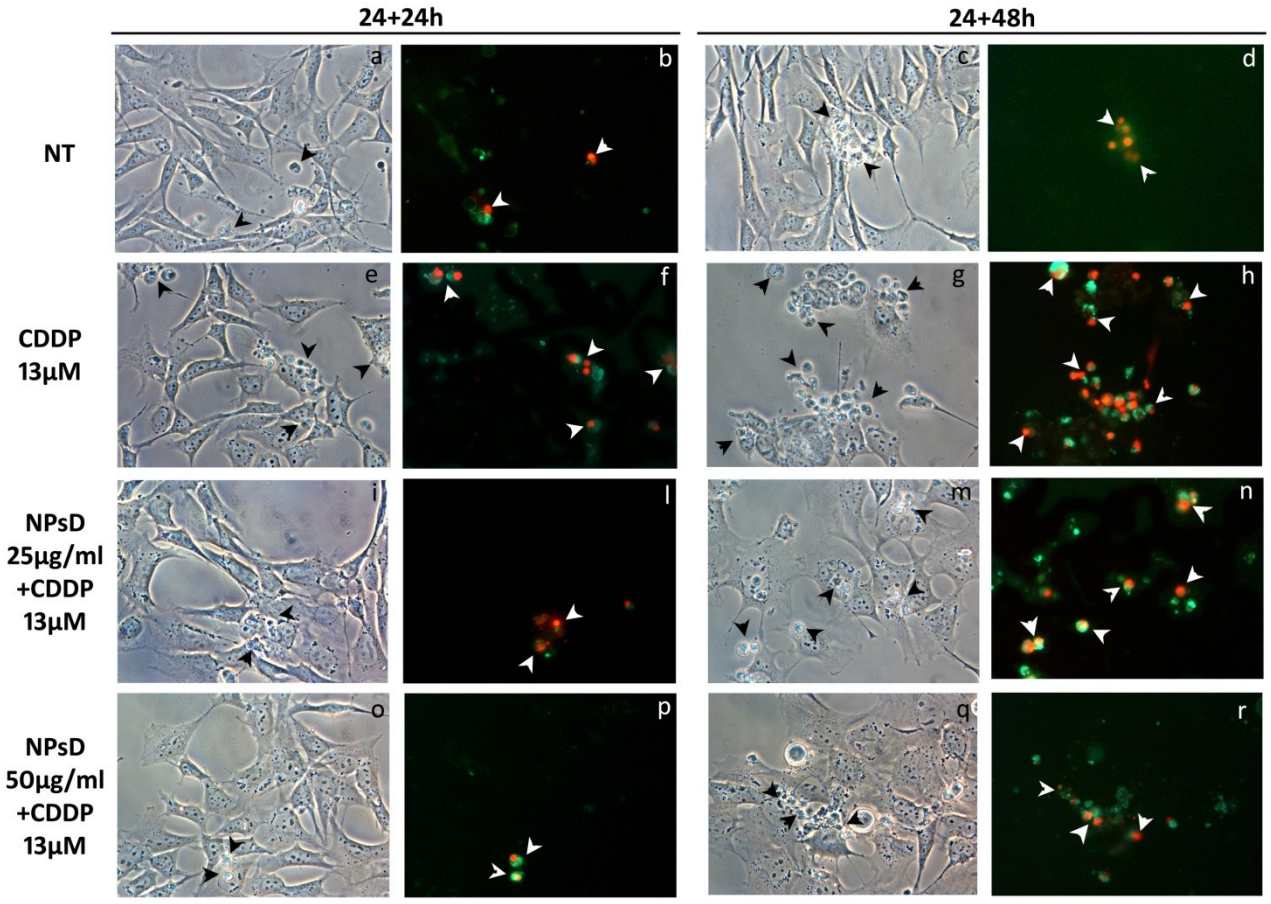

Fig. 4.64. Morphological investigations with annexin V-FITC (green) and PI (red) on OC-k3 cells pre-treated for 24 hours with NPsD (25 and 50 µg/ml), then co-treated with CDDP 13 µM and the same NPsD concentrations for 24 and 48 hours. White arrowheads indicate cells in apoptosis. Images a, c, e, g, i, m, o, q are phase contrast. NT, untreated control. Magnification 40x.

The morphological investigations with DAPI and phalloidin-TRITC on OC-k3 cells, pre-treated for 24 hours with NPsD, then co-treated with CDDP and NPsQ for 24 and 48 hours, revealed that at 24 hours of treatment with CDDP 13 µM most cells were deformed, with very enlarged nuclei and shorter cytoskeletal fibres (Fig. 4.65). Some multi-lobed nuclei were also visible. These effects were more evident at 48 hours: only few adhering cells were visible and those still attached to the substrate were swollen, with frayed cytoskeleton, scarce cytoplasm and multi-lobed nuclei (Fig.

4.65 H). In co-treatments with NPsD, the OC-k3 cells were more similar to untreated controls: the number of adhering cells was higher, most cells appeared elongated again and only few had multi-lobed nuclei.

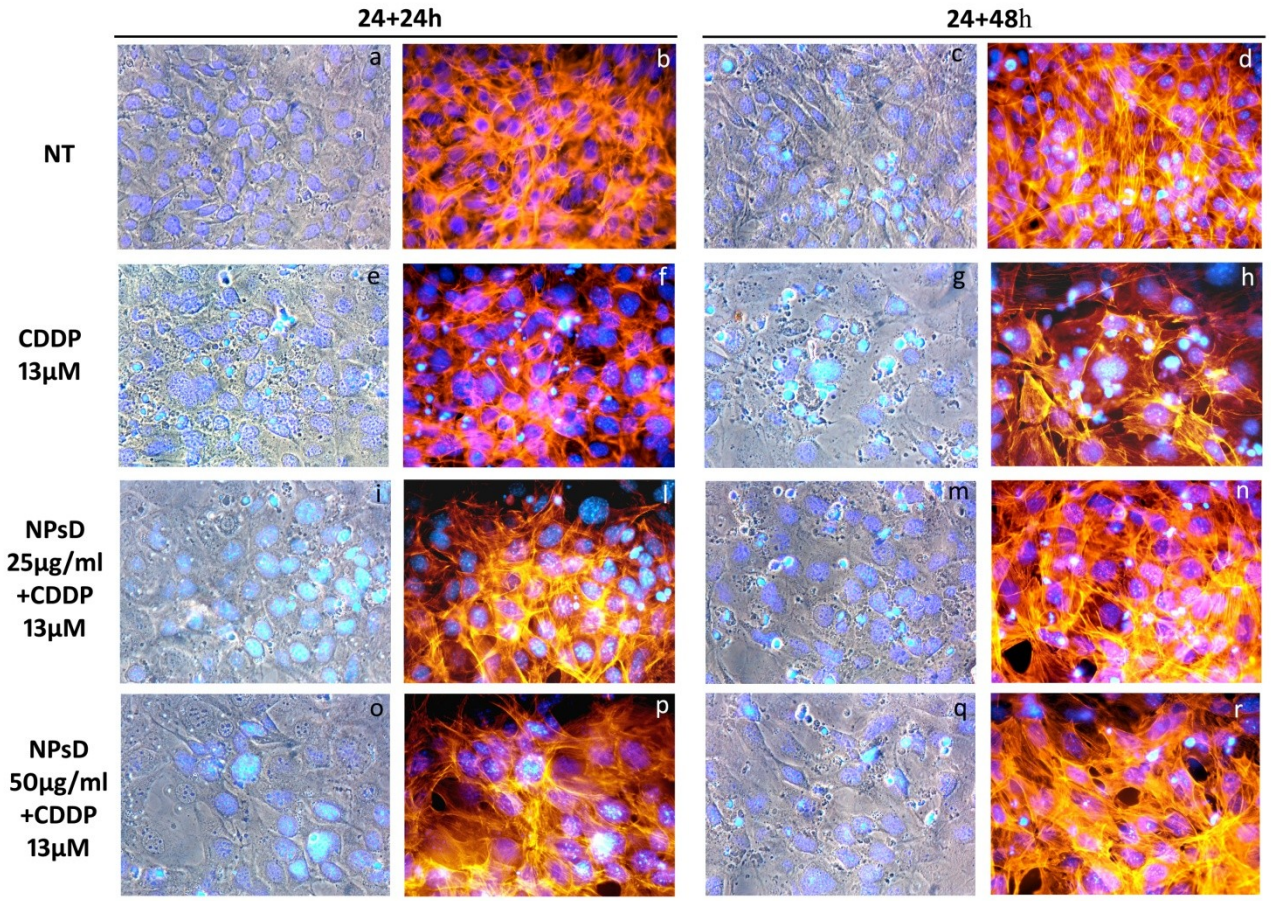

Fig. 4.65. Morphological investigations with DAPI (blue) and phalloidin-TRITC (red) on OC-k3 cells pre-treated for 24 hours with NPsD (25 and 50 µg/ml), then co-treated with CDDP 13 µM and the same NPsD concentrations for 24 and 48 hours. Images a, c, e, g, i, m, o, q are colour-combined DAPI-phase contrast. NT, untreated control. Magnification 40x.

The expression of genes involved in apoptosis, investigated by RTqPCR on OC-k3 cells pre-treated with NPsD 25 and 50 µg/ml, then co-treated with CDDP 13 µM and the same concentrations of NPsD for 24 and 48 hours, indicated that all transcripts were underexpressed in co-treatments with NPsD in comparison to CDDP 13 µM (Fig. 4.66). The NPsD concentration with the lower gene expression in comparison to CDDP was 25 µg/ml. The caspase 8 gene was significantly underexpressed in comparison to CDDP 13 µM only at 48 hours ($p<0.001$). The genes involved in the apoptotic cascade followed the same trend: Bid ($p<0.01$), BAX ($p<0.001$) and caspase 3

(p<0.001) were significantly underexpressed at 48 hours of co-treatement at NPsD 25 µg/ml. The same trend was observed for the antitumoral gene p53.

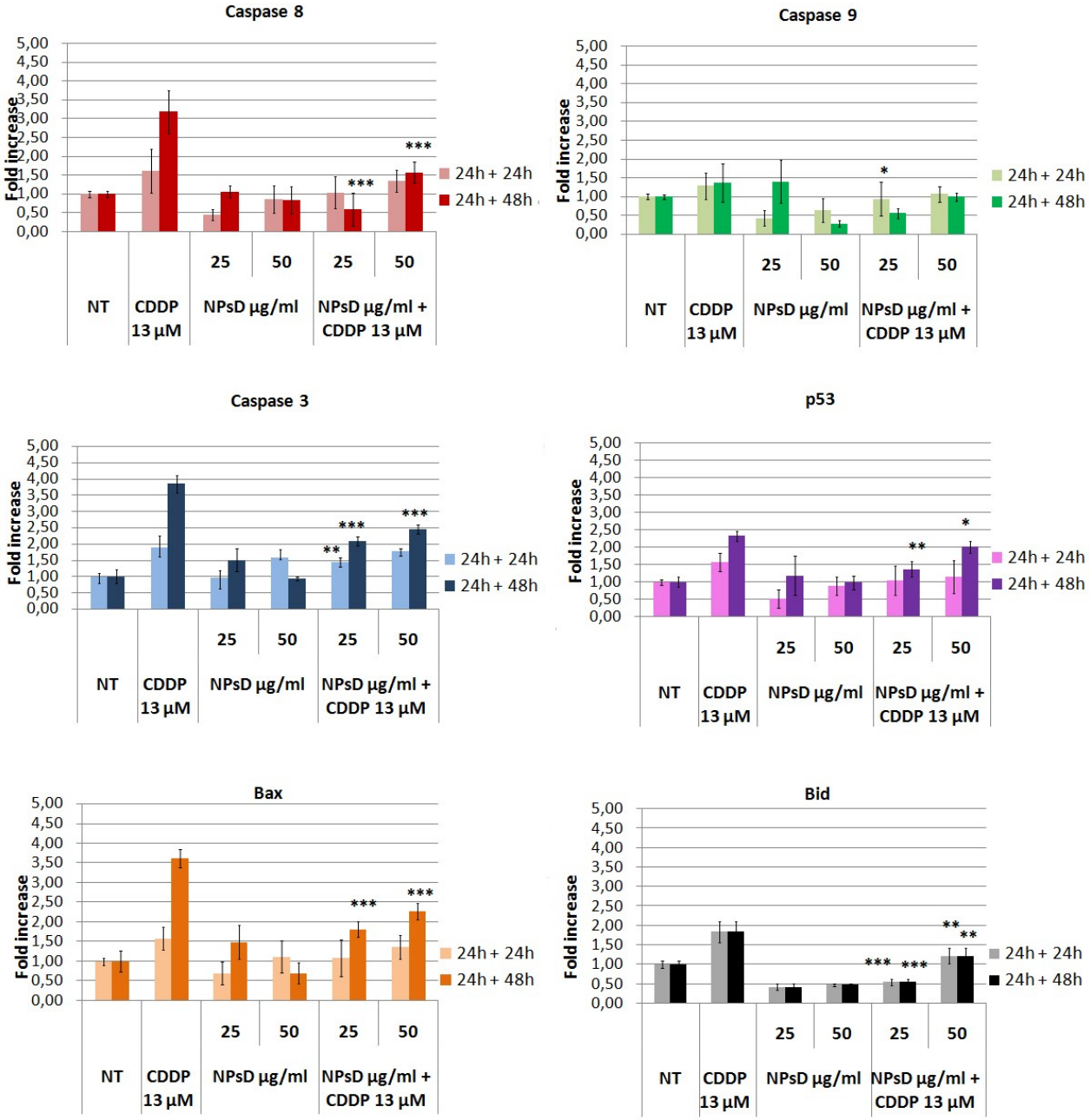

Fig. 4.66. Analyses of relative gene expression by RTqPCR on OC-k3 cells pre-treated for 24 hours with NPsD (25 and 50 µg/ml), then co-treated with CDDP 13 µM and the same NPsQ concentrations for 24 and 48 hours, expressed as normalized fluorescence intensity with standard errors as bars. Asterisks indicate significant values in comparison to CDDP 13 µM (* = p<0.05; **= p<0.01; ***=p<0.001).

The results of analyses of protein markers related to apoptosis by Western blot in OC-k3 cells pre-treated for 24 hours with NPsD, then co-treated with CDDP and NPsD for 24 and 48 hours, generally showed a protective effect against the chemotherapeutic drug (Fig. 4.67). The CDDP 13 μM caused an increase of cleaved caspase 3, pERK and PARP both at 24 and 48 hours of treatment. The co-treatment with NPsD reduced the expression of these apoptotic markers in a time dependent way. A NPsD concentration of 25 μg/ml induced a significantly lower expression of cleaved PARP ($p<0.001$) and pERK ($p<0.01$) at 48 hours of co-treatment. The level of caspase 3 decreased according to dose and time of exposure to NPsD, in a significant way in comparison to CDDP alone, both at 24 and 48 hours of co-treatment ($p<0.001$).

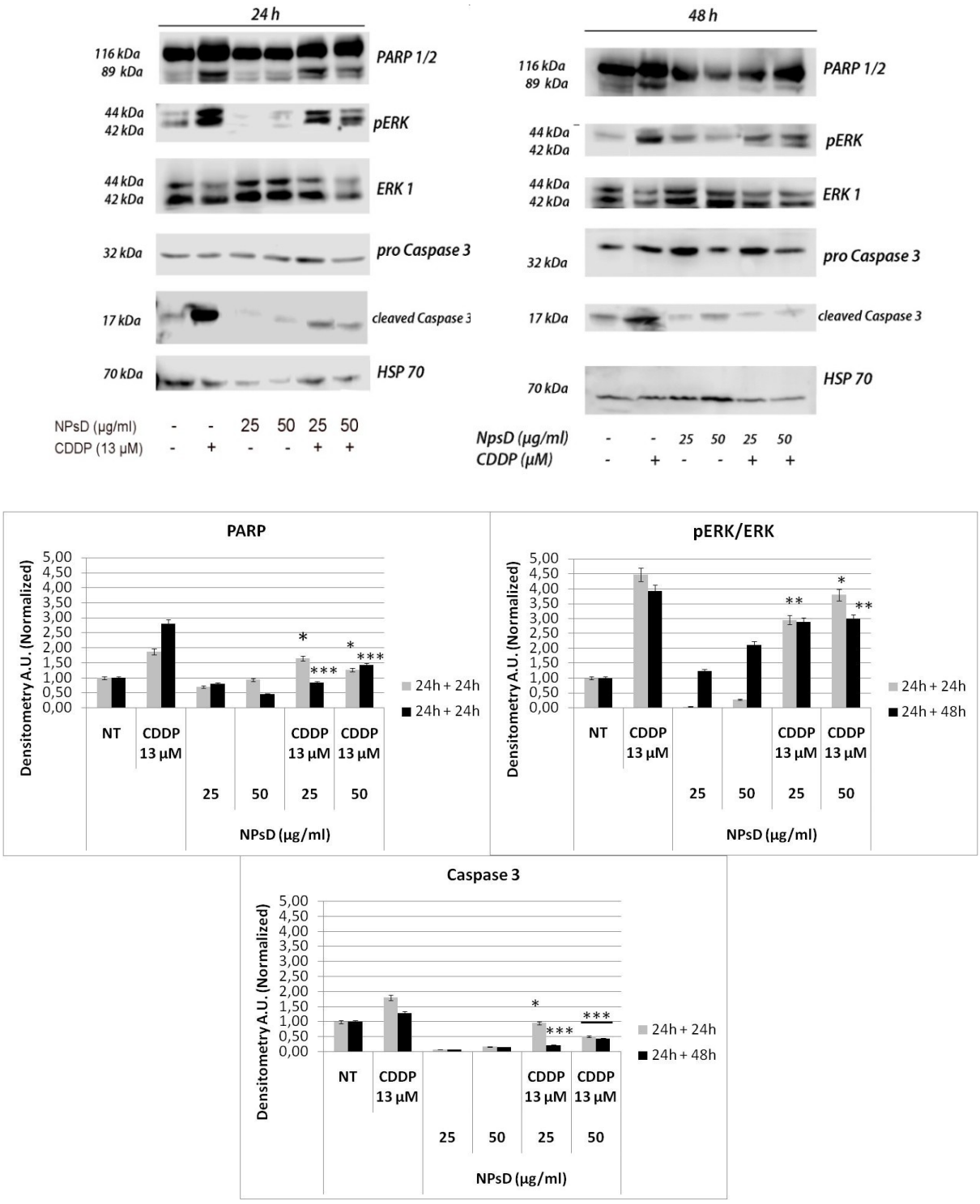

Fig. 4.67. Western Blot after SDS-PAGE and densitometric analysis of key proteins related to apoptosis (with HSP-70 as standard marker) in OC-k3 cells pre-treated for 24 hours with NPsD (25 and 50 µg/ml), then co-treated with CDDP 13 µM and the same NPsD concentrations for 24 and 48 hours. Bars represent standard errors. Asterisks indicate significant values in comparison to CDDP 13 µM (* = $p<0.05$; **=$p<0.01$; ***$p<0.001$).

Based on the results of protection tests with NPsD against CDDP in OC-k3, other tests were performed by ultra high performance liquid chromatography (UHPLC), in order to obtain quantitative data on concentration of the pharmacological drug released along time by NPsD in cells, using the NPsD concentrations able to exert a protective effect in co-treatments.

Starting from a given amount of NPsD, the analyses by UHPLC allowed to obtain the concentration of the drug inside NPsD: at the protective concentration of NPsD 50 µg/ml, about 38 ng/ml of conjugated dexamethasone are released.

The amount of nanoparticle-conjugated drug released and internalized when cells were treated by NPsD was analysed by UHPLC and compared to that in OC-k3 cells treated with a corresponding amount of drug alone at 24 hours of treatment (Fig. 4.68). After 24 hours the culture medium, the cell lysate and the cellular pellet were analysed in the treated cells lysate. The results showed that the amount of dexamethasone detected after 24 hours in cells treated with NPsD was significantly higher ($p<0.001$) in comparison to those treated with the drug alone.

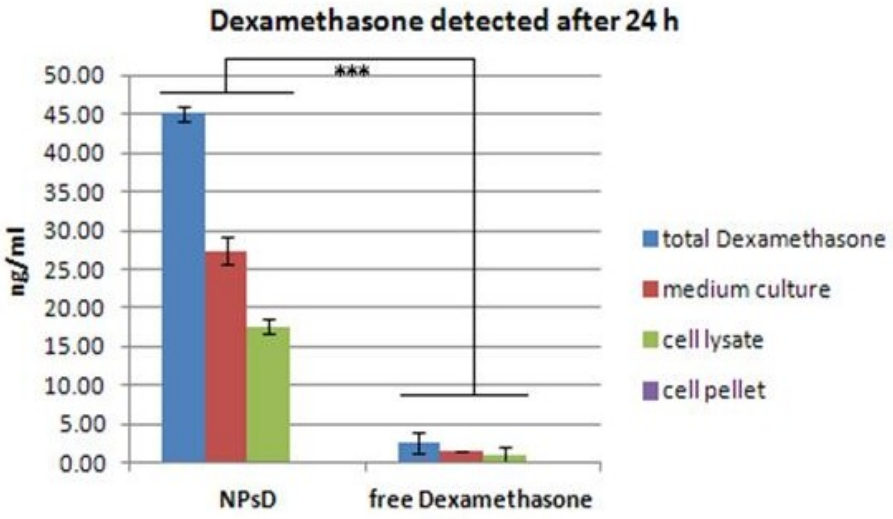

Fig.4.68. Amounts of dexamethasone (ng/ml) measured by ultra high performance liquid chromatography (UHPLC) in extracts of OC-k3 cells treated for 24 hours either with NPsD 50 µg/ml or with a corresponding amount of dexamethasone only for the same time. Bars represent standard errors. Asterisks indicate significant values between extracts treated with NPsD and treated with dexamethasone only (***=$p<0.001$).

The time-release profile of dexamethasone from NPsD 50 µg/ml after 4, 24 and 48 hours from treatment was also analysed by UHPLC. The results showed that the highest dexamethasone release occurred after 24 hours (Fig. 4.69): at that time, the drug concentration in the culture medium or in the cell lysate was significantly higher ($p<0.001$) in comparison to what observed at 4 hours. After 4 and 24 hours of treatment, the highest dexamethasone concentration was detected in the culture medium and the amount was significantly higher (at 4 hours, $p<0.01$; at 24 hours, $p<0.001$) in comparison to what detected in the cell lysate. At 48 hours of treatment, the trend was reversed: the amount of dexamethasone was significantly higher in the cell lysate ($p<0.01$) than in the culture medium.

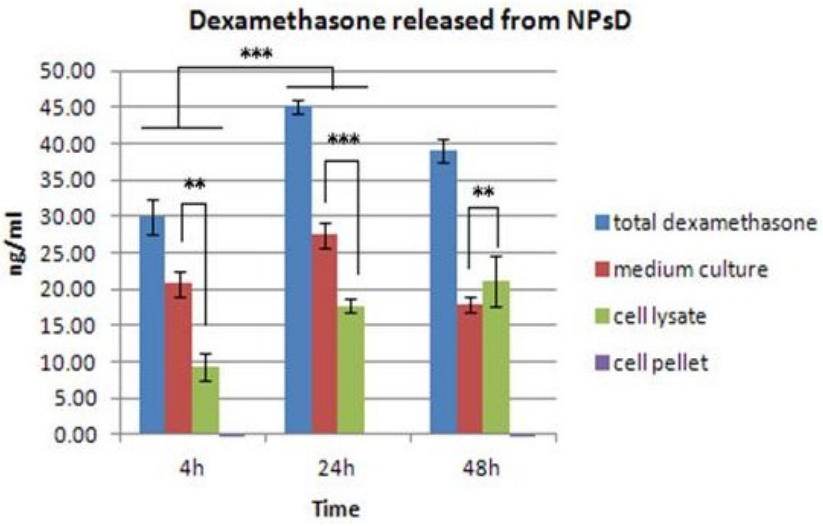

Fig. 4.69. Amounts of dexamethasone (ng/ml) measured by UHPLC in extracts of OC-k3 cells treated for 4, 24 and 48 hours with NPsD 50 µg/ml. Bars represent standard errors. Asterisks indicate significant values between extracts treated with NPsD at different times (**=$p<0.01$; ***=$p<0.001$).

5 Discussion

According to World Health Organization data, in 2015 about 360 million people worldwide were affected by hearing loss, defined as a partial or total impairment of the hearing ability due to pathologies of the inner ear (5). Epidemiologic data about hearing loss also indicate a raising incidence rate over time: from 2005 to 2015 the number of people suffering from hearing disability increased by 29.5%, due to increasing people age and environmental noise levels.

Hearing damage due to trauma, noise exposure or drug ototoxicity is irreversible because mammalian hair cells and cochlear neurons, responsible for elaboration and transmission of the auditory signal, are not able to regenerate (2, 179).

Although several studies have investigated new pharmacological compounds to prevent or protect these cells from effects of ototoxic agents (180), no specific drug has been presently developed (135). Moreover, drug delivery (DD) of therapeutic compounds to the inner ear has to deal with problems such as the small size of the cochlea, its difficult access and the limited blood flow from systemic circulation (73).

Nanoparticles (NPs) used as vehicle for DD in the inner ear may improve the existing therapeutic strategies (77), providing sustained release, increased half-life, improved drug diffusion and target specificity (78).

During this study, liquid crystalline nanoparticles (LCN NPs) based on the endogenous lipid glycerol monooleate were developed and tested, conjugated with two different hydrophobic drugs, coenzyme Q10 and dexamethasone. These two compounds are currently tested for inner ear therapies but have limited solubility and bioavailability. The analyses have been performed *in vitro* on two different cell lines, PC12 and OC-k3, used as a model of inner ear cell populations. The effectiveness of NPs delivery has been verified against the cytotoxicity of cisplatin ((SP-4-2)-diamminedichloroplatinum (II)) (CDDP), a well known ototoxic agent.

5.1 Nanoparticles production and *in vitro* characterization

Nanoparticles (NPs), artificial compounds with size lower than 1μm, may be used in research and clinical applications as a drug delivery (DD) system to improve the existing therapeutic strategies

(77). Besides the potential applications of these studies for hearing loss therapy, the cochlea is also a suitable model for studying the local applicationof NPs for DD, due to its isolated structure and to the cochlear fluid rheology that facilitate the distribution of compounds. Recently, innovative technical approaches for NP-based DD in inner ear have been tested, among them magnetic NPs (155), poly-D/L-lactic/glicolic acid (PGLA) (156), silicon NPs marked by a fluorochrome (181), hyperbranched poly-L-lysine (HBPL) and lipid core NPs (132). In all these studies NPs were applied near the round window membrane (RWM) and were detected in all parts of the cochlea (spiral ganglium, stria vascularis and hair cells), simultaneously releasing the conjugated drugs (134, 163).

The ideal NPs should have the following properties: simple preparation processes, low cost of raw materials, high biocompatibility, temperature stability, integrity of the structure in a diluted media, high exchange surface and solid-like viscosity (30). For all the above reasons it was decided to test liquid crystalline NPs (LCN) based on the polar lipid glycerol monooleate (GMO). The LCN possess a versatile internal structure able to encapsulate both hydrophilic and hydrophobic compounds (90). Depending on the surrounding environment and/or the conjugated compounds, the LCN components may assemble in different phases, lamellar, hexagonal or bicontinuous cubic (100). The cubic phase is composed by a lipid bilayer arranged in a three-dimensional internal folding, converted into a viscous gel (103) that can be dispersed into NPs (cubosomes) in presence of an excess of water (182). The material exploits the properties of GMO, a widely studied lipid used in food, cosmetic and pharmaceutical preparations, which is nontoxic, biocompatible and biodegradable (99). In a diluted solution, the GMO bicontinuous cubic phase is thermodynamically stable and exhibits mechanical stiffness (112, 113). The specific preparation protocol of the cubosomes in this study is based on the method by Spicer and Hyden (103).

The control cubosomes produced for this study (NPsA) have size about 200 nm, as previously reported in similar production processes (123, 183), exhibit the typical cubic-like structure and have a high sample homogeneity indicated by the low polydispersity index (PDI). They also exhibit a slight negative external charge (about 20 mV), a relevant parameter preventing the aggregation of particles when dispersed in a solution. Although positively charged cubosomes may be better detected when used in experiments in the cochlea (135), they exhibit a higher toxicity on cochlear tissues, therefore the negative charges ones were chosen for this study. The stability of particles in aqueous solution was verified by monitoring their physical chemical parameters for a period of two months, along which no significant variation was observed.

As reported in literature, cubosomes may be combined with numerous compounds for DD, among which peptides (98), proteins (114, 119, 121, 122) and drugs(123-126). Previous studies also showed that the inclusion of hydrophobic compounds in a cubic bicontinuous phase induced a shift to an hexagonal phase(98, 113, 183). The effects of different cubic or hexagonal structures of liquid crystalline NPs used for DD in cells, bacteria or organs are still under investigation (98, 184). This interesting property has been observed in the present study by adding two hydrophobic drugs, coenzyme Q10 (CoQ10) and dexamethasone, to the NPs preparation process. The resulting NPs, respectively called NPsQ and NPsD, showed a roughly hexagonal shape when observed at the transmission electron microscope (TEM). The physical chemical analyses of NPsQ and NPsD yielded very similar results to those of NPsA, and the data of the toxicity tests *in vitro* were compared with those of NPsA to verify whether the structure shifts could yield different results.

Concerning the numerous studies on nanomaterials for therapeutic applications (115), few of them have analysed the possible toxic effects of NPs and the outcome of treatment of cells with cubosomes (185, 186). According to the results obtained in this study, the viability assays on both OC-k3 and PC12 cell lines, performed with the three types of NPs, generally show that these nanoparticles cause a dose dependent effect on cells, as reported for similar NPs formulations (131, 183). However, the tolerance of OC-k3 and PC12 cell lines towards NPs appears very different. These results agree with previous reports showing that the *in vitro* toxicity of NPs is influenced by size, proliferation and embryonic origin of the selected cell lines (187, 188).

The NPs were tested on PC12 cells at concentrations 0-200 µg/ml for 24 and 48 hours. Both NPsA and NPsQ induced an increase in cell viability, significant for concentrations 50-100 µg/ml at 24 hours and for 25-125 µg/ml at 48 hours. However, NPsD caused toxic effects on PC12, inducing a significant decrease of viability at concentrations 13-25 µg/ml at 24 hours and 13-75 µg/ml at 48 hours, a recover at values similar to untreated controls at 100 µg/ml and a significant toxicity at higher concentrations. On OC-k3 cells, NPs were tested at concentrations 0-150 µg/ml, again at 24 and 48 hours and the viability assays yielded similar results for NPsA, NPsQ and NPsD. All NPs induced a comparable dose dependent decrease of cell viability, significant from 50 µg/ml onwards. A phase transition from cubic to roughly hexagonal phase was observed in both NPsQ and NPsD, therefore the different results obtained on PC12 and OC-k3 support the hypothesis that these differences are unrelated to the physical chemical structure but are due to the conjugated drug. The effects on DD of NPs phase transitions have not been further investigated in this study, but this interesting point deserves supplementary research in the future.

The dexamethasone effects described in literature are controversial and change according to the organ or cell line tested (68, 70, 189, 190). The molecular tests performed in this study confirm the toxic effects of NPsD on PC12, therefore it was chosen to interrupt the dexamethasone treatment on this cell line.

The analysis of cell cycle in PC12 cells treated with NPsA and NPsQ at concentrations up to 100 μg/ml did not reveal significant differences in the distribution of cell populations in comparison to untreated controls, therefore in PC12 the increment of viability was not apparently related to alterations of the cell cycle but only to a normal cell proliferation rate. The same results were obtained in OC-k3 cell line treated with all types of NPs, with no significant differences among cell population distribution for NPs concentrations between 0 and 50 μg/ml.

The morphological analyses with fluorescence microscopy, conducted by treating the cells with NPs tagged with rhodamine B, allowed to verify the interactions of NPs inside cells and track them over time. The uptake of fluorescent NPs occurred 4 hours after treatment for OC-k3 cells and 8 hours after treatment in PC12 cells. The time difference in NPs uptake between the two cell lines could be related to different viability cell responses and could also depend on NPs-cell membrane interactions, since the two cell lines have a different composition of phospholipid and membrane proteins (187, 188). The NPs uptake appeared dose dependent and the clearest and strongest signals were acquired 24 hours after treatment, although a quantitative analysis of the fluorescent signal was not performed. Several fluorescent spots could be identified inside the cells, suggesting that NPs do not self-aggregate. These results confirm that NPs are able to deliver the conjugated compound inside the cells, as previously reported (183, 191). The exact location of the dye could not be identified, but there are literature reports showing that rhodamine dyes tend to associate with mitochondria in living cells (192).

The interactions of NPs with cells and the dose dependent responses led to investigate the morphological and molecular responses of cells to the treatment. Cells were observed by fluorescence microscopy in presence of cytoplasmic and nuclear morphological markers. The results showed that in cells treated with high doses of NPs (75 and 200 μg/ml for PC12 and 25 and 50 μg/ml for OC-k3), a dose dependent formation of numerous intracellular vesicles and a cell swelling could be detected. Although the type of vesicles was not investigated in detail ,it is possible to advance the hypothesis that they are produced by exocitosis. An exocytotic process of NPs from the cell *in vitro* depending on particle doses and on proteins in the culture medium has been recently described (193). The authors indicate three possible exocytosis mechanisms: lysosome secretion, vesicle-related secretion and non-vesicle-related secretion. The dose dependent

vesicle formation observed in this study has not been investigated in detail, but it could be a cell mechanism to prevent osmotic stress death due to high concentration of NPs. Other morphological analyses were performed in this study to verify whether osmotic stress in the cell could induce cell death by apoptosis. A typical marker of the initial step of apoptosis is phosphatidylserine (PS), a lipid component of the cell membrane that can be tracked by annexin V fluorescent marker. The analyses of OC-k3 treated with 50 µg/ml of all types of NPs, and of PC12 treated with 100 µg/ml of NPsA and NPsQ did not reveal an increased exposition of PS in comparison to untreated controls. The analyses of the cytoskeleton of the two cell lines by the specific marker phalloidin at the same NPs concentrations did not show any alteration or degradation in the cytoskeleton. The nuclei stained with 4',6-diamidino-2-phenylindole (DAPI)did not appear multi-lobed and no chromatin degradation or cell swelling were observed on both cell lines.

These results suggest that the cells underwent a dose dependent stress while treated with NPs, but NPs were not able to trigger cell apoptosis. To verify this hypothesis, the RNA and protein lysate from cells treated with all types of NPs were analysed by quantitative PCR (RTqPCR) and Western blot to investigate the expression of key markers related to the apoptotic process. Few data are presently available in literature about the molecular effects of treatment with non-conjugated GMO NPs of cells and organs. Recently it has been shown that Chinese hamster ovary (CHO) and human lung adenocarcinoma cells (A549) exposed to GMO NPs show in the first four hours after treatment a significant increase in expression of some apoptosis markers, such as interferon α (IFN-α) and BAX. An overexpression of the oxidative stress marker heme oxygenase 1, but not of glutathione reductase, was also observed in these cell lines. The expression of these genes decreased after 24 hours of treatment, returning to control levels (183).

The results in the present study indicate a higher expression over time of the genes investigated: after 24 and 48 hours of treatment, some of the analysed transcripts were still overexpressed in comparison to controls. In PC12 cells treated with NPsA a significant increase in expression of caspase 8 and caspase 9 was observed at 25 µg/ml after 24 hours and 75 µg/ml after 48 hours. At the same concentrations caspase 3 after 48 hours while BAX was significantly overexpressed only at 75 µg/ml at 48 hours. On the contrary, the treatment with NPsQ induced a significant increase only of caspase 9 after 48 hours. In OC-k3 cells the treatment with NPsA induced an overexpression dose and time dependent of caspases 8 and 3, Bid, BAX and p53. The level of caspase 9 was lower than in controls. In treatments with NPsQ ,the transcripts were less expressed than with NPsA, except for caspase 3 which was significantly overexpressed over time. A similar pattern of reduction in gene expression was observed in treatments with NPsD, in which all

transcripts were expressed at the same level of controls or lower, except for caspase 3 at 50 µg/ml after 24 hours.

The three types of NPs therefore induced different cell responses, that could be related to the different cell lines and their NPs uptake, and within cell lines, to the type of drug conjugated to NPs. According to literature data, the NPs preparation methods could also be involved. Concerning the NPs uptake, the results obtained in this study by RTqPCR are in contrast with the only other literature data available by RTqPCR analyses, reporting a down-expression of apoptotic marker genes after 24 hours (21). The differences could be explained by the later cell uptake in the cell lines tested in this study, unlike what described by other authors (132-134).

Although qPCR analyses indicate that the treatment with NPs affected the cell environment and induced a stress response at mRNA level, these data were not confirmed by the subsequent translational analyses of some key apoptosis markers, such as ERK, caspase 3 and PARP. In PC12 cells treated with NPsA or NPsQ at 50-100 µg/ml, none of the apoptotic marker proteins was overexpressed. The same results were obtained in OC-k3 treated with NPsA and NPsD at 10-50 µg/ml and with NPsQ at 10-75 µg/ml, except for PARP, significantly overexpressed with NPsQ 75 µg/ml after 48 hours, and phosphorylated ERK with NPsD 50 µg/ml after 48 hours. A high concentration of NPs had been previously associated to a higher toxicity on cells by the viability assay. These results agree with those of the previous morphological analyses with annexin V and propidium iodide (PI), performed at the same doses of NPs, indicating that no apoptotic process was undergoing in cells. It could therefore be advanced the hypothesis that NPs are tolerated by PC12 and OC-k3 cells at different concentration ranges and that they could induce a specific stress response, according to the presence or not of the conjugated drug. Nevertheless, even when the cell environment is perturbed by the presence of NPs, at the tested concentrations the NPs did not cause any cell apoptosis.

5.2 Cisplatin cytotoxicity

Cisplatin (CDDP) is a widely used chemotherapeutic agent, currently administered in clinical practice for a broad variety of solid tumours (7). Its use in cancer therapy involves numerous side effects, including ototoxicity (194, 195). Clinical evaluations and *in vivo* studies on animal models have verified that CDDP ototoxicity affects the cochlear hair cells, the supporting cells, the spiral ganglion neurons and the stria vascularis. This drug exerts the highest damage in the outer hair cells

of the basal turn of the cochlea, causing cell death (26, 49, 196) and impairment of the signal transduction. It also induces calcium accumulation in the cells (22) and in neurons of the spiral ganglion causes disruption of neuronal processes, loss of the myelin sheath (197) and eventually cell death (198).

In this study two different cell lines were selected for *in vitro* analyses as representative of inner ear cell populations affected by the CDDP ototoxicity: the OC-k3 cells express specific markers of epithelial cells, auditory sensory cells and supporting cells (169), and the PC12 cells may differentiate into nerve cells when exposed to nerve growth factor (174). Because of their properties, both cell lines have already been used for investigations concerning exposure to cisplatin (177, 199). The results of the present study generally agree with previous data: CDDP causes a dose and time dependent cytotoxicity (13, 170, 177) and cell death by apoptosis (200, 201). The toxicity of the chemotherapeutic agent was higher on PC12 cells than on OC-k3 at the same dose. At 5 μM, CDDP was significantly toxic on PC12 after 24 hours and on OC-k3 after 48 hours; at 13 μM CDDP induced on PC12 cells a 80% decrease in cell viability after 48 hours, in comparison to a 60% decrease on OC-k3 ($p<0.001$). In protection experiments, the value of 5 μM was therefore chosen as the limit CDDP concentration for PC12 cells because this concentration was already significantly toxic after 48 hours, and that of 13 μM was chosen for OC-k3.

Previous studies showed that CDDP caused apoptosis by binding DNA, forming adducts (7), arresting the cell cycle (20), inducing ROS production (24-26) and activating both extrinsic and intrinsic apoptotic pathways (202). Since the three pathways to apoptosis are related to each other, it is likely that CDDP may be affect all of them. Moreover, different cell lines show different apoptosis related effects when exposed to CDDP: in differentiated pot-mitotic lines, the damage by CDDP is exerted mostly through the ROS pathway, but in undifferentiated or scarcely differentiated cells, actively in mitosis, the CDDP-induced DNA damage pathway is prevalent (30).

Inside the cell, chloride ions allow the formation of reactive hydrated species of CDDP, but also nucleophilic groups containing oxygen, nitrogen or sulphur atoms with unpaired electrons, such as those contained in purine DNA bases, may bind to CDDP in place of chloride. Moreover, the hydrated CDDP form is positively charged, therefore it may electrostatically bind the negatively charged DNA helix (22, 202). Among the effects of cross-linking between CDDP and DNA, there is the arrest of the cell-cycle in G2 and the consequent triggering of apoptosis (203). The results obtained in this study on cell population distribution of OC-k3 and PC12 cells along the cell cycle generally support the above hypothesis, but in OC-k3 cells the treatment with low concentrations of CDDP (2.5 and 5 μM) after 24 and 48 hours did not induce a decrease of cells in G2. At these low

concentrations the cells could still be able to activate the DNA repairing systems, as shown by the increase of cells in S. The cell response to CDDP also appears to be time dependent. For example, in OC-k3 the viability assays showed the same damage at CDDP 5 μM after 48 hours and 13 μM after 24 hours, but the distribution of cells in the cell cycle was different at the two times of exposure: in the first case the apoptotic cells increased in number, and in the second one the cells accumulated in G0.

The same trend was observed in PC12 at 5 μM. Thus, when damages to DNA become too relevant or irreversible, the cell arrests the repairing mechanism and triggers the apoptosis process. The different responses of the two cell lines to CDDP toxicity could also depend on different intracellular accumulation of chloride and consequent formation of the CDDP active form (204).

Apoptosis is characterized by typical morphological changes such as cell shrinkage, cytoskeleton disruption, cytoplasm condensation and internucleosomal DNA fragmentation (205). As previously mentioned, one of the initial markers of apoptosis is PS. Both OC-k3 and PC12 treated with CDDP were positive to this marker at 24 hours, at concentrations 5 μM for PC12 and 13 μM for OC-k3, in correspondence of increasing effects of CDDP detected in viability assays.

The irreversible DNA damages and the arrest of cell cycle are both events able to activate the pro-apoptotic cell response, which involves numerous molecular pathways, and are also related to overexpression of the anti-tumour transcription factor p53 (206). The p53is a powerful upregulator of Bid and BAX proteins (42), which induce the release of cytochrome *c* from mitochondria and the activation of the intrinsic pathway of apoptosis (43). It has been shown that CDDP is able to trigger apoptosis through the extrinsic pathway, via cell surface death receptors and cleavage of pro-caspase 8 (38). The CDDP also causes an intracellular ROS production, which may induce activation of the intrinsic pathway of apoptosis (30). The connection between the two pathways occurs when the initial apoptotic signal initiated by caspase 8 is amplified at the level of mitochondria, resulting in cytochrome *c* release and upregulation of the effector caspases 3 (202). These results have been verified by numerous *in vitro* studies on different cell lines and *in vivo* (202, 207-209).

The expression of markers of the apoptotic process have been analysed by RTqPCR on OC-k3 cells and PC12: the results indicate a general overexpression of RNA transcripts of the initiator caspases 8 and 9, of the proapoptotic factor p53, of the mitochondrial protein Bid and BAX and the effector caspases 3 on both cell lines. These results agree with previous studies indicating that induction of apoptosis by CDDP does not occur through a single signal pathway, but triggers several factors in

different pathways. In the present study, the expression of caspase 8 is significantly high at 5 μM for both cell lines and increases with dose and time of exposure to the chemotherapeutic agent.

At CDDP 25 μM the expression of caspase 8 transcript in OC-k3 cells is lower in comparison to 13 μM dose, probably because of activation of other pathways by the high concentration of CDDP. At low doses of CDDP, caspase 9 already results overexpressed in comparison to controls, but the difference is significant only after 48 hours of treatment with CDDP 25 μM. The higher expression of caspase 8 in comparison to that of caspase 9 indicates a major activation of the extrinsic pathway in comparison to the intrinsic one. This is however in contrast to results of previous studies *in vitro* on HEI-OC1 cells (202) in which a transient overexpression of caspase 8 in the first 6 hours of CDDP treatment and a shift to a prolonged overexpression of caspase 9 within the first 12 hours of treatment was observed. Caspase 3 results significantly expressed over time and dose of CDDP already at 5 μM at 24 hours on both cell lines. These results are in agreement with previous studies suggesting that caspase 3 is activated downstream of activation of both caspase 8 and 9. The transcript of p53 is overexpressed in accordance to CDDP concentration and time of exposure on both cell lines. The levels of Bid and BAX transcripts follow the same expression trend, indicating that p53 upregulates the two mitochondrial factors, in agreement with literature data (210). Overall, these data indicate a multifactorial apoptosis triggered by CDDP; a hypothesis could be advanced that apoptosis is activated on these cells mainly through the extrinsic pathway (high levels of caspase 8) and by DNA damages (high p53 levels), and less through the intrinsic way related to ROS production. These results on these undifferentiated cell lines are in agreement with a hypothesis suggesting that the main cause of apoptosis by CDDP in differentiated post-mitotic cochlear cells is related to ROS production and not to DNA damages(30).

The results obtained by RTqPCR analyses clearly correlate with those of protein apoptotic markers examined by Western blot. Apoptosis induced by CDDP involves the MAPK family, and the ERK subfamily is relevant for regulation of cell growth and differentiation(211). It has been shown on HeLa cells that the activation of ERK plays a role in induction of apoptosis by CDDP (13). The results presented in this study support the fact that in both cell lines the significant increase of phosphorylated ERK is in accordance to concentration and time of exposure to CDDP. Another apoptotic key protein analysed was cleaved caspase 3, whose expression reflected the same trend observed for its transcript. The action of caspase 3 influences the protein PARP, involved in DNA repairing system, which is inactivated by protein cleavage directly from caspase 3 (212). The results of this study agree with literature data showing a significant increase in PARP and caspase 3 levels in cells.

5.3 Protection analyses

It is known that the effects of cisplatin in cells have a broad spectrum and may induce apoptosis by activation of both the intrinsic and extrinsic pathway. The ideal protector against CDDP should then possess the ability to interfere with CDDP action mechanisms and prevent, block or lower its cytotoxic effects. In this study dealing with exogenous NPs, the first issue to be investigated was the interaction among cells, nanomaterials and activated pathways within the cells. The results of this study indicate that NPs alone induce a cellular stress at high concentrations, but the presence of conjugated drugs lowers the expression of stress markers, thus apoptosis is not triggered in the studied cell lines.

It was therefore important to discriminate between the effects of NPs and those of CDDP treatment on cells, in order to avoid a cumulative toxic effect when treating the cells with both compounds. In order to prevent or reduce the toxic effects of CDDP, it was chosen to pretreat cells with the protective agents conjugated with NPs. The two selected drugs, CoQ10 and dexamethasone, exhibit a very low solubility and bioavailability, and have already been tested against ototoxicity induced by CDDP.

Although several literature studies have focused on delivery of protective drugs in cells or organs including the inner ear, none of them has up to date proposed a model of study of co-treatment using both the toxic agent and the NPs based system on the same substrate.

5.3.1 NPsQ vs CDDP

The coenzyme Q10 (CoQ10) is a vitamin-like antioxidant, involved in numerous energy-producing metabolic pathways of cells and regulating the mitochondrial respiratory chain. It is also able to scavenge oxygen radicals and inhibit lipid peroxidation, preventing damages to cells and tissues (56-58). As a ROS scavenger,CoQ10 works by inhibiting the mitochondrial membrane depolarization, blocking the release of cytochrome *c* in the cytoplasm and the activation of the intrinsic apoptotic pathway (60). The CoQ10 is an ubiquitous factor, essential for cell respiration and other key functions; any deficiency in its availability or biosynthesis may disrupt normal cellular function (213). Several factors have been shown to decrease CoQ10 levels, among which illness, inflammation, stress and aging(214). Because of its relevant role in physiological processes

and its ubiquity, it has been the subject of a broad range of studies to reduce oxidative stress conditions, achieved by replenishing CoQ10 shortage or by administering supplementary amounts of it. This has occurred for example in cardiovascular diseases (215), in onset and progression of breast cancer (216), for neuroprotection (217) and in case of hearing loss (218, 219). The local administration of antioxidants has been connected with increased glutathione levels and decreased noise hearing loss (62). Other authors showed that the preventive application of local antioxidants reduced the noise induced hearing loss (63).

Regardless of its therapeutic benefits, the delivery of CoQ10 is challenging due to its low aqueous solubility (<4 ng/ml), high molecular weight and thermosensitivity (220). Previous studies investigated the oral bioavailability increment of CoQ10 conjugated in GMO NPs *in vivo* (220) and the actual release of the drug *in vitro* by tracking the lipase activity (221). To date, there are no reports about the potential delivery to the inner ear of CoQ10 by GMO NPs.

According to the protective effects of antioxidants on inner ear tissues (62), and to the timing for NPs uptake in cells detected in this study, cells were pretreated with NPsQ 24 before applying CDDP. Although CoQ10 is broadly used as antioxidant agent, its delivery *in vitro* by GMO NPs did not provide significant protection against highly cytotoxic doses of CDDP. The NPsQ were tested on PC12 at concentrations 25-75 μg/ml and on OC-k3 at 10-50 μg/ml, based on previous biocompatibility results by viability assays. The CDDP was tested in co-treatments at 5-25 μM, but a protective effect of NPsQ was obtained only against CDDP 5 μM in both cell lines. On PC12 cells, CDDP 5 μM caused a high dose and time dependent toxicity; the results of viability assays showed that co-treatment with NPsQ could induce a slight recover at 75-100 μg/ml at 24 hours, and at 25 and 75 μg/ml after 48 hours. However, despite the recovery, the cell viability was too low compared to controls after 48 hours, and at 24 hours the variation was minimal. On OC-k3 cells, the recover from CDDP 5 μM toxicity was very low for NPsQ 10-25 μg/ml. Moreover, with NPsQ 50 μg/ml a decreased viability of the cells was observed, probably because of a synergic effect between stress induced by the high NPsQ concentration and CDDP toxicity. The analysis of the cell cycle confirmed these results: for both cell lines co-treated with the same concentrations used for the viability assays, no significant difference was observed in the cell population distribution compared to the treatment by CDDP alone. However, in treatment with only NPsQ it was also observed that NPs did not induce any significant change in the cell cycle.

The morphological analyses highlighted a better response of cells to co-treatments: with CDDP 5 μM the number of cells attached to substrate significantly decreased, but the number of observed cells increased with high NPsQ concentrations. The PC12 cells appeared less deformed and with a

lower number of multi-lobed nuclei. On the other hand, the OC-k3 cell aspect in co-treatments appeared similar to that of the same cells treated with CDDP 5 μM. In analyses with annexin V-FITC, regardless of co-treatments, numerous cells stained in green and their number increased for high doses of NPsQ. In these cells, the CoQ10 did not directly affect the status of the cytoskeleton, since cells undergoing co-treatments appeared shrunk and with shorter cytoskeleton filaments, typical effects of CDDP.

No oxidative stress markers were analysed in molecular tests, but CoQ10 is known to directly influence the release of cytochrome *c* from mitochondria, blocking the cleavage of caspase 9 and3 and therefore the intrinsic apoptotic pathway (59, 60). However, on PC12 cells the expression of caspase 9 was not lowered by co-treatments and the enzyme was overexpressed in comparison to CDDP at 24 hours with NPsQ 25 μg/ml. Caspase 3 and BAX were generally overexpressed, significantly after 24 hours of co-treatment. These results suggest an absence of protection from apoptosis by NPsQ in this cell line. All analysed transcripts were also under expressed over time: these results agree with those of viability assays indicating at 48 hours of co-treatment a higher recover of cell viability in comparison to 24 hours. The results of protein expression by Western blot in co-treatments indicate a dose and time dependent under expression of apoptotic markers in comparison to CDDP: this is in agreement with the results of analyses with NPsQ only, where, regardless of an overexpression of mRNA transcripts, no overexpression of the apoptotic proteins was observed in comparison to untreated controls. However, although a significant decrease in caspase 3 and PARP levels was detected in co-treatments, the expression of these proteins remained significantly higher than controls, indicating a high apoptotic rate.

In OC-k3 cells, the mRNA transcripts were generally overexpressed over time in co-treatments, except for caspase 8 and 9. These results are in agreement with those obtained by treatments with NPsQ only, which were able to reduce the expression of early apoptosis markers at 24 hours in comparison to untreated controls. Other late apoptosis markers such as BAX, Bid and caspase 3 were however overexpressed in co-treatments in comparison to CDDP.

All these results suggest that CoQ10 conjugated to NPs, although able to exert a slight protective effect on both cell lines against CDDP damages, was not able to significantly prevent CDDP-induced apoptosis in comparison to cells not exposed to this highly cytotoxic agent.

5.3.2 NPsD vs CDDP

Dexamethasone is a glucocorticoid used for a broad variety of clinical therapies, and in the inner ear as an anti-inflammatory and antioxidant (26). Its classical systemic administration causes numerous side effects due to the steroid accumulation in other organs (190, 222), therefore the local application is preferred for therapies of the inner ear. Concerning drug induced hearing loss, it has been shown that preventive local applications of dexamethasone may reduce the ototoxicity caused by aminoglycosides *in vivo* (68) and reduce CDDP ototoxicity by increasing antioxidant levels in cells (69) and by decreasing levels of NADPH oxidase 3 (70). Dexamethasone has however a low solubility: in order to overcome this problem, and also to develop a more targeted local therapy and reduce the administered dose, this drug has been recently associated to steroid-eluting electrodes (223) or lipid nanoparticles (136).

Literature data about the effects of dexamethasone are still controversial, depending on the different cell lines tested or on associated compounds. For example, some authors suggested that the use of dexamethasone in addition to antibiotic therapy against acute bacterial meningitis increased hippocampal neuronal apoptosis (189).These data could be related to the results of this study, in which dexamethasone induced a significant toxicity on PC12 neuronal cells when conjugated with NPs, while an opposite effect was detected on OC-k3 epithelial cells. Given the different effects on the two cell lines analysed in this study, the protection by NPsD against CDDP toxicity was fully investigated only on OC-k3 cells.

The NPsD were tested at 10-50 µg/ml against different CDDP concentrations: they were able to protect against the highly cytotoxic CDDP concentration of 13 µM. In viability assays there was no recover after 24 hours, but after 48 hours of co-treatment a highly significant increase in cell viability was observed with NPsD 50 µg/ml compared to CDDP 13 µM. The analysis of the cell cycle confirmed that after 48 hours of co-treatment with NPsD 25-50 µg/ml, a significant increase was found in G2/M phase and a decrease (although not significant) in hypodiploid cell population; the number of cells in G0 or S did not show significant differences. A significant number of OC-k3 mitotic cells could be observed also in morphological results with NPsD 50 µg/ml. In agreement with previous results, the number of adhering cells increased with co-treatments at 48 hours, the cells had shape and cytoskeleton similar to untreated controls and a minor number of them exhibited the green annexin V-FITC stain.

The results obtained by RTqPCR on OC-k3 cells are very promising and indicate a significant under-expression of all transcripts analysed, including caspase 3. Even in contrast to the results of viability assays, the expression of transcripts increased over time, remaining significantly lower than CDDP 13 μM. No oxidative stress marker was analysed in this study, but the underexpression of caspase 9, directly activated by intracellular oxidative stress, allows to advance the hypothesis that dexamethasone conjugated to NPs may protect against CDDP-induced ROS toxicity. Moreover, the significant low expression of caspase 8 and 3 (compared to CDD 13 μM) agrees with results by other authors showing that in human eosinophils the dexamethasone treatment does no trigger the cleavage of caspase 8 and 3 (71). It is interesting to notice that the most protective concentration of NPsD in morphological and viability tests is 50 μg/ml, while in RTqPCR data an NPsD concentration of25 μg/ml induces a lower transcript expression. It may be assumed that a higher amount of NPsD induces a higher cellular stress, increasing cell response through the expression of genes related to apoptosis, whereas the high amount of internalized dexamethasone actively protects against cytotoxicity caused by CDDP and allows a higher cell survival rate. These data agree with those of protein expression analysed by Western blot, indicating a significant underexpression of cleaved caspase 3, PARP and pERK in comparison to CDDP only. At protein levels, the most protective NPsD concentration is again 25 μg/ml.

Based on these results, further analyses were performed to quantify the amount of dexamethasone released from NPsD and internalized in OC-k3 cells. The analysis by ultra performance liquid chromatography (UPLC) of OC-k3 treated with NPsD 50 μg/ml compared to cells treated with a corresponding amount of dexamethasone only (about 40 ng/ml) indicate that NPs significantly improve the cell uptake of dexamethasone, as previously shown *in vivo* (136). By tracking the drug release over time it was also possible to show that the highest amount of the compound was released in culture medium and inside cells after 24 hours from treatment, in accordance with observations conducted with NPs conjugated to the fluorescent dye rhodamine B and with timing employed in co-treatment analyses. Overall, these results clearly suggest that NPs induced a higher internalization of dexamethasone in cells in comparison to treatments with the compound alone. Based on UPLC results, it is also likely that the conjugation to NPs may protect dexamethasone from degradation, increasing its half-life.

6. Conclusions and future developments

The nanoparticles (NPs) based on glycerol monooleate produced in this study are stable in the liquid dispersion and are able to internalize hydrophobic drugs of interest. These NPs were conjugated with two drugs currently used in inner ear therapies, coenzyme Q10 (NPsQ) and dexamethasone (NPsD). Non-conjugated nanoparticles (NPsA) tagged with a fluorescent dye (rhodamine B) applied *in vitro* on inner ear cell models, the PC12 and OC-k3 cell lines, were uptaken in the first 4-8 hours after treatment. The administration of NPsD on OC-k3 revealed a significant improvement of the delivery of the conjugated drug inside cells after 4, 24 and 48 hours of treatment, compared to the drug alone. On PC12 cells, NPsA and NPsQ were not toxic up to 100 µg/ml and did not induce signs of apoptosis, while NPsD resulted toxic on this cell line at low concentrations. All other NPs produced were not toxic on OC-k3 cells up to 50 µg/ml and did not induce signs of apoptosis.

The NPsQ and NPsD were tested *in vitro* to reduce the cytotoxicity of cisplatin, a antitumor agent causing a high dose and time dependent cytotoxicity on both PC12 and OC-k3 cells by inducing apoptosis. The NPs carrying coenzyme Q10 were able to induce a slight reduction of toxicity of cisplatin 5 µM on PC12 and OC-k3 cells after 24 and 48 hours, while NPs conjugated with dexamethasone were able to significantly reduce the toxicity of cisplatin 13 µM on OC-k3 cells, especially after 48 hours.

Based on these promising *in vitro* results on inner ear cell models, the future developments could concern the application of NPs carrying therapeutic agents *in vivo* on animal models, mostly focusing on dexamethasone delivery. Local application of NPsD in the inner ear could improve the half-life and the distribution of the conjugated compound in the cochlea and lead to reduce ototoxicity caused by systemic treatment with cisplatin, without affecting its efficacy as antitumor drug.

The NP-based system have a high potential for inner ear delivery of therapeutic drugs. Their use could minimize the side effects of treatments, allow a better target specificity and provide a sustained release of drugs in inner ear fluids. The type of NPs may be modified, different drugs may be carried and several formulations could be tested. The NPs could also be combined with other nanomaterials, such as hydrogels, to improve the local application of drugs. However, several issues have yet to be solved and more *in vivo* studies are necessary to verify NPs bioavailability and effectiveness before successful clinical applications.

7 Bibliography

1. El Kechai N, Agnely F, Mamelle E, Nguyen Y, Ferrary E and Bochot A: Recent advances in local drug delivery to the inner ear. Int J Pharm 494: 83-101, 2015.
2. Grandori F, Martini A: Potenziali evocati uditivi - Basi teoriche e applicazioni cliniche. 1995.
3. Igarashi M, Ohashi K and Ishii M: Morphometric comparison of endolymphatic and perilymphatic spaces in human temporal bones. Acta Otolaryngol 101: 161-164, 1986.
4. Lee K, Das S: Essential Otolaryngology: Head & Neck Surgery. McGraw-Hill, Medical Pub Division 1993.
5. Ekborn A, Lindberg A, Laurell G, Wallin I, Eksborg S and Ehrsson H: Ototoxicity, nephrotoxicity and pharmacokinetics of cisplatin and its monohydrated complex in the guinea pig. Cancer Chemother Pharmacol 51: 36-42, 2003.
6. Rossof AH, Slayton RE and Perlia CP: Preliminary clinical experience with cis-diamminedichloroplatinum (II) (NSC 119875, CACP). Cancer 30: 1451-1456, 1972.
7. Eastman A: Mechanisms of resistance to cisplatin. Cancer Treat Res 57: 233-249, 1991.
8. Katzung BG: Farmacologia generale e clinica. 2006.
9. Goodsell DS: The molecular perspective: Cisplatin. Stem Cells 24: 514-515, 2006.
10. Gately DP and Howell SB: Cellular accumulation of the anticancer agent cisplatin: a review. Br J Cancer 67: 1171-1176, 1993.
11. Andrews PA and Howell SB: Cellular pharmacology of cisplatin: perspectives on mechanisms of acquired resistance. Cancer Cells 2: 35-43, 1990.
12. Dive C and Hickman JA: Drug-target interactions: only the first step in the commitment to a programmed cell death? Br J Cancer 64: 192-196, 1991.
13. Wang X, Martindale JL and Holbrook NJ: Requirement for ERK activation in cisplatin-induced apoptosis. J Biol Chem 275: 39435-39443, 2000.
14. Laurell G and Bagger-Sjoback D: Degeneration of the organ of Corti following intravenous administration of cisplatin. Acta Otolaryngol 111: 891-898, 1991.
15. Bokemeyer C, Berger CC, Hartmann JT*, et al*: Analysis of risk factors for cisplatin-induced ototoxicity in patients with testicular cancer. Br J Cancer 77: 1355-1362, 1998.
16. Rybak LP, Husain K, Whitworth C and Somani SM: Dose dependent protection by lipoic acid against cisplatin-induced ototoxicity in rats: antioxidant defense system. Toxicol Sci 47: 195-202, 1999.

17. Evans P and Halliwell B: Free radicals and hearing. Cause, consequence, and criteria. Ann N Y Acad Sci 884: 19-40, 1999.

18. Alam SA, Ikeda K, Oshima T*, et al*: Cisplatin-induced apoptotic cell death in Mongolian gerbil cochlea. Hear Res 141: 28-38, 2000.

19. Huang T, Cheng AG, Stupak H*, et al*: Oxidative stress-induced apoptosis of cochlear sensory cells: otoprotective strategies. Int J Dev Neurosci 18: 259-270, 2000.

20. Huang H, Zhu L, Reid BR, Drobny GP and Hopkins PB: Solution structure of a cisplatin-induced DNA interstrand cross-link. Science 270: 1842-1845, 1995.

21. Kharbanda S, Pandey P, Ren R, Mayer B, Zon L and Kufe D: c-Abl activation regulates induction of the SEK1/stress-activated protein kinase pathway in the cellular response to 1-beta-D-arabinofuranosylcytosine. J Biol Chem 270: 30278-30281, 1995.

22. Jordan P and Carmo-Fonseca M: Molecular mechanisms involved in cisplatin cytotoxicity. Cell Mol Life Sci 57: 1229-1235, 2000.

23. Kartalou M and Essigmann JM: Mechanisms of resistance to cisplatin. Mutat Res 478: 23-43, 2001.

24. Rybak LP and Somani S: Ototoxicity. Amelioration by protective agents. Ann N Y Acad Sci 884: 143-151, 1999.

25. Clerici WJ, Di Martino DL and Prasad MR: Direct effects of reactive oxygen species on cochlear outer hair cell shape in vitro. Hear Res 84: 30-40, 1995.

26. Kopke RD, Liu W, Gabaizadeh R*, et al*: Use of organotypic cultures of Corti's organ to study the protective effects of antioxidant molecules on cisplatin-induced damage of auditory hair cells. Am J Otol 18: 559-571, 1997.

27. Evans RM and Simpkins H: Cisplatin induced intermediate filament reorganization and altered mitochondrial function in 3T3 cells and drug-sensitive and -resistant Walker 256 cells. Exp Cell Res 245: 69-78, 1998.

28. Rybak LP, Whitworth C and Somani S: Application of antioxidants and other agents to prevent cisplatin ototoxicity. Laryngoscope 109: 1740-1744, 1999.

29. Feghali JG, Liu W and Van De Water TR: L-n-acetyl-cysteine protection against cisplatin-induced auditory neuronal and hair cell toxicity. Laryngoscope 111: 1147-1155, 2001.

30. Poirrier AL, Pincemail J, Van Den Ackerveken P, Lefebvre PP and Malgrange B: Oxidative stress in the cochlea: an update. Curr Med Chem 17: 3591-3604, 2010.

31. Dehne N, Lautermann J, Petrat F, Rauen U and de Groot H: Cisplatin ototoxicity: involvement of iron and enhanced formation of superoxide anion radicals. Toxicol Appl Pharmacol 174: 27-34, 2001.

32. Banfi B, Malgrange B, Knisz J, Steger K, Dubois-Dauphin M and Krause KH: NOX3, a superoxide-generating NADPH oxidase of the inner ear. J Biol Chem 279: 46065-46072, 2004.

33. Bowers WJ, Chen X, Guo H, Frisina DR, Federoff HJ and Frisina RD: Neurotrophin-3 transduction attenuates cisplatin spiral ganglion neuron ototoxicity in the cochlea. Mol Ther 6: 12-18, 2002.

34. Eguchi Y, Shimizu S and Tsujimoto Y: Intracellular ATP levels determine cell death fate by apoptosis or necrosis. Cancer Res 57: 1835-1840, 1997.

35. Lewis K: Programmed death in bacteria. Microbiol Mol Biol Rev 64: 503-514, 2000.

36. Leist M and Jaattela M: Four deaths and a funeral: from caspases to alternative mechanisms. Nat Rev Mol Cell Biol 2: 589-598, 2001.

37. Bohm I and Schild H: Apoptosis: the complex scenario for a silent cell death. Mol Imaging Biol 5: 2-14, 2003.

38. Ashkenazi A and Dixit VM: Death receptors: signaling and modulation. Science 281: 1305-1308, 1998.

39. Srinivasula SM, Ahmad M, Fernandes-Alnemri T, Litwack G and Alnemri ES: Molecular ordering of the Fas-apoptotic pathway: the Fas/APO-1 protease Mch5 is a CrmA-inhibitable protease that activates multiple Ced-3/ICE-like cysteine proteases. Proc Natl Acad Sci U S A 93: 14486-14491, 1996.

40. Green DR and Reed JC: Mitochondria and apoptosis. Science 281: 1309-1312, 1998.

41. Kroemer G, Zamzami N and Susin SA: Mitochondrial control of apoptosis. Immunol Today 18: 44-51, 1997.

42. Li H, Zhu H, Xu CJ and Yuan J: Cleavage of BID by caspase 8 mediates the mitochondrial damage in the Fas pathway of apoptosis. Cell 94: 491-501, 1998.

43. Kluck RM, Bossy-Wetzel E, Green DR and Newmeyer DD: The release of cytochrome c from mitochondria: a primary site for Bcl-2 regulation of apoptosis. Science 275: 1132-1136, 1997.

44. Soengas MS, Alarcon RM, Yoshida H*, et al*: Apaf-1 and caspase-9 in p53-dependent apoptosis and tumor inhibition. Science 284: 156-159, 1999.

45. Slee EA, Harte MT, Kluck RM*, et al*: Ordering the cytochrome c-initiated caspase cascade: hierarchical activation of caspases-2, -3, -6, -7, -8, and -10 in a caspase-9-dependent manner. J Cell Biol 144: 281-292, 1999.

46. Srinivasula SM, Ahmad M, Fernandes-Alnemri T and Alnemri ES: Autoactivation of procaspase-9 by Apaf-1-mediated oligomerization. Mol Cell 1: 949-957, 1998.

47. Saraste A and Pulkki K: Morphologic and biochemical hallmarks of apoptosis. Cardiovasc Res 45: 528-537, 2000.

48. Sakahira H, Enari M and Nagata S: Cleavage of CAD inhibitor in CAD activation and DNA degradation during apoptosis. Nature 391: 96-99, 1998.

49. Liu X, Zou H, Slaughter C and Wang X: DFF, a heterodimeric protein that functions downstream of caspase-3 to trigger DNA fragmentation during apoptosis. Cell 89: 175-184, 1997.

50. Siddik ZH: Cisplatin: mode of cytotoxic action and molecular basis of resistance. Oncogene 22: 7265-7279, 2003.

51. Micheau O, Solary E, Hammann A, Martin F and Dimanche-Boitrel MT: Sensitization of cancer cells treated with cytotoxic drugs to fas-mediated cytotoxicity. J Natl Cancer Inst 89: 783-789, 1997.

52. Muller M, Wilder S, Bannasch D*, et al*: p53 activates the CD95 (APO-1/Fas) gene in response to DNA damage by anticancer drugs. J Exp Med 188: 2033-2045, 1998.

53. Choi BK, Choi CH, Oh HL and Kim YK: Role of ERK activation in cisplatin-induced apoptosis in A172 human glioma cells. Neurotoxicology 25: 915-924, 2004.

54. Zhuang S and Schnellmann RG: A death-promoting role for extracellular signal-regulated kinase. J Pharmacol Exp Ther 319: 991-997, 2006.

55. Makin GW, Corfe BM, Griffiths GJ, Thistlethwaite A, Hickman JA and Dive C: Damage-induced Bax N-terminal change, translocation to mitochondria and formation of Bax dimers/complexes occur regardless of cell fate. EMBO J 20: 6306-6315, 2001.

56. Astolfi L, Simoni E, Valente F*, et al*: Coenzyme Q10 plus Multivitamin Treatment Prevents Cisplatin Ototoxicity in Rats. PLoS One 11: e0162106, 2016.

57. Tsuneki H, Sekizaki N, Suzuki T*, et al*: Coenzyme Q10 prevents high glucose-induced oxidative stress in human umbilical vein endothelial cells. Eur J Pharmacol 566: 1-10, 2007.

58. Sohet FM, Neyrinck AM, Pachikian BD*, et al*: Coenzyme Q10 supplementation lowers hepatic oxidative stress and inflammation associated with diet-induced obesity in mice. Biochem Pharmacol 78: 1391-1400, 2009.

59. Lenaz G, Cavazzoni M, Genova ML*, et al*: Oxidative stress, antioxidant defences and aging. Biofactors 8: 195-204, 1998.

60. Papucci L, Schiavone N, Witort E*, et al*: Coenzyme q10 prevents apoptosis by inhibiting mitochondrial depolarization independently of its free radical scavenging property. J Biol Chem 278: 28220-28228, 2003.

61. Cascella V, Giordano P, Hatzopoulos S*, et al*: A new oral otoprotective agent. Part 1: Electrophysiology data from protection against noise-induced hearing loss. Med Sci Monit 18: BR1-8, 2012.

62. Hight NG, McFadden SL, Henderson D, Burkard RF and Nicotera T: Noise-induced hearing loss in chinchillas pre-treated with glutathione monoethylester and R-PIA. Hear Res 179: 21-32, 2003.

63. Kopke RD, Coleman JK, Liu J, Campbell KC and Riffenburgh RH: Candidate's thesis: enhancing intrinsic cochlear stress defenses to reduce noise-induced hearing loss. Laryngoscope 112: 1515-1532, 2002.

64. Parnes LS, Sun AH and Freeman DJ: Corticosteroid pharmacokinetics in the inner ear fluids: an animal study followed by clinical application. Laryngoscope 109: 1-17, 1999.

65. Haynes BF, Pikus A, Kaiser-Kupfer M and Fauci AS: Successful treatment of sudden hearing loss in Cogan's syndrome with corticosteroids. Arthritis Rheum 24: 501-503, 1981.

66. Kanzaki J, T Ou and Tsuchihashi N: Steroid-responsive sensorineural hearing loss: combination therapy with prednisolone and Sairei-to. ORL J Otorhinolaryngol Relat Spec 55: 24-29, 1993.

67. Shea JJ, Jr. and Ge X: Dexamethasone perfusion of the labyrinth plus intravenous dexamethasone for Meniere's disease. Otolaryngol Clin North Am 29: 353-358, 1996.

68. Himeno C, Komeda M, Izumikawa M*, et al*: Intra-cochlear administration of dexamethasone attenuates aminoglycoside ototoxicity in the guinea pig. Hear Res 167: 61-70, 2002.

69. Daldal A, Odabasi O and Serbetcioglu B: The protective effect of intratympanic dexamethasone on cisplatin-induced ototoxicity in guinea pigs. Otolaryngol Head Neck Surg 137: 747-752, 2007.

70. Dinh CT, Chen S, Bas E*, et al*: Dexamethasone Protects Against Apoptotic Cell Death of Cisplatin-exposed Auditory Hair Cells In Vitro. Otol Neurotol 36: 1566-1571, 2015.

71. Zhang JP, Wong CK and Lam CW: Role of caspases in dexamethasone-induced apoptosis and activation of c-Jun NH2-terminal kinase and p38 mitogen-activated protein kinase in human eosinophils. Clin Exp Immunol 122: 20-27, 2000.

72. Chen G, Zhang X, Yang F and Mu L: Disposition of nanoparticle-based delivery system via inner ear administration. Curr Drug Metab 11: 886-897, 2010.

73. Juhn SK and Rybak LP: Labyrinthine barriers and cochlear homeostasis. Acta Otolaryngol 91: 529-534, 1981.

74. Inamura N and Salt AN: Permeability changes of the blood-labyrinth barrier measured in vivo during experimental treatments. Hear Res 61: 12-18, 1992.

75. Lefebvre PP and Staecker H: Steroid perfusion of the inner ear for sudden sensorineural hearing loss after failure of conventional therapy: a pilot study. Acta Otolaryngol 122: 698-702, 2002.

76. Minor LB, Schessel DA and Carey JP: Meniere's disease. Curr Opin Neurol 17: 9-16, 2004.
77. Malam Y, Loizidou M and Seifalian AM: Liposomes and nanoparticles: nanosized vehicles for drug delivery in cancer. Trends Pharmacol Sci 30: 592-599, 2009.
78. Gelperina S, Kisich K, Iseman MD and Heifets L: The potential advantages of nanoparticle drug delivery systems in chemotherapy of tuberculosis. Am J Respir Crit Care Med 172: 1487-1490, 2005.
79. Pararas EE, Borkholder DA and Borenstein JT: Microsystems technologies for drug delivery to the inner ear. Adv Drug Deliv Rev 64: 1650-1660, 2012.
80. Banerjee A and Parnes LS: The biology of intratympanic drug administration and pharmacodynamics of round window drug absorption. Otolaryngol Clin North Am 37: 1035-1051, 2004.
81. Goycoolea MV and Lundman L: Round window membrane. Structure function and permeability: a review. Microsc Res Tech 36: 201-211, 1997.
82. Goycoolea MV: The round window membrane under normal and pathological conditions. Acta Otolaryngol Suppl 493: 43-55, 1992.
83. Salt AN and Plontke SK: Local inner-ear drug delivery and pharmacokinetics. Drug Discov Today 10: 1299-1306, 2005.
84. Jahnke K: Permeability barriers of the inner ear. Fine structure and function. Fortschr Med 98: 330-336, 1980.
85. Jahnke K: The blood-perilymph barrier. Arch Otorhinolaryngol 228: 29-34, 1980.
86. Saito T, Zhang ZJ, Tokuriki M*, et al*: Expression of p-glycoprotein is associated with that of multidrug resistance protein 1 (MRP1) in the vestibular labyrinth and endolymphatic sac of the guinea pig. Neurosci Lett 303: 189-192, 2001.
87. Hongzhuo Liu JH, kevin S. Li: Current strategies for drug delivery to the inner ear. Acta Pharmaceutica Sinica B 3: 86-96, 2013.
88. Swan EE, Mescher MJ, Sewell WF, Tao SL and Borenstein JT: Inner ear drug delivery for auditory applications. Adv Drug Deliv Rev 60: 1583-1599, 2008.
89. McCall AA, Swan EE, Borenstein JT, Sewell WF, Kujawa SG and McKenna MJ: Drug delivery for treatment of inner ear disease: current state of knowledge. Ear Hear 31: 156-165, 2010.
90. Tamura T, Kita T, Nakagawa T*, et al*: Drug delivery to the cochlea using PLGA nanoparticles. Laryngoscope 115: 2000-2005, 2005.
91. Horie RT, Sakamoto T, Nakagawa T, Ishihara T, Higaki M and Ito J: Stealth-nanoparticle strategy for enhancing the efficacy of steroids in mice with noise-induced hearing loss. Nanomedicine (Lond) 5: 1331-1340, 2010.

92. Bowe SN and Jacob A: Round window perfusion dynamics: implications for intracochlear therapy. Curr Opin Otolaryngol Head Neck Surg 18: 377-385, 2010.
93. De Ceulaer G, Johnson S, Yperman M*, et al*: Long-term evaluation of the effect of intracochlear steroid deposition on electrode impedance in cochlear implant patients. Otol Neurotol 24: 769-774, 2003.
94. Paulson DP, Abuzeid W, Jiang H, Oe T, O'Malley BW and Li D: A novel controlled local drug delivery system for inner ear disease. Laryngoscope 118: 706-711, 2008.
95. Hahn H, Kammerer B, DiMauro A, Salt AN and Plontke SK: Cochlear microdialysis for quantification of dexamethasone and fluorescein entry into scala tympani during round window administration. Hear Res 212: 236-244, 2006.
96. Ciorba AL, Jolly C and Martini A: Cochlear Implants and Inner Ear Based Therapy. European Journal of Nanomedicine 2: 4, 2009.
97. Salt AN: Pharmacokinetics of Drug Entry into Cochlear Fluids. Volta Rev 105: 277-298, 2005.
98. Boge L, Bysell H, Ringstad L*, et al*: Lipid-Based Liquid Crystals As Carriers for Antimicrobial Peptides: Phase Behavior and Antimicrobial Effect. Langmuir 32: 4217-4228, 2016.
99. Norling T, Lading P, Engstrom S, Larsson K, Krog N and Nissen SS: Formulation of a drug delivery system based on a mixture of monoglycerides and triglycerides for use in the treatment of periodontal disease. J Clin Periodontol 19: 687-692, 1992.
100. Lutton ES: Phase behavior of aqueous systems of monoglycerides. J Am Oil Chem Soc 42: 1068-1070, 1965.
101. Qiu H and Caffrey M: The phase diagram of the monoolein/water system: metastability and equilibrium aspects. Biomaterials 21: 223-234, 2000.
102. Bei D, Meng J and Youan BB: Engineering nanomedicines for improved melanoma therapy: progress and promises. Nanomedicine (Lond) 5: 1385-1399, 2010.
103. Spicer PT HK: Novel Process for Producing Cubic Liquid Crystalline Nanoparticles. Langmuir 17: 9, 2001.
104. Lawrence MJ: Surfactant systems: microemulsions and vesicles as vehicles for drug delivery. Eur J Drug Metab Pharmacokinet 19: 257-269, 1994.
105. Larsson K: Cubic liquid water-phases: Structures and biomembrane aspects. Journal of Physical Chemistry 93: 10, 1989.
106. Barauskas J, Johnsson M, Joabsson F and Tiberg F: Cubic phase nanoparticles (Cubosome): principles for controlling size, structure, and stability. Langmuir 21: 2569-2577, 2005.

107. Fidber S, Fei L, Yang H, Patel R, Aikens P A: Vesicle formation and disintegration: a water-hydrotrope-nonionic surfactant system. Colloids and Surfaces A: Physicochemical and Engineering Aspects 129-130: 8, 1997.

108. Gustaffson J , Almgren M, Larsson K Cubic Lipid−Water Phase Dispersed into Submicron Particles. Langmuir 12: 3, 1996.

109. Gustaffson J L-WH, Almgren M, Larsson K Submicron Particles of Reversed Lipid Phases in Water Stabilized by a Nonionic Amphiphilic Polymer. Langmuir 13: 8, 1997.

110. Nakano M, Matsuoka H, Handa T: Small-Angle X-ray Scattering and 13C NMR Investigation on the Internal Structure of "Cubosomes". Langmuir 17: 6, 2001.

111. Milak S and Zimmer A: Glycerol monooleate liquid crystalline phases used in drug delivery systems. Int J Pharm 478: 569-587, 2015.

112. Hyde ST, Andersson S: A cubic structure consisting of a lipid bilayer forming an infinite periodic minimum surface of the gyroid type in the glycerolmonooleat-water system. Zeitschrift für Kristallographie - Crystalline Materials 168: 8, 1984.

113. Drummond CJ, Fong C: Surfactant self-assembly objects as novel drug delivery vehiclres. Current Opinion in Colloid & Interface Science 4: 8, 2000.

114. Rizwan SB, Boyd BJ, Rades T and Hook S: Bicontinuous cubic liquid crystals as sustained delivery systems for peptides and proteins. Expert Opin Drug Deliv 7: 1133-1144, 2010.

115. Angelova A, Angelov B, Mutafchieva R, Lesieur S and Couvreur P: Self-assembled multicompartment liquid crystalline lipid carriers for protein, peptide, and nucleic acid drug delivery. Acc Chem Res 44: 147-156, 2011.

116. Caboi F, Amico GS, Pitzalis P, Monduzzi M, Nylander T and Larsson K: Addition of hydrophilic and lipophilic compounds of biological relevance to the monoolein/water system. I. Phase behavior. Chem Phys Lipids 109: 47-62, 2001.

117. Jager E, Venturini CG, Poletto FS*, et al*: Sustained release from lipid-core nanocapsules by varying the core viscosity and the particle surface area. J Biomed Nanotechnol 5: 130-140, 2009.

118. Salentinig S, Sagalowicz L and Glatter O: Self-assembled structures and pKa value of oleic acid in systems of biological relevance. Langmuir 26: 11670-11679, 2010.

119. Chung H, Kim J, Um JY, Kwon IC and Jeong SY: Self-assembled "nanocubicle" as a carrier for peroral insulin delivery. Diabetologia 45: 448-451, 2002.

120. Rizwan SB, Assmus D, Boehnke A*, et al*: Preparation of phytantriol cubosomes by solvent precursor dilution for the delivery of protein vaccines. Eur J Pharm Biopharm 79: 15-22, 2011.

121. Cervin C, Vandoolaeghe P, Nistor C, Tiberg F and Johnsson M: A combined in vitro and in vivo study on the interactions between somatostatin and lipid-based liquid crystalline drug carriers and bilayers. Eur J Pharm Sci 36: 377-385, 2009.
122. Lopes LB, Ferreira DA, de Paula D*, et al*: Reverse hexagonal phase nanodispersion of monoolein and oleic acid for topical delivery of peptides: in vitro and in vivo skin penetration of cyclosporin A. Pharm Res 23: 1332-1342, 2006.
123. Wyatt DM, Dorschel D: A cubic phase delivery system composed of glycerol monooleate and water for sustained release of water soluble drugs. Pharmaceutical Technologies 15, 1992.
124. Alfons K and Engstrom S: Drug compatibility with the sponge phases formed in monoolein, water, and propylene glycol or poly(ethylene glycol). J Pharm Sci 87: 1527-1530, 1998.
125. Chang C-M, Bodmeier R: Binding Drugs to Monoglyceride based drug delivery systems. Internation Journal of Pharmacology 147: 135, 1997.
126. Lindell K, Engblom S, Engstrom M, Jonstromer M, Carlsson A: Influence of a charged phospholipid on the release pattern of timolol maleate from cubic liquid crystalline phases. 108: 9, 1998.
127. Gordon S, Young K, Wilson R*, et al*: Chitosan hydrogels containing liposomes and cubosomes as particulate sustained release vaccine delivery systems. J Liposome Res 22: 193-204, 2012.
128. Engstrom S, Lindahl L, Wallin R, Engblom J: A study of polar lipid drug carrier system undergoing a thermoversatile lamellar-to-cubic phase transition. Internation Journal of Pharmacology 86: 9, 1992.
129. Sadhale Y and Shah JC: Biological activity of insulin in GMO gels and the effect of agitation. Int J Pharm 191: 65-74, 1999.
130. Chang C-M, Bodmeier R: Monoglyceride based liquid crystalline topical drug delivery systems. Pharmacological Research 11: 1994.
131. Hureaux J, Lagarce F, Gagnadoux F*, et al*: Toxicological study and efficacy of blank and paclitaxel-loaded lipid nanocapsules after i.v. administration in mice. Pharm Res 27: 421-430, 2010.
132. Scheper V, Wolf M, Scholl M*, et al*: Potential novel drug carriers for inner ear treatment: hyperbranched polylysine and lipid nanocapsules. Nanomedicine (Lond) 4: 623-635, 2009.
133. Zhang Y, Zhang W, Lobler M*, et al*: Inner ear biocompatibility of lipid nanocapsules after round window membrane application. Int J Pharm 404: 211-219, 2011.
134. Zou J, Saulnier P, Perrier T*, et al*: Distribution of lipid nanocapsules in different cochlear cell populations after round window membrane permeation. J Biomed Mater Res B Appl Biomater 87: 10-18, 2008.

135. Liu H, Chen S, Zhou Y*, et al*: The effect of surface charge of glycerol monooleate-based nanoparticles on the round window membrane permeability and cochlear distribution. J Drug Target 21: 846-854, 2013.
136. Chen G, Hou SX, Hu P, Hu QH, Guo DD and Xiao Y: [In vitro dexamethasone release from nanoparticles and its pharmacokinetics in the inner ear after administration of the drug-loaded nanoparticles via the round window]. Nan Fang Yi Ke Da Xue Xue Bao 28: 1022-1024, 2008.
137. Bozzuto G and Molinari A: Liposomes as nanomedical devices. Int J Nanomedicine 10: 975-999, 2015.
138. Wang AZ, Langer R and Farokhzad OC: Nanoparticle delivery of cancer drugs. Annu Rev Med 63: 185-198, 2012.
139. Zou J, Sood R, Ranjan S*, et al*: Size-dependent passage of liposome nanocarriers with preserved posttransport integrity across the middle-inner ear barriers in rats. Otol Neurotol 33: 666-673, 2012.
140. Zou J, Sood R, Ranjan S*, et al*: Manufacturing and in vivo inner ear visualization of MRI traceable liposome nanoparticles encapsulating gadolinium. J Nanobiotechnology 8: 32, 2010.
141. Letchford K and Burt H: A review of the formation and classification of amphiphilic block copolymer nanoparticulate structures: micelles, nanospheres, nanocapsules and polymersomes. Eur J Pharm Biopharm 65: 259-269, 2007.
142. Farokhzad OC and Langer R: Nanomedicine: developing smarter therapeutic and diagnostic modalities. Adv Drug Deliv Rev 58: 1456-1459, 2006.
143. Lin JJ, Ghoroghchian PP, Zhang Y and Hammer DA: Adhesion of antibody-functionalized polymersomes. Langmuir 22: 3975-3979, 2006.
144. Buckiova D, Ranjan S, Newman TA*, et al*: Minimally invasive drug delivery to the cochlea through application of nanoparticles to the round window membrane. Nanomedicine (Lond) 7: 1339-1354, 2012.
145. Yoon JY, Yang KJ, Kim da E*, et al*: Intratympanic delivery of oligoarginine-conjugated nanoparticles as a gene (or drug) carrier to the inner ear. Biomaterials 73: 243-253, 2015.
146. Grottkau BE, Cai X, Wang J, Yang X and Lin Y: Polymeric nanoparticles for a drug delivery system. Curr Drug Metab 14: 840-846, 2013.
147. Cai H, Wen X, Wen L*, et al*: Enhanced local bioavailability of single or compound drugs delivery to the inner ear through application of PLGA nanoparticles via round window administration. Int J Nanomedicine 9: 5591-5601, 2014.
148. Pritz CO, Dudas J, Rask-Andersen H, Schrott-Fischer A and Glueckert R: Nanomedicine strategies for drug delivery to the ear. Nanomedicine (Lond) 8: 1155-1172, 2013.

149. Le VH, Thuc CN and Thuc HH: Synthesis of silica nanoparticles from Vietnamese rice husk by sol-gel method. Nanoscale Res Lett 8: 58, 2013.
150. Sameti M, Bohr G, Ravi Kumar MN, *et al*: Stabilisation by freeze-drying of cationically modified silica nanoparticles for gene delivery. Int J Pharm 266: 51-60, 2003.
151. Ahola M, Rich J, Kortesuo P, Kiesvaara J, Seppala J and Yli-Urpo A: In vitro evaluation of biodegradable epsilon-caprolactone-co-D, L-lactide/silica xerogel composites containing toremifene citrate. Int J Pharm 181: 181-191, 1999.
152. Sun C, Lee JS and Zhang M: Magnetic nanoparticles in MR imaging and drug delivery. Adv Drug Deliv Rev 60: 1252-1265, 2008.
153. Cao ZG, Zhou SW, Sun K, Lu XB, Luo G and Liu JH: [Preparation and feasibility of superparamagnetic dextran iron oxide nanoparticles as gene carrier]. Ai Zheng 23: 1105-1109, 2004.
154. Ye F, Laurent S, Fornara A, *et al*: Uniform mesoporous silica coated iron oxide nanoparticles as a highly efficient, nontoxic MRI T(2) contrast agent with tunable proton relaxivities. Contrast Media Mol Imaging 7: 460-468, 2012.
155. Kopke RD, Wassel RA, Mondalek F, *et al*: Magnetic nanoparticles: inner ear targeted molecule delivery and middle ear implant. Audiol Neurootol 11: 123-133, 2006.
156. Ge X, Jackson RL, Liu J, *et al*: Distribution of PLGA nanoparticles in chinchilla cochleae. Otolaryngol Head Neck Surg 137: 619-623, 2007.
157. Zou J, Sood R, Zhang Y, Kinnunen PK and Pyykko I: Pathway and morphological transformation of liposome nanocarriers after release from a novel sustained inner-ear delivery system. Nanomedicine (Lond) 9: 2143-2155, 2014.
158. Roy S, Johnston AH, Newman TA, *et al*: Cell-specific targeting in the mouse inner ear using nanoparticles conjugated with a neurotrophin-derived peptide ligand: potential tool for drug delivery. Int J Pharm 390: 214-224, 2010.
159. Wu TH, Liu CP, Chien CT and Lin SY: Fluorescent hydroxylamine derived from the fragmentation of PAMAM dendrimers for intracellular hypochlorite recognition. Chemistry 19: 11672-11675, 2013.
160. Kim DK, Park SN, Park KH, *et al*: Development of a drug delivery system for the inner ear using poly(amino acid)-based nanoparticles. Drug Deliv 22: 367-374, 2015.
161. Du X, Chen K, Kuriyavar S, *et al*: Magnetic targeted delivery of dexamethasone acetate across the round window membrane in guinea pigs. Otol Neurotol 34: 41-47, 2013.

162. Sheppard WM, Wanamaker HH, Pack A, Yamamoto S and Slepecky N: Direct round window application of gentamicin with varying delivery vehicles: a comparison of ototoxicity. Otolaryngol Head Neck Surg 131: 890-896, 2004.
163. Thaler M, Roy S, Fornara A*, et al*: Visualization and analysis of superparamagnetic iron oxide nanoparticles in the inner ear by light microscopy and energy filtered TEM. Nanomedicine 7: 360-369, 2011.
164. Lajud SA, Nagda DA, Qiao P*, et al*: A novel chitosan-hydrogel-based nanoparticle delivery system for local inner ear application. Otol Neurotol 36: 341-347, 2015.
165. Wang X, Dellamary L, Fernandez R*, et al*: Dose-dependent sustained release of dexamethasone in inner ear cochlear fluids using a novel local delivery approach. Audiol Neurootol 14: 393-401, 2009.
166. Salt AN and Plontke SK: Principles of local drug delivery to the inner ear. Audiol Neurootol 14: 350-360, 2009.
167. Astolfi L, Guaran V, Marchetti N*, et al*: Cochlear implants and drug delivery: In vitro evaluation of dexamethasone release. J Biomed Mater Res B Appl Biomater 102: 267-273, 2014.
168. Wu WJ, Sha SH, McLaren JD, Kawamoto K, Raphael Y and Schacht J: Aminoglycoside ototoxicity in adult CBA, C57BL and BALB mice and the Sprague-Dawley rat. Hear Res 158: 165-178, 2001.
169. Kalinec F, Kalinec G, Boukhvalova M and Kachar B: Establishment and characterization of conditionally immortalized organ of corti cell lines. Cell Biol Int 23: 175-184, 1999.
170. Bertolaso L, Martini A, Bindini D*, et al*: Apoptosis in the OC-k3 immortalized cell line treated with different agents. Audiology 40: 327-335, 2001.
171. Bertolaso L, Bindini D, Previati M*, et al*: Gentamicin-induced cytotoxicity involves protein kinase C activation, glutathione extrusion and malondialdehyde production in an immortalized cell line from the organ of corti. Audiol Neurootol 8: 38-48, 2003.
172. Previati M, Lanzoni I, Corbacella E*, et al*: RNA expression induced by cisplatin in an organ of Corti-derived immortalized cell line. Hear Res 196: 8-18, 2004.
173. Previati M, Lanzoni I, Astolfi L*, et al*: Cisplatin cytotoxicity in organ of Corti-derived immortalized cells. J Cell Biochem 101: 1185-1197, 2007.
174. Greene LA and Tischler AS: Establishment of a noradrenergic clonal line of rat adrenal pheochromocytoma cells which respond to nerve growth factor. Proc Natl Acad Sci U S A 73: 2424-2428, 1976.
175. Garber SS, Hoshi T and Aldrich RW: Regulation of ionic currents in pheochromocytoma cells by nerve growth factor and dexamethasone. J Neurosci 9: 3976-3987, 1989.

176. Piga R, Saito Y, Chen Z, Yoshida Y and Niki E: Characterization of monochloramine toxicity on PC12 cells and protective effect of tocopherol via antioxidative function. Arch Biochem Biophys 436: 101-109, 2005.
177. Lee YW, So C, Chi WH, Lee SH: Underlying Mechanism of Cisplatin-induced Apoptosis in PC-12 Cells. Journal of Korean Neurosurgery Society 27: 6, 1998.
178. Klein R, Brown D and Turnley AM: Phenoxodiol protects against Cisplatin induced neurite toxicity in a PC-12 cell model. BMC Neurosci 8: 61, 2007.
179. Ruben RJ: Development of the inner ear of the mouse: a radioautographic study of terminal mitoses. Acta Otolaryngol Suppl 220:221-244, 1967.
180. Wang J, Lloyd Faulconbridge RV, Fetoni A, Guitton MJ, Pujol R and Puel JL: Local application of sodium thiosulfate prevents cisplatin-induced hearing loss in the guinea pig. Neuropharmacology 45: 380-393, 2003.
181. Praetorius M, Brunner C, Lehnert B*, et al*: Transsynaptic delivery of nanoparticles to the central auditory nervous system. Acta Otolaryngol 127: 486-490, 2007.
182. K L: Cubic liquid water-phases: Structures and biomembrane aspects. Journal of Physical Chemistry 93: 10, 1989.
183. Hinton T, Grusche F, Acharya D, Shukla R, Bansal V, Waddington L, Monaghan P, Muir B: Bicontinuous cubic phase nanoparticle lipid chemistry affects toxicity in cultured cells Toxicology Research 3: 12, 2014.
184. Guo C, Wang J, Cao F, Lee RJ and Zhai G: Lyotropic liquid crystal systems in drug delivery. Drug Discov Today 15: 1032-1040, 2010.
185. Barauskas J, Cervin C, Jankunec M*, et al*: Interactions of lipid-based liquid crystalline nanoparticles with model and cell membranes. Int J Pharm 391: 284-291, 2010.
186. Murgia S, Falchi AM, Mano M*, et al*: Nanoparticles from lipid-based liquid crystals: emulsifier influence on morphology and cytotoxicity. J Phys Chem B 114: 3518-3525, 2010.
187. Oberdorster G, Oberdorster E and Oberdorster J: Concepts of nanoparticle dose metric and response metric. Environ Health Perspect 115: A290, 2007.
188. Zook JM, Maccuspie RI, Locascio LE, Halter MD and Elliott JT: Stable nanoparticle aggregates/agglomerates of different sizes and the effect of their size on hemolytic cytotoxicity. Nanotoxicology 5: 517-530, 2011.
189. Spreer A, Gerber J, Hanssen M*, et al*: Dexamethasone increases hippocampal neuronal apoptosis in a rabbit model of Escherichia coli meningitis. Pediatr Res 60: 210-215, 2006.

190. Belgaumi AF, Al-Bakrah M, Al-Mahr M*, et al*: Dexamethasone-associated toxicity during induction chemotherapy for childhood acute lymphoblastic leukemia is augmented by concurrent use of daunomycin. Cancer 97: 2898-2903, 2003.

191. Shen HH, Crowston JG, Huber F, Saubern S, McLean KM and Hartley PG: The influence of dipalmitoyl phosphatidylserine on phase behaviour of and cellular response to lyotropic liquid crystalline dispersions. Biomaterials 31: 9473-9481, 2010.

192. Johnson L V, Walsh ML, Chen L B: Localization of mitochondria in living cells with rhodamine. Proc Natl Acad Sci U S A 77: 4, 1980.

193. Oh N and Park JH: Endocytosis and exocytosis of nanoparticles in mammalian cells. Int J Nanomedicine 9 Suppl 1: 51-63, 2014.

194. Humes HD: Insights into ototoxicity. Analogies to nephrotoxicity. Ann N Y Acad Sci 884: 15-18, 1999.

195. Huang X, Whitworth CA and Rybak LP: Ginkgo biloba extract (EGb 761) protects against cisplatin-induced ototoxicity in rats. Otol Neurotol 28: 828-833, 2007.

196. Rybak LP, Ravi R and Somani SM: Mechanism of protection by diethyldithiocarbamate against cisplatin ototoxicity: antioxidant system. Fundam Appl Toxicol 26: 293-300, 1995.

197. van Ruijven MW, de Groot JC, Klis SF and Smoorenburg GF: The cochlear targets of cisplatin: an electrophysiological and morphological time-sequence study. Hear Res 205: 241-248, 2005.

198. Cardinaal RM, de Groot JC, Huizing EH, Veldman JE and Smoorenburg GF: Histological effects of co-administration of an ACTH((4-9)) analogue, ORG 2766, on cisplatin ototoxicity in the albino guinea pig. Hear Res 144: 157-167, 2000.

199. Borgatti P, Zauli G, Colamussi ML*, et al*: Extracellular HIV-1 Tat protein activates phosphatidylinositol 3- and Akt/PKB kinases in CD4+ T lymphoblastoid Jurkat cells. Eur J Immunol 27: 2805-2811, 1997.

200. Forge A: Outer hair cell loss and supporting cell expansion following chronic gentamicin treatment. Hear Res 19: 171-182, 1985.

201. Vago P, Humbert G and Lenoir M: Amikacin intoxication induces apoptosis and cell proliferation in rat organ of Corti. Neuroreport 9: 431-436, 1998.

202. Devarajan P, Savoca M, Castaneda MP*, et al*: Cisplatin-induced apoptosis in auditory cells: role of death receptor and mitochondrial pathways. Hear Res 174: 45-54, 2002.

203. Chu G: Cellular responses to cisplatin. The roles of DNA-binding proteins and DNA repair. J Biol Chem 269: 787-790, 1994.

204. McDonald ES, Randon KR, Knight A and Windebank AJ: Cisplatin preferentially binds to DNA in dorsal root ganglion neurons in vitro and in vivo: a potential mechanism for neurotoxicity. Neurobiol Dis 18: 305-313, 2005.

205. Vaux DL and Strasser A: The molecular biology of apoptosis. Proc Natl Acad Sci U S A 93: 2239-2244, 1996.

206. Zhang M DDL, Salvi R: Cisplatin activates caspase 3 and the p-53 inhibitor, pifithrin-alpha attenuates caspase 3 labelling. 25th ARO Midwinter Meeting 528A 2002

207. Kalinec G LDJ, Webster P: A cochlear cell line as an in vitro system for drug ototoxicity screening. Audiology and neuro-otology 8: 13, 2003.

208. Liu Y, Xing H, Han X*, et al*: Apoptosis of HeLa cells induced by cisplatin and its mechanism. J Huazhong Univ Sci Technolog Med Sci 28: 197-199, 2008.

209. Rybak LP, Whitworth CA, Mukherjea D and Ramkumar V: Mechanisms of cisplatin-induced ototoxicity and prevention. Hear Res 226: 157-167, 2007.

210. Liu W, Staecker H, Stupak H, Malgrange B, Lefebvre P and Van De Water TR: Caspase inhibitors prevent cisplatin-induced apoptosis of auditory sensory cells. Neuroreport 9: 2609-2614, 1998.

211. Johnson GL, Villancourt RR: Sequential protein kinase reactions controlling cell growth and differentiation. Current Opinion in Cell Biology 6: 9, 1994.

212. Brauns SC, Dealtry G, Milne P, Naude R and Van de Venter M: Caspase-3 activation and induction of PARP cleavage by cyclic dipeptide cyclo(Phe-Pro) in HT-29 cells. Anticancer Res 25: 4197-4202, 2005.

213. Folkers K: The potential of coenzyme Q 10 (NSC-140865) in cancer treatment. Cancer Chemother Rep 2 4: 19-22, 1974.

214. Scheer JF: Getting to the heart of the matter with CoQ10. Better Nutrition 61: 3, 1999.

215. Langsjoen PH and Langsjoen AM: Overview of the use of CoQ10 in cardiovascular disease. Biofactors 9: 273-284, 1999.

216. Lockwood K, Moesgaard S and Folkers K: Partial and complete regression of breast cancer in patients in relation to dosage of coenzyme Q10. Biochem Biophys Res Commun 199: 1504-1508, 1994.

217. Koenig ML and Meyerhoff JL: In vitro neuroprotection against oxidative stress by pre-treatment with a combination of dihydrolipoic acid and phenyl-butyl nitrones. Neurotox Res 5: 265-272, 2003.

218. Ciuman RR: Inner ear symptoms and disease: pathophysiological understanding and therapeutic options. Med Sci Monit 19: 1195-1210, 2013.

219. Sato K: Pharmacokinetics of coenzyme Q10 in recovery of acute sensorineural hearing loss due to hypoxia. Acta Otolaryngol Suppl 458: 95-102, 1988.
220. Swarnakar NK, Jain AK, Singh RP, Godugu C, Das M and Jain S: Oral bioavailability, therapeutic efficacy and reactive oxygen species scavenging properties of coenzyme Q10-loaded polymeric nanoparticles. Biomaterials 32: 6860-6874, 2011.
221. Swarnakar NK, Thanki K and Jain S: Lyotropic liquid crystalline nanoparticles of CoQ10: implication of lipase digestibility on oral bioavailability, in vivo antioxidant activity, and in vitro-in vivo relationships. Mol Pharm 11: 1435-1449, 2014.
222. Nabih M, Peyman GA, Tawakol ME and Naguib K: Toxicity of high-dose intravitreal dexamethasone. Int Ophthalmol 15: 233-235, 1991.
223. Astolfi L, Simoni E, Giarbini N*, et al*: Cochlear implant and inflammation reaction: Safety study of a new steroid-eluting electrode. Hear Res 336: 44-52, 2016.